2016

In Situ Geochemistry of Middle Ordovician Dolomites of the Upper Mississippi Valley: Evaluation of the Dorag Model and New Implications for Dolomitizing Fluids

John Michael Callen
Louisiana State University and Agricultural and Mechanical College

IN SITU GEOCHEMISTRY OF MIDDLE ORDOVICIAN DOLOMITES OF THE UPPER MISSISSIPPI VALLEY: EVALUATION OF THE DORAG MODEL AND NEW IMPLICATIONS FOR DOLOMITIZING FLUIDS

A Thesis

Submitted to the Graduate Faculty of the
Louisiana State University and
Agricultural and Mechanical College
in partial fulfillment
of the requirements for the degree of
Master of Science

in

The Department of Geology and Geophysics

by
John Michael Callen
B.S., Centenary College of Louisiana, 2012
May 2016

TABLE OF CONTENTS

ABSTRACT

The dolomitization and diagenetic history of Ordovician carbonates of southern Wisconsin has been studied for over a century. Previous studies attributed dolomitization to various single or multiple diagenetic factors and environments. The goal of the study was to resolve arguments regarding dolomitization models, including Badiozamani's often cited but recently questioned mixing zone model, using LA-ICP-MS focusing on REE to determine the nature of dolomitizing fluids.

Analysis revealed that particulate material incorporated into the dolomite affected the geochemical results of many of the samples. Integrating geochemical data with petrographic evidence for diagenetic history, the studied Decorah Formation dolomites were assigned to two realms: shallow burial and hydrothermal. Shallow burial dolomites exhibit three distinct REE patterns. Dolomite from the middle portion of the Guttenberg formed inside a trilobite fossil maintained a seawater-like REE pattern, while dolomite in lime mud inside this fossil and dolomite in micrite from another sample in this interval exhibit LREE enrichment consistent with early burial. Carimona, Specht's Ferry, and Lower Guttenberg dolomites are often burrow associated and exhibit MREE enrichment associated with Fe-oxide desorption in anoxic porewaters. The proximity of these dolomites to samples to K-bentonite beds is interpreted as having been the result of Mg leaching from the volcanic ash during alteration. Extensively dolomitized samples in the upper Guttenberg and Ion Member exhibit evidence of hydrothermal dolomitization. The relation of these heavily dolomitized samples to interbedded limestones provides evidence for a recently proposed hydrothermal dolomitization model invoking pressure solution of calcite and precipitation of dolomite.

These early burial and hydrothermal depositional models are consistent with models proposed for overlying and underlying Ordovician dolomites. This study revealed no evidence of extensive dolomitization due to Badiozamani's mixing zone model. Due to the location of this outcrop relative to the Wisconsin Arch, this study cannot directly disprove that dolomitization in eastern Wisconsin is the result of Badiozamani's Dorag dolomitization. Despite this, Luczaj's argument that the Dorag model should not have been widely applied to dolomites of the southern Wisconsin area seems appropriate.

1. INTRODUCTION

Dolomite has been the focus of laboratory research and field observations for more than 150 years. Dolomite ($CaMg(CO_3)_2$) is a common component of carbonate rocks throughout the geologic record. This mineral is very common among carbonates of the Paleozoic and Proterozoic; however, dolomite is uncommon in modern marine carbonate environments (Holland and Zimmerman, 2000; Warren, 2000; McKenzie and Vasconcelos, 2009). In the case of dolomites, the present is not the key to the past. In order to overcome the lack of modern analogues to large-scale dolomitization present in the rock record, scientists have developed many different depositional and diagenetic models of dolomitization (Warren, 2000). These models serve to overcome barriers associated with the formation of dolomite. The application and relevance of these models to ancient dolomites has been a source debate among scientists as our understanding and the tools scientists use to study dolomite evolve. The general acceptance that special geochemical conditions are required for dolomitization has resulted in many rock-based studies focusing on the geochemistry of dolomitizing fluids (Whitaker et al., 2004). By incorporating new geochemical analysis and methods to increase our understanding of dolomitizing fluid, scientists can work to apply these dolomitization models more accurately.

The drive to develop and apply predictive models for dolomitization is motivated not only by scientific curiosity, but also by the economic importance of dolomite and dolomitization processes. Dolomite accounts for 80% of North American and almost 50% of international carbonate petroleum reservoirs (Warren, 2000). Dolomitized strata surrounding the Michigan Basin in northern Illinois and eastern Wisconsin have been studied due to the hydrocarbon

reservoir production potential of these Ordovician rocks (Yoo et al., 2000; Luczaj, 2006). Several recent studies incorporating rare earth element (REE) data have been conducted on dolomite in or on updip basin edges in order to constrain the nature, origin, and potential flow patterns of diagenetic fluids. These studies were conducted in the Illinois Basin (Banner et al., 1988), Newfoundland (Azomani et al., 2013 and Azmy et al., 2013), and the Tarim Basin (Wang et al., 2009; Wang et al., 2014; Zhang et al., 2014) due to the economic potential of dolomitized carbonate units as hydrocarbon reservoirs in these areas.

Dolomite is also a key host of Mississippi Valley-Type Pb-Zn deposits (Van Heyl, 1959). The Upper Mississippi Valley (UMV) Pb-Zn mining district (Figure 1, A) of southwest Wisconsin has been extensively studied due to the mining potential of these hydrothermal precipitates in Ordovician rocks (Tupas, 1950; Agnew et al., 1956; Hall et al., 1963; Deininger, 1964; Van Heyl, 1959; Heyl et al., 1974, 1982; Smith, 1991; Brannon et al., 1992; Rowan et al., 1995; Smith and Simo, 1997; Fouke et al., 2012). The economic importance of Pb-Zn sulfides and its association with dolomite in southern Wisconsin has resulted in many studies focused on the occurrence of dolomite. These studies have attributed the occurrence of dolomite in these Ordovician rocks to a wide range of dolomitization models.

Before discussing dolomitization models of southern Wisconsin, it is important to understand why these models must be developed. Despite the oversaturation of seawater with respect to dolomite, dolomite rarely precipitates under normal marine conditions (Badiozamani, 1973). Laboratory experiments have revealed that dolomite formation from seawater is inhibited by several kinetic factors including Mg/Ca ratios, CO_3^{2-} activity and temperature, ionic strength, 1973). Laboratory experiments have revealed that dolomite formation from seawater is inhibited

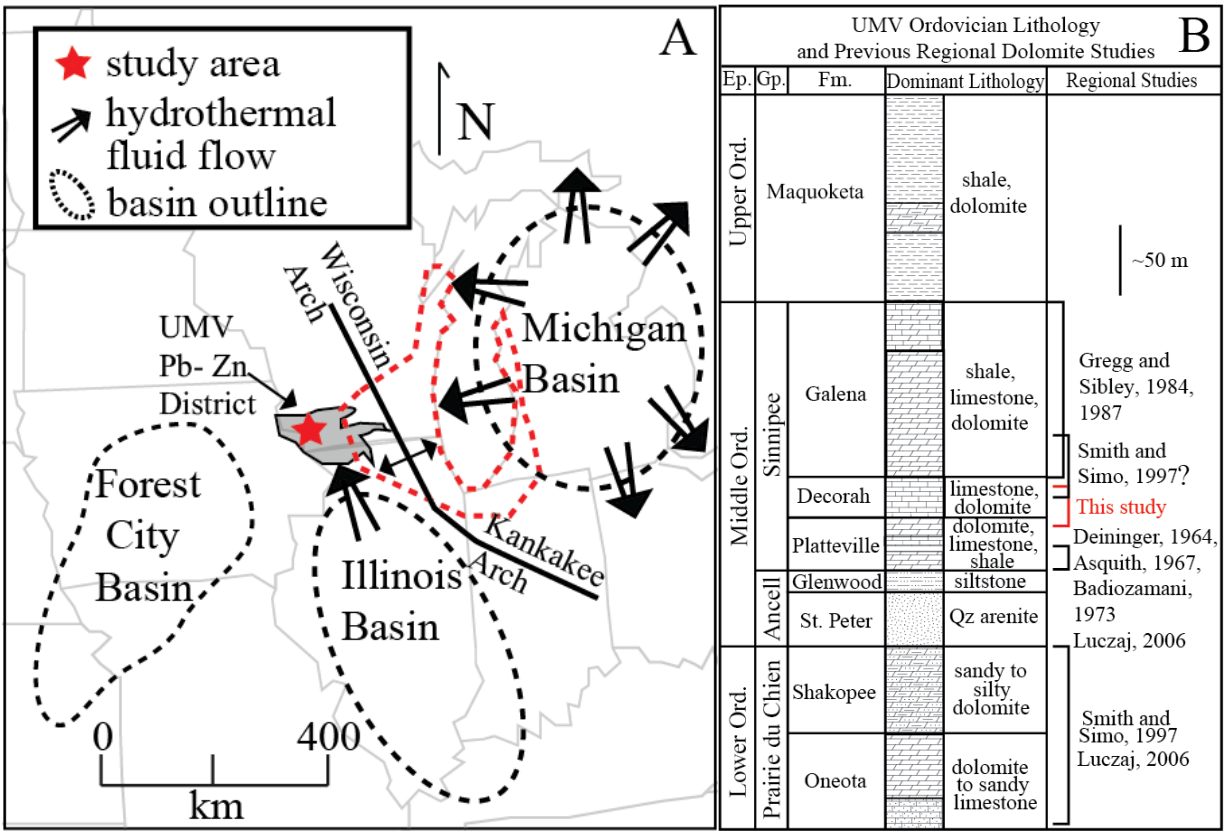

Figure 1, A (left) – This figure provides insight into the regional structural features surrounding the study area. The red dotted outline is the extent of dolomite surrounding the Wisconsin Arch from the Luczaj study (2006). Large arrows indicate suggested flow directions of basinal hydrothermal fluids. Hydrothermal fluids affecting the Pb-Zn district were likely derived from the Illinois Basin, and dolomitization along the Wisconsin Arch resulted from hydrothermal fluids expelled radially from the Michigan Basin (Luczaj, 2006). Figure 1, B (right) – Generalized stratigraphic column for Ordovician strata typical of southwest Wisconsin with previous studies of dolomitization marked by the formation which was studied (modified from Smith and Simo, 1997). Abbreviations are Ep. (Epoch), Gp. (Group), and Fm. (Formation).

by several kinetic factors including Mg/Ca ratios, CO_3^{2-} activity and temperature, ionic strength, and time required for dolomitization (Whitaker et al., 2004). Another problem is that dolomite has not been synthetically formed under low temperature conditions in the laboratory without bacterial mediation (Warren, 2000; McKenzie and Vasconcelos, 2009). These mechanisms inhibiting dolomite formation have been discussed since the early 20th century and are referred to

as the “Dolomite Problem” (Van Tuyl, 1914). Therefore, models that could be used to understand the kinetic and thermodynamic inhibitors related to dolomite formation and overcome them must be invoked.

Several studies have focused on the formation and occurrence of dolomite in the Lower and Middle Ordovician strata of southern Wisconsin (Figure 1, B) (Deininger, 1964; Asquith, 1967; Badiozamani; 1973; Gregg and Sibley, 1984; Smith and Simo, 1997; Luczaj, 2006). The “Dorag” model proposed by Badiozamani (1973) involved mixing of meteoric water from runoff with seawater. He argued that this mixing provided a means of overcoming the kinetic barriers to dolomite formation and used the geometry of dolomitization surrounding the Wisconsin Arch (Figure 1, A) as field evidence. His second argument was that dolomitization of Wisconsin Arch strata occurred during regression resulting in subaerial exposure and creating a freshwater-saltwater mixing zone. His evidence was the geometric pattern of dolomitization surrounding the Arch, and he related the movement of the dolomite-limestone transition boundary to phases of transgression and regression. The Wisconsin Arch became the type locality for this model, and it became the most well-known model for dolomitization in the region. This model quickly became a popular and widely referenced key dolomite model in the 1980s and 1990s (Hardie, 1987; Luczaj, 2006).

More recently, the validity of this model has been called into question. Hardie (1987) revealed several weaknesses of this model. It was noted that mixing zone waters with respect to temperature, pCO_2, pH, and initial meteoric water composition do not likely behave in the ideal manner used in Badiozamani’s thermodynamic arguments (Hardie, 1987). Thermodynamic calculations were reevaluated resulting in smaller range of seawater and meteoric mixtures that

could promote dolomite formation (Hardie, 1987). Furthermore, in the case of many studies attributed to mixing-zone dolomitization, dolomite was precipitated without dissolution of the precursor calcite, which negates a fundamental principle of the mixing zone model. Recent research by Luczaj (2006) provided more evidence against the "Dorag" model when his field observations of the occurrence of dolomite surrounding the Wisconsin Arch did not match the geometry used by Badiozamani as evidence in support of his model. Luczaj instead revealed evidence that dolomitization extended further east towards the margin of the Michigan Basin than previously studied (Figure 1, A). He proposed that this dolomite formed as the result of hydrothermal fluid flow out of the Michigan Basin (Figure 1, A) and supported this claim with field evidence, petrographic and cathodoluminescence (CL) analysis, fluid inclusion data, and stable isotope ($\delta^{13}C$ and $\delta^{18}O$) data.

The majority of previous studies of diagenesis and dolomitization in southern Wisconsin (Figure 1, B) have relied on these same analysis techniques (Agnew, 1956; Deininger, 1964; Asquith, 1967; Badiozamani, 1973; Gregg and Sibley, 1987; Smith and Simo, 1997; Luczaj, 2006). These studies have attributed dolomitization to a number of different, sometimes conflicting, models. Despite the previous research, some questions remain. Is the "Dorag" model potentially incorrect in its type area? Have dolomites been formed in multiple diagenetic environments, as some studies suggest? If so, what dolomitization model or models provide the best explanation for dolomitization in the region? Finally, what additional data can scientists use in order to provide better and more accurate depositional models?

Recent studies of carbonate diagenesis, particularly dolomite, have incorporated new analysis techniques such as inductively coupled mass spectrometry (ICP-MS) major, trace, and

rare earth element (REE) geochemical analyses to provide insight into the nature of diagenetic conditions (Qing and Mountjoy, 1994; Bau et al., 1997; Hecht et al., 1999; Frimmel, 2009; Azmy et al., 2013; Azomani et al., 2013; Zhao and Jones, 2013; Wang et al., 2014; Zhang et al., 2014). Even more recently *in situ* analysis via laser ablation inductively coupled mass spectrometry (LA-ICP-MS) measuring REE has proven to be effective in dolomite studies. This analysis technique provides indicators as to the geochemistry of the diagenetic fluid (Carmichael et al., 2008; Wang et al., 2009; Corlett and Jones, 2012, Xuefeng, 2008; Zhang et al., 2014).

This study focused on applying LA-ICP-MS REE analysis in combination with petrographic and cathodoluminescence analysis to provide new insights into the arguments concerning the nature of diagenetic fluids, which formed this dolomite. By understanding the nature of the diagenetic fluids, we aim to settle arguments concerning the appropriate dolomitization model or models for dolomites of the Upper Mississippi Valley region of southern Wisconsin. Furthermore, this study is important in providing further information contributing to understanding the origin and flow of hydrothermal diagenetic fluids because UMV-type Pb-Zn deposits, which were precipitated from these fluids, are of economic importance in regional mining operations.

2. BACKGROUND

2.1 PALEOGEOGRAPHY AND REGIONAL STRUCTURAL FEATURES

During the Late Ordovician (460-443 Ma) the majority of Laurentia was situated at a low paleolatitude in the southern hemisphere (Scotese and McKerrow, 1990; Scotese, 2004; Cocks and Torsvik, 2011) (Figure 2, A). Much of central and eastern North America was inundated by a shallow epeiric sea (Figure 2, B) (Scotese and McKerrow, 1991). This sea was bounded to the south by the Taconic Highlands (Figure 2, B), separating this shallow sea from the Iapetus Ocean (Kolata et al., 2001; Scotese, 2004). The Taconic Highlands formed due to the subduction-driven Taconic orogeny that produced a volcanic arc complex off the southeastern margin of Laurentia (Kolata et al., 2001; Young et al., 2005). The sea was bounded to the north and the northeast by the Transcontinental Arch and Canadian Shield, but was open to the Iapetus Ocean along its southwestern border (Scotese and McKerrow, 1990; Fanton and Holmden, 2007). The Transcontinental Arch provided an important source of terrigenous sediments for Specht's Ferry shale deposition (Figures 3 and 4) in the studied outcrop and Decorah shale deposition regionally, as well as a source of freshwater runoff into the midcontinent sea (Ludvigson et al., 1996; Choi and Simo, 1998; Simo et al., 2003). The Wisconsin Dome extended southward into central and southern Wisconsin from the Transcontinental Arch (Figure 2, B) (Simo et al., 2003). The Wisconsin Dome was periodically subjected to exposure coincident with changing sea level (Fanton and Holmden, 2007).

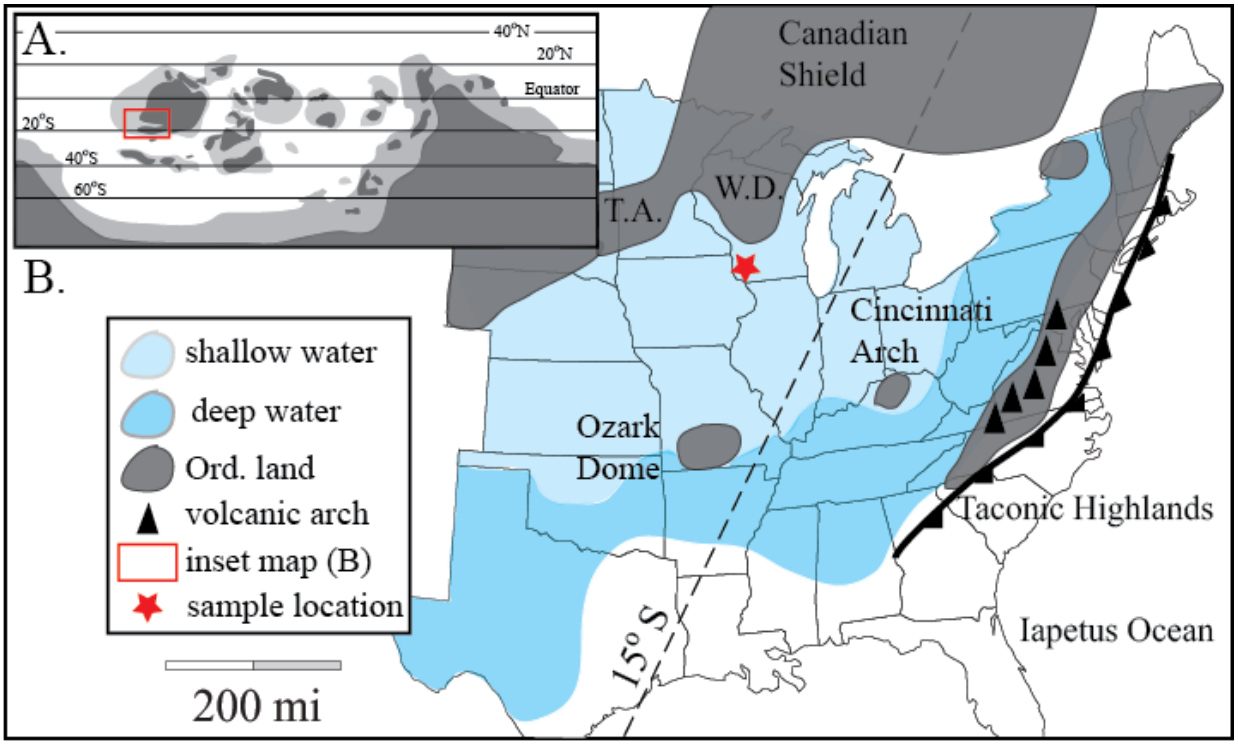

Figure 2, A. Global paleogeographic reconstruction for the Middle Ordovician period (460 Ma) was modified from Pohl et al. (2015) after reconstructions by Torsvick and Cocks (2009). Exposed land is shown in dark gray, shallow seas in light grey, and deep oceans in white. 2, B. Inset map of the eastern portion of Laurentia. Relative depth zones of the epeiric sea are differentiated by shades of blue, and (modified from Fanton and Holmden, 2007). Paleogeographic reconstruction modified after Fanton and Holmden (2007) and Cocks and Torsvik (2015). Abbreviations of features include the Transcontinental Arch (T.A.) and the Wisconsin Dome (W.D.).

2.2 REGIONAL STRATIGRAPHY

Upper Ordovician strata in southern Wisconsin and the surrounding area were deposited in subtidal environments ranging from inner ramp to outer ramp depositional settings (Choi and Simo, 1998; Choi, 1999; Witzke and Ludvigson, 2005). As illustrated in Figure 1, A, Figure 3, and Figure 4, stratigraphic units in this study include sections of the upper Platteville Formation and the Decorah Formation. The upper portion of the Platteville Formation is the Quimby's Mill Member (Figure 3 and Figure 4), a very dense brown micritic mudstone that exhibits conchoidal

fracturing, giving it the name “glass rock” (Agnew, 1946, 1956). These latest Platteville Formation rocks were interpreted to have been deposited at the end of an upward shallowing sequence terminated by a sequence boundary at the top (Choi and Simo, 1998). This was similarly interpreted as a drowning surface by Ludvigson et al. (2004).

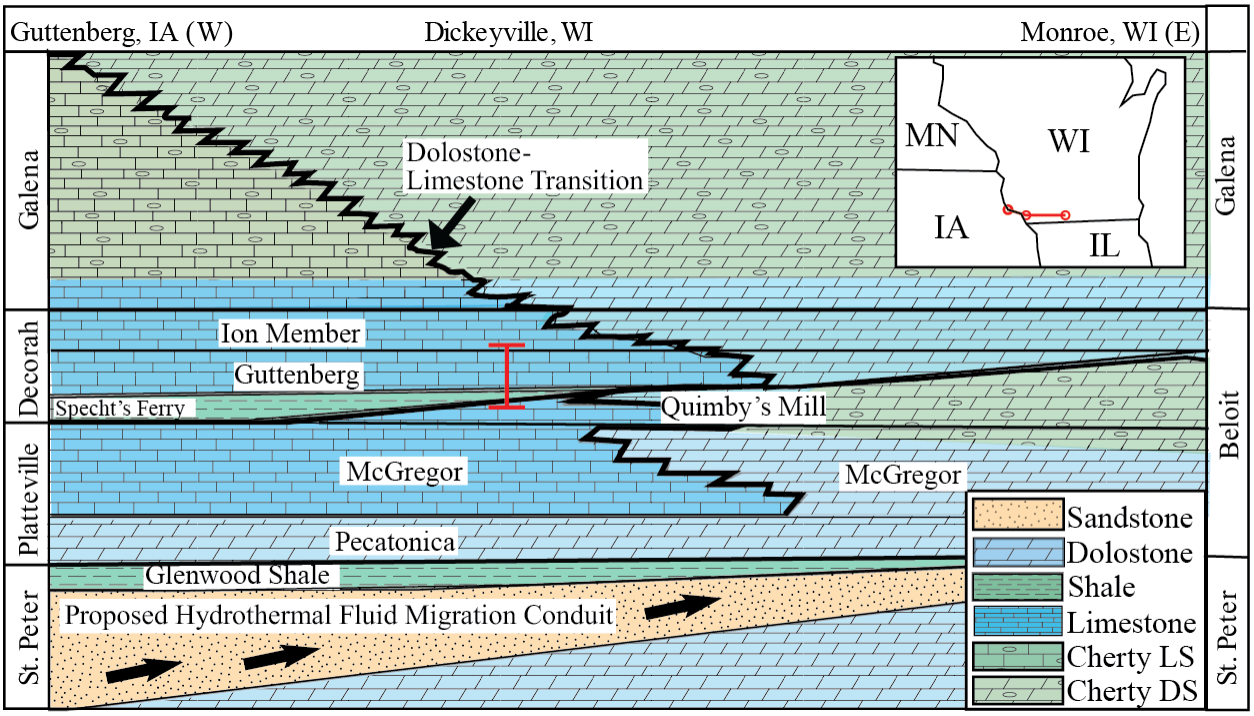

Figure 3-West-East diagrammatic cross-section of Middle and Upper Ordovician formations of southwest Wisconsin that reveals the pattern of shifting dolostone-limestone transition points from east to west (modified from Agnew et al., 1956) that Badiozamani used for his argument of Dorag dolomitization. Smith and Simo (1997) proposed that the underlying St. Peter sandstone was a potential conduit for migration of hydrothermal diagenetic fluids associated with UMV-type mineralization from the south in the Illinois Basin (Figure 2A). Agnew’s Ion Member lithology and that of this outcrop study (Figure 4) are different. Red bracket indicates the approximate location of the Dickeyville outcrop along this transect as well as the vertical extent of the sampled section.

Platteville Formation strata are overlain by the Carimona, Specht’s Ferry, Guttenberg, and Ion Members of the Decorah Formation. The Decorah Formation is the earliest deposition of the Galena Group (McLaughlin et al., 2011). At the Dickeyville outcrop, the Carimona Member

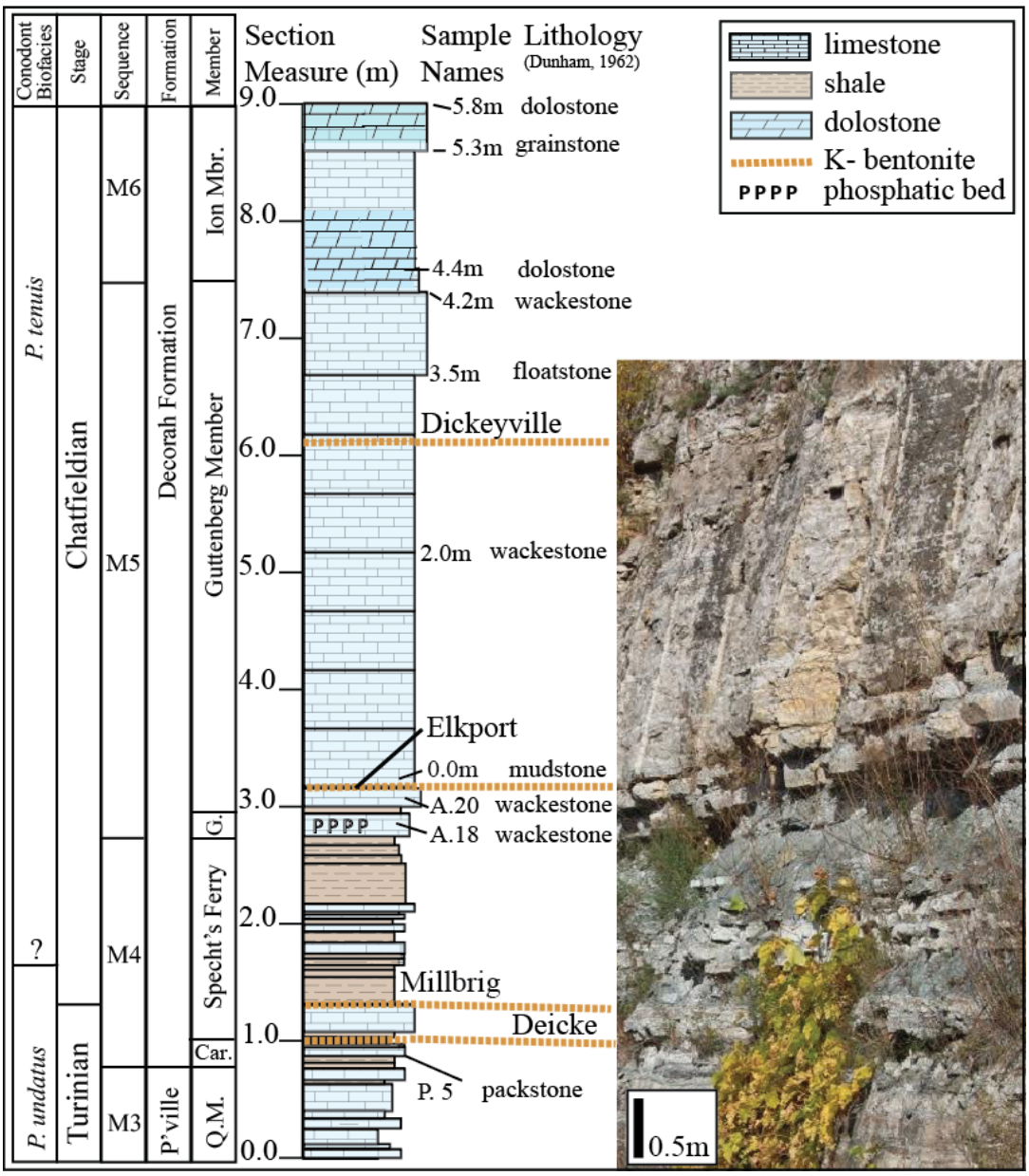

Figure 4-Stratigraphic column of the Highway 151 roadcut at Dickeyville, Wisconsin. Tentative Midcontinent conodont biozones from Sell et al. (2015) from nearby Hwy. 61 Dickeyville outcrop. Zones were correlated using trace element correlation of apatite from K-bentonites. "?" indicates tentative biostratigraphic boundary. "M" sequence stratigraphic nomenclature from Holland and Patzkowsky (1997) originally developed on the Nashville Dome and correlated to the UMV region by McLaughlin et al. (2011) using lithologic changes from shale to carbonate deposition and faunal changes in brachiopods. Regional stratigraphic nomenclature from Agnew et al. (1956) applied to this outcrop by McLaughlin et al (2011). Abbreviated formations and members include the Platteville (P'ville), Quimby's Mill (Q.M.), and the Carimona (Car.), and the Garnavillo (G.).

is 0.3M and consists of thicker limestone beds with shale partings. The Specht's Ferry is a 1.8 m green to grey-green shale-dominated unit with thin limestone interbeds. The Deicke K-bentonite is overlain by the Specht's Ferry. The Specht's Ferry is a shale-dominated unit with thin, discontinuous fossiliferous limestone interbeds. The Millbrig K-bentonite is located in the lower portion of the Specht's Ferry. Overlying the shale-dominated Specht's Ferry is the thin, phosphatic grain rich Garnavillo limestone bed, the lowermost member of the Decorah Formation. This phosphate-grain rich bed likely marks sea level rise and condensation of sediments (Ludvigson et al., 2004; Witzke and Ludvigson, 2005). The Elkport K-bentonite lies between the Garnavillo limestone and the overlying Guttenberg Member of the Decorah Formation. The Guttenberg Member is a predominantly limestone unit that is ~4.8 m thick with occasional minor shale partings. This limestone unit was deposited in a shallowing upward sequence from below storm wave base to above fair weather wave base (Choi et al., 1999). The Dickeyville K-bentonite is in the upper portion of the Guttenberg Member. The Guttenberg-Ion Member contact is interpreted as another transgressive drowning surface (Ludvigson et al., 2004). The highest 2.5 m of samples is from the Ion Member, which is a mixed limestone-dolomite rock unit at the Dickeyville outcrop.

2.3 PREVIOUS REGIONAL DOLOMITE STUDIES

Ordovician dolomites and dolomitization processes in and around the UMV mining district of southwest Wisconsin have been studied for over a century (Van Tuyl, 1914) (Figure 2, A). In this time researchers have drawn different conclusions as to the cause of dolomite formation (Agnew et al., 1956; Deininger, 1964; Asquith, 1967; Badiozamani, 1973; Gregg and

Sibley, 1984; Smith and Simo, 1997; Luczaj, 2006). This section will serve to step through the evolution of hypotheses regarding dolomitization in southern Wisconsin.

In his overview of knowledge of dolomite formation, Van Tuyl (1914) used geochemical, field, and petrographic evidence from the Upper Mississippi Valley region as one of his study locations. In his discussion of dolomite models, Van Tuyl hypothesized that abrupt dolomite-limestone contacts must have formed by seawater or very early alteration at or near the sediment-water interface. His argument was that burial fluids would interact with rocks equally and not result in abrupt transitions exhibited by dolomites in the region. He stated that the cloudy, clastic inclusion-rich nature of some dolomites also could only be the result of primary deposition. He also argued for burial dolomitization due to evidence of dolomite replacement in fossils and creation of secondary porosity due to limestone to dolomite molar reduction in heavily dolomitized units.

Deininger (1964) studied the lower portion of the Platteville Formation. His interpretations pointed to three different diagenetic fluids mediating dolomitization in a burial model following lithification. His first argument was for seawater, which he quickly dismissed due to the volume of dolomite and the problem of Mg-sourcing from seawater for dolomitization of the observed scale. Ground water was another fluid considered. Deininger pointed out two weaknesses to this fluid as well. Porosity associated with fluid flow might have formed after dolomitization, and that the relationship between the water table and dolomitization was tenuous because the water table has changed through time. Deininger's last hypothesis was hydrothermal fluid flow, given that dolomitization was associated with sulfide mineralization, which was his preferred dolomitization model.

Three years later Asquith (1967) attributed dolomite formation in the same formation to precipitation from seawater or evaporative brines, although his study recognized and intentionally ignored the hydrothermal dolomitization and what he considered to be groundwater dolomitization. His interpretation of dolomitization was two stages: shallow burial and during or around the time of lithification.

As previously discussed, Badiozamani (1973) conducted one of the largest regional studies that focused mainly on Platteville Formation dolomitization in southern Wisconsin. His research resulted a newly introduced model, the Dorag mixing zone model. Badiozamani's field evidence that the geometry of dolomitization was associated with the positive feature known as the Wisconsin Arch. Badiozamani claimed that eustatic changes in sea level and subsequent exposure of the Wisconsin Arch (Figure 1, A) provided a means for meteoric water to penetrate strata and mix with seawater. He argued by thermodynamic calculations that this mixing provided a means of increased saturation of dolomite with respect to calcite in pore fluids, resulting in dolomitization. This study also sought to link the shifts in the dolomite-limestone boundary along the Wisconsin Arch with marine-meteoric water mixing zone dolomitization and explaining the abrupt transition from limestone to dolomite. Badiozamani also argued that no evidence or mechanism existed by which dolomitization at elevated temperatures (>50^{o}C) could have occurred, ruling out hydrothermal diagenesis. Although this study was widely accepted and applied in the 1980s and 1990s, more recent research revealed issues with his model (Hardie, 1987; Luczaj, 2006).

The first weakness of Badiozamani's Dorag model of dolomitization was addressed in a reevaluation of the thermodynamic calculations by which seawater-meteoric water mixing could

facilitate dolomitization and greatly reducing the effective range of seawater-meteoric mixing within which the model can be applied (Hardie, 1987). Luczaj (2006) found that dolomitization was not tied to the geometry of the Wisconsin Arch, instead dolomite extended off the flank of the structure toward the western side of the Michigan Basin (Figure 1, A). Luczaj argued that the regional geometry of dolomitization and geochemical evidence pointed to a hydrothermal fluid flow system from the Michigan Basin that replaced any precursor carbonate materials. Luczaj also argued that hydrothermal fluids traveled along bedding planes and fractures, potentially explaining abrupt limestone-dolomite contacts explained as mixing zone evidence by Badiozamani (1973).

Gregg and Sibley (1984) and Sibley and Gregg (1987) focused their research on Galena Group dolomites. Their samples were collected from strata that was influenced by Pb-Zn precipitating hydrothermal fluids. They argued that dolomite in these intervals had been neomorphosed from precursor limestone and dolomite by hydrothermal fluids. They also claimed that dolomite texture is related to temperature, and that above 50^{o}C (but potentially up to 100 ^{o}C), the texture of the resulting dolomite changes from idiotopic (rhombic euhedral-subhedral) to xenotopic (nonrhombic). Critically, however their point counts revealed that this both idiotopic and xenotopic dolomites of hydrothermal nature occurred in the Galena Group. The occurrence of idiotopic dolomite in these strata was ascribed to stabilization of crystal faces by impurities (organic material or clays) or pore spaces.

Dolomitization in the Prairie du Chien Group (Smith and Simo, 1997) was attributed to multiple diagenetic realms. Later stages of diagenesis, such as hydrothermal fluids, seemed to have erased evidence of earlier stages of dolomite by replacement or neomorphism. They

cautioned that this can result in incorrect and oversimplified assumptions about diagenetic fluid histories and the origin of dolomites. Syndepositional dolomite was preserved in lime-mud dominated facies. This dolomite is finely crystalline (<0.1mm) and exhibited red-orange luminescence. This dolomite was interpreted as having been precipitated with the aid of sulfate reducing bacteria. Shallow burial, fabric-destructive replacement dolomite was attributed to subaerial exposure. This dolomite was idiotopic subhedral or euhedral in nature. These dolomites (0.1-0.5 mm) nucleated on the smaller precursor syndepositional dolomite and exhibit microzoning of red-orange and orange CL. The last dolomitization stage was hydrothermal in nature. These crystals were described as mainly idiotopic and less commonly xenotopic in texture. They argued that the replacement of much of the precursor dolomite was due to the thermodynamic instability of Ca-rich, disordered low temperature dolomites. These dolomites exhibited a sequence of colors: dull orange, microzoned red and black, red, dark red, and black. Although there focus and discussion was devoted to the Prairie du Chien Group dolomites, Smith and Simo also analyzed samples from the Platteville, Galena, and Decorah Formations. Their results indicated that Platteville Formation dolomites were generally formed from seawater-like fluids, while Decorah and Galena Formation dolomites were formed from hydrothermal fluids. Smith and Simo also proposed that the St. Peter sandstone was a major hydrothermal fluid conduit from the Illinois Basin (Figure 3).

2.4 APPLICATION OF REE AND TRACE ELEMENT ANALYSIS TO DOLOMITES

2.4.1 Application of REE to Dolomites

REE concentration measurements are a valuable tool in geochemical analysis. This series of fifteen elements, the lanthanides, are mainly trivalent, the common exceptions being Ce^{4+} and

Eu^{2+} that occur in certain diagenetic environments, with their chemistry largely controlled by ionic radius (Azomani et al., 2013). This results in a systematic change across the series, the mechanism responsible for preferential fractionation among light rare earth (LREE; La to Nd), middle rare earth elements (MREE; Sm to Dy), and heavy rare earth elements (HREE; Ho to Lu) (Azomani et al., 2013). These elements have very low abundances (ppb) in seawater and living marine organisms with carbonate shells or components, however these REE abundances are much higher in seafloor and buried carbonate sediments (Banner et al., 1988). This REE enrichment occurs by interaction with pore-waters near the sediment-water interface (Banner et al., 1988; Shields and Webb, 2004; Bau and Alexander, 2006; Zhao and Jones, 2012). Interaction with later diagenetic fluids can potentially erase or overprint the geochemical signatures of the original carbonate material (Wang et al., 2014; Zhang et al., 2014). Incorporation of REE can occur by several different means; substitution for Ca^{2+} and Mg^{2+} in the carbonate lattice, filling lattice positions formed by defects, or incorporation by adsorption due to remnant ionic charges (Qing and Mountjoy, 1994). Carbonate REE data can also be overprinted by the incorporation into carbonates of non-carbonate phases like Fe or Mn oxides, clay minerals, quartz, or sulfides. Due to the high concentration of REE in these phases relative to carbonates, even small amounts of contamination by these phases will overprint the REE pattern of diagenetic fluids in carbonates (Qing and Mountjoy, 1994; Nothdurft et al., 2004; Frimmel, 2009; Zhang et al., 2014).

LA-ICP-MS analysis of REE has successfully been used in recent studies of ancient and modern carbonates including limestones and dolomites (Carmichael et al., 2008; Wang et al., 2009, 2014; Corlett and Jones, 2012; Gromek et al., 2012; Li et al., 2014; Zhang et al., 2014).

Comparison of REE signatures to potential proxies for sources of REE such as Upper Continental Crust (UCC) (Taylor and McLennan, 1985, 1995) provide a basis for delineating different trends in REE patterns and making inferences regarding the diagenetic history and alteration of carbonate materials. For instance, Post Archean Australian Shale (PAAS) or UUC-normalized REE patterns of seawater and carbonates retaining seawater or seawater-like geochemical signatures exhibit LREE depletion relative to HREE and a distinctly noticeable negative Ce anomaly due to the oxic nature of normal seawater (Sholkovitz and Shen, 1995; Azomani et al., 2013). This occurs due to the systematic chemical changes across the series. Variation from this seawater-like REE trend is an indication influence by fluids with distinctly non-seawater like geochemical properties (Banner et al., 1988).

As noted earlier, two elements in the lathanide series, Ce and Eu, commonly occur in multiple oxidation states. In the case of Ce (Ce^{4+}/Ce^{3+}) oxidation state is controlled by oxidation condition (anoxic vs. oxic fluids) (Bau and Alexander, 2006; Bolhar and Van Kranendonk, 2007; Zhao and Jones, 2013; Zhang et al., 2014). Eu oxidation state (Eu^{3+}/Eu^{2+}) is controlled primarily by temperature, and to lesser extent by pressure and pH, making it an invaluable tool in the identification of high temperature burial brines or hydrothermal diagenetic fluids (Frimmel, 2009; Zhang et al., 2014). These sensitive oxidation states, controlled by varying conditions of diagenetic fluids, makes them valuable analytical tools.

2.4.2 Application of Trace Elements to Dolomites

REE results and interpretations can be supplemented by analysis of trends in various other elements to aid in interpretation of diagenetic environment and fluid characteristics. The

elements Al and Th are important indicators of incorporation of clay minerals contaminants, which would greatly affect the REE patterns of dolomites (Zhang et al., 2014). Ba, Fe, and Sr in comparison to Mn can help in estimating diagenetic fluid characteristics like hydrothermal influence, redox state, and recrystallization respectively (Frimmel, 2009; Azomani et al., 2013; Zhang et al., 2014).

3. METHODS

3.1 SAMPLE COLLECTION

Samples were taken from the Highway 151 roadcut in Dickeyville, WI, along Highway 151, described as the bypass roadcut of the 2007 WGWA Fall Field Trip Guide (WGWA, 2007) as well as Stop 5 from McLaughlin et al. (2011). A stratigraphic column based on field notes and measurements was drafted for the outcrop (Figure 4). Sample names and measurements relative to the Deicke K-bentonite are compiled in Appendix 1.

3.2 PETROGRAPHIC PREPARATION AND ANALYSIS

Sample chips were cut to size and sent to National Petrographic Service, Inc. for mounting. A total of 35 thin sections were made from 32 carbonate intervals. Specific attention was paid to dolomite, the basis of geochemical work. Petrographic analysis was completed with a Leica DM750P petrographic microscope. The thin sections were classified using the Dunham carbonate rock classification scheme (Dunham, 1962) (Appendix 1). Analysis was conducted using Flügel (2004) as a guide in identifying and interpreting sedimentary structures, fabrics, cements, skeletal assemblages, and diagenetic components (i.e. stylolites, dolomite, post-depositional cements) (Appendix 1). These dolomites were classified based on petrographic characteristics after Sibley and Gregg (1987). Cathodoluminescence (CL) analysis was conducted with a Relion III cathodoluminescence stage and Leica M125 stereomicroscope with the conditions of a -4.7-5.7 kV beam voltage, pressure of 32-40 mTorr, and a current of 0.509-0.78 mA (Appendix 1). Descriptions and interpretations were completed using cathodoluminescence petrography reviews outlined by Hiatt and Pufahl (2014).

3.3 LASER ABLATION ANALYSIS

A Thermo iCap Qc ICP-MS was connected to a Cetac G2-213 Nd:YAG laser system for analysis. Helium was used as the carrier gas in the ablation cell because helium enhances the transport efficiency of ablated material (Zhang et al., 2014). The carrier gas was then mixed with argon makeup gas prior to entering the torch. Laser settings were optimized in order to attain an optimum balance between signal intensity and duration prior to burning through the thin section samples. ICP-MS and laser settings were compiled below in Table 1, A and 1, B respectively. Elements analyzed included ^{24}Mg, ^{27}Al, ^{43}Ca, ^{48}Ti, ^{43}Ca, ^{55}Mn, ^{57}Fe, ^{88}Sr, ^{89}Y, ^{90}Zr, ^{137}Ba, ^{232}Th, and the lanthanide series (REE) ^{57}La-^{71}La.

Table 1- ICP-MS and Laser Ablation System Settings

A. Thermo iCap Qc ICP-MS	
Parameter	Setting
RF power/ W	1550
Cool gas flow rate (1 min $^{-1}$)	14
Carrier gas (Ar) flow rate (1 min $^{-1}$)	0.74
Carrier gas (He) flow rate (1 min $^{-1}$)	0.67

B. Cetac G2-213 laser system	
Parameter	Setting
Laser Type	Nd:YAG
Wavelength (nm)	213
Laser Fluence (%)	3
Pulse Repetition Rate (Hz)	4
Shutter Delay (s)	10
Ablation time (s)	40
Washout times (s)	30
Spot Size (µm)	100

The National Institute of Standards and Technology (NIST) has produced synthetic glass standards which have been used previously for instrument calibration when analyzing calcium carbonates (Jochum et al., 2012; Li et al., 2014; Zhang et al., 2014). NIST SRM 612 was used as the external standard as this reference material has been certified. IAEA B7 marine limestone and NIST SRM 1d argillaceous limestone standards were used as secondary standards ("known

unknowns") to monitor analytical quality. IAEA B7 is a Miocene marine limestone from Maiella Massif in the Abruzzo region of Italy. This standard material is a nearly pure calcite with rare glauconite (Tonarini et al., 2003). EPMA results from this study show 94.3-99.9% $CaCO_3$ with the other constituent mainly being $MgCO_3$. SRM 1d limestone standard was collected from a quarry in Putnam County, Indiana and is composed of argillaceous limestone ("Certificate of Analysis", 2005). Despite this impure and variable nature of these samples with respect to Ca content, an ideal stoichiometric composition of calcite, 40.04 % Ca, was used for these samples. IAEA B7 and SRM 1d were also cross-referenced as external standards during data reduction to insure the greatest accuracy and precision available, with the result that NIST 612 offered the same or better accuracy than either SRM 1d or IAEA B7 as the external standards. IAEA B7 experimental results were compared to IAEA B7 reference values compiled in Tonarini et al. (2003). NIST SRM 1d experimental results were compared to those compiled in Barca (2011). Tonarini et al. (2003) and Barca (2011) trace element data were collected using LA-ICP-MS analysis. These data can be found in supporting material (Appendix 2).

Data reduction was conducted using the Iolite v2.5 (Hellstrom et al., 2008) application extension for IGOR PRO 6.3.7.2 software (Wavemetrics, 2014). The Trace Element data reduction scheme utilized, and DRS setting are compiled in Table 2 (Paton et al., 2011).

A total of 330 dolomites were ablated from 10 samples based on availability of potential targets in each sample. The maximum number of dolomites ablated in a thin section was 40. Ba/Ca and Zr/Ca ratios were used in signal selection to avoid any signal compromised by burn through into the underlying glass slide. This also aided in eliminating dolomite samples most altered due to terrigenous contaminants (clays). This is because Zr is an element commonly

Table 2- Igor Pro 6.3.7.2 software Data Reduction Settings

Sample	Purpose	DRS Scheme	Internal Standard	Index Content %	Signal Selection Method
NIST 612	external standard	trace element	^{43}Ca	8.5	Manual (peak, consistent Ca)
SRM 1d	known unknown	trace element	^{43}Ca	40.04	Automatic (Ca count)
IAEA B7	known unknown	trace element	^{43}Ca	40.04	Automatic (Ca count)
dolomite	experiment	trace element	^{43}Ca	21.73	Low Ba/Ca ratio Low Zr/Ca ratio

found in terrigenous material (Frimmel, 2009; Zhang et al., 2014). Dolomite crystals that experienced premature burnthrough, cracked immediately when ablated, or were likely compromised due to laser targeting were eliminated based on observations during the ablation process. Data for 219 dolomites were compiled for this study and element concentration averages were calculated for each sample.

To further evaluate the presence of siliciclastic material within the remaining samples, dolomite REE concentrations were normalized to UCC (Upper Continental Crust), a proxy for terrigenous material from the Canadian Shield. Al and Th concentrations of UCC are ~8% for Al and 10.5-10.7 ppm for Th (Rudnick and Gao, 2003). Clay content of greater than 2% has been shown to be sufficient enough to alter REE patterns (Webb and Kamber, 2000; Nothdurft et al., 2004; Zhang et al., 2008; Frimmel, 2009). For this study, a 2% cutoff compared to UCC values was used as similarly executed by Frimmel (2009). Contamination cutoff limits for dolomite signatures were 1600 ppm for Al and 0.2 ppm for Th.

REE values were normalized to Upper Continental Crust values (UCC) from Taylor and McLennan (1985, 1995) compiled in Rudnick and Gao (2003). This serves to provide a means of

comparing dolomite geochemical signatures to potential sources of terrigenous material from nearby cratonic sources. Modern seawater and the carbonate standard materials were plotted against samples for comparison. Modern seawater values were magnified by $x10^6$ after Alibo and Nozaki (1999) and Zhang et al. (2014) due to the low ∑REE concentrations of seawater. Eu, Ce, and Pr anomalies were calculated using the following formulas: $Eu/Eu^* = Eu_N /(0.67Eu_N + 0.33Tb_N)$, $Ce/Ce^* = Ce_N/(0.5La_N + 0.5Pr_N)$, and $Pr/Pr^* = Pr_N/(0.5Ce_N + 0.5Nd_N)$ after Bau and Dulski (1996) and Zhang et al. (2014). Error bars for graphs represent standard error of the analyzed element or anomaly from each sample set.

4. RESULTS

4.1 PETROGRAPHY AND CATHODOLUMINESCENCE ANALYSIS RESULTS

4.1.1 Thin Section Description

Descriptions of thin sections of dolomite capable of geochemical analysis are listed in stratigraphic order from the lowest analyzed thin section in the outcrop to the highest. Matrix, allochems, represented taxa, and diagenetic features were characterized. The results presented focus on those characteristics that provide evidence regarding the nature and origin of the dolomite. Subdivision of these intervals was completed following geochemical analysis of the dolomites. Intervals were divided based predominantly on REE patterns but also on CL characteristics of the dolomite.

The lower interval samples include P. 5 from the Carimona, A. 18 and DV A. 20 from the Specht's Ferry, and DV 0.0M from the lowermost Guttenberg (Figure 4). These samples are all closely stratigraphically associated with the Deicke (DV P. 5 underlies) and Millbrig K-bentonites (A. 18 and A. 20 are below, DV 0.0M is directly above). Sample P. 5 is classified as a packstone, but there are burrowed portions of the slide that are purely micritic or micrite partially replaced by dolomite (Figure 5, A). The micritic mud matrix is gray-tan and sugary with portions of skeletal material and micrite replaced by clearer, blocky sparite. Dolomites are located primarily along the upper edges of the sample and in a micritic burrow in the upper portion of the slide. Many skeletal grains have been partially to completely replaced by small pyrite overgrowths. Pyrite concentrations increase toward the upper portion of the sample. Sample A. 18 is a wackestone with a slightly darker gray micritic matrix with portions of lighter, slightly

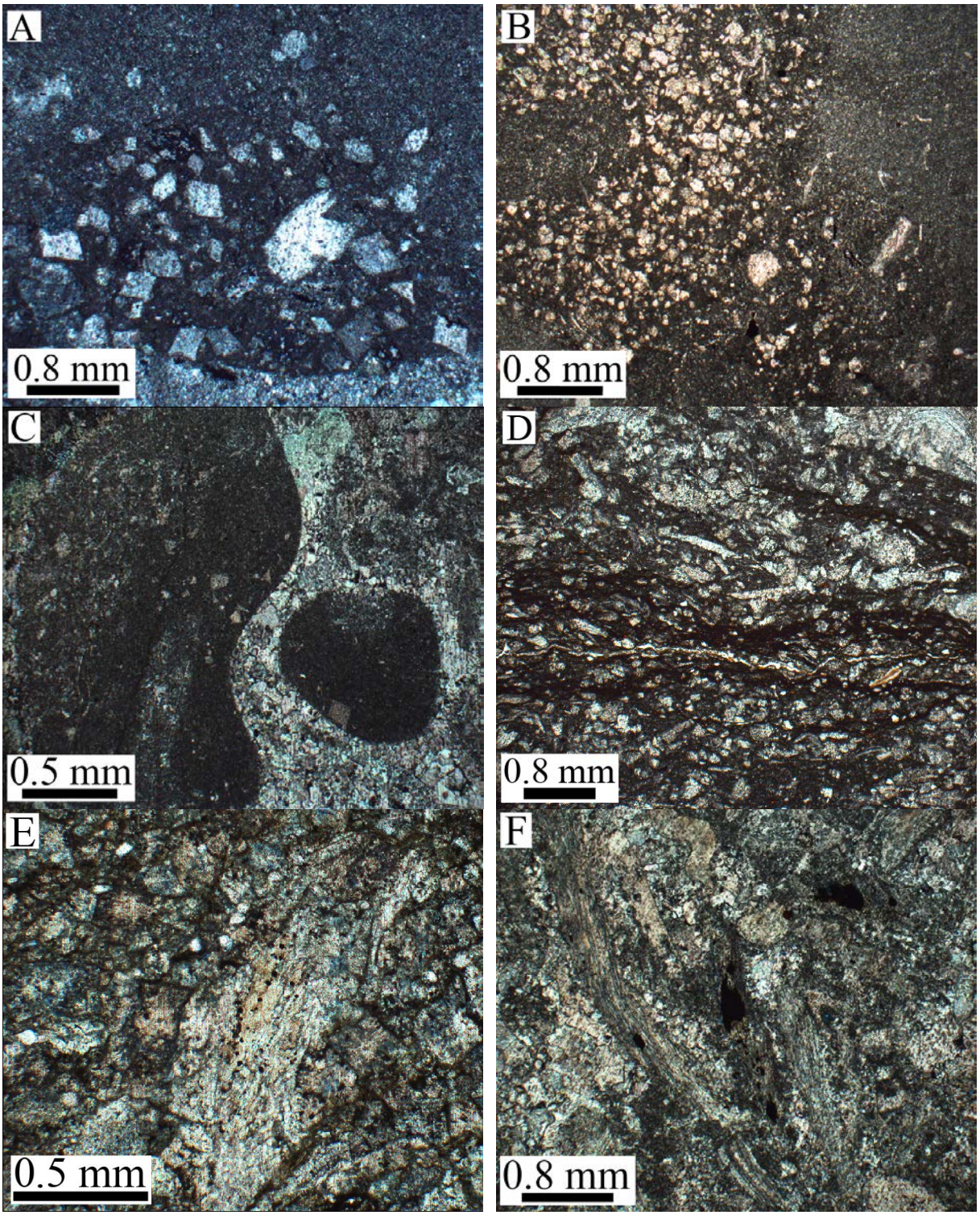

Figure 5- (A) Sample DV P. 5 XPL, (B) Sample DV A. 20 PPL, (C) Sample DV 3.5M XPL, (D) Sample DV 4.2M PPL, (E) Sample DV 5.8M PPL, (F) Sample DV 5.3M PPL.

coarser burrow infill. Burrows in this sample appear to be oriented both vertically and horizontally. Small pyrite grains have overgrown skeletal grains in varying degrees from minor to almost complete replacement by sparry calcite. Dolomites are spread fairly evenly throughout the sample in the micritic matrix and do not generally share grain boundaries. Some of the dolomite in each of these samples is partially dissolved. DV A. 20 and DV 0.0M are both light tan mudstones. The majority of the sparse (<10% of slide) skeletal grains in these samples have been neomorphosed and lost all original texture or replaced by pyrite. Pyrite replacement is common in DV A. 20. These samples both have small sparite-filled fractures. Dolomites are concentrated in burrows in each slide and surrounded by a much darker matrix (Figure 5, B). These portions were likely subjected to greater diagenetic influence than the surrounding matrix.

The middle stratigraphic interval includes three analyzed samples, DV 2.0M, DV 3.5M, and DV 4.2M, from the middle and upper portion of the Guttenberg Member. These samples have light grey, slightly tan, micritic matrices. DV 2.0M and 4.2M are wackestones, and DV 3.5M is a floatstone. DV 2.0M does not exhibit signs of heavy diagenesis, with partial pyrite replacement of a few skeletal grains and recrystallization into sparite of other skeletal grains. The strongest diagenetic feature is the dolomite concentrated toward the lower portion of the slide. DV 3.5M is extensively altered by sparite infill and grain and matrix replacement (Figure 5, C). Much of this sparite exhibits a clear, granular-blocky texture. The dolomite in this sample is generally limited to grains preserved inside unaltered micritic shell infill and replacement of fossils. DV 4.2M exhibits more diagenetic features toward the upper portion of the slide including hummocky anastomosing stylolites, neomorphosed skeletal grains, and some dolomite at the top, while just below this area in the upper middle portion of the slide dolomite is much more prevalent (Figure

5, D). These samples exhibit far less pyritization compared to the underlying and overlying intervals.

The final set of upper interval samples include 4.4M, DV 5.3M and DV 5.8M from the Ion Member. DV 4.4M and 5.8M are very similar in composition, these samples are almost entirely composed of dolomite. Many smaller skeletal grains in both samples have been replaced by pyrite, while sparite is preserved in the void spaces of some skeletal grains. Theses samples have voids and high porosity due to dissolution from diagenetic fluids or the volume reduction associated with the replacement or recrystallization associated with conversion from calcite to dolomite mineralogy (Figure 5, E). The darker material filling the intercrystalline pore space between dolomites is likely a combination of iron oxides, organic material, and sulfide minerals, similarly to observations by Agnew et al. (1956) and Gregg and Sibley (1984). This opaque, brown material is more prevalent in DV 4.4M than DV 5.8M.

DV 5.3M exhibits different characteristics than the samples (Samples DV 4.4M and DV 5.8M) it is found between. There is evidence of pressure solution in upper portion of this sample, as some skeletal grains that are in contact with one another have been partially dissolved (Figure 5, F). The sparite cement making up the majority of the slide ranges from granular to opaque or clear blocky sparite. Dolomite in this sample is concentrated in two portions of the slide; a circular feature that appears to have once been a burrow, and a thin upper portion of the slide slide surrounded by darker material of similar composition to that found in the DV 5.3M and DV 5.8M.

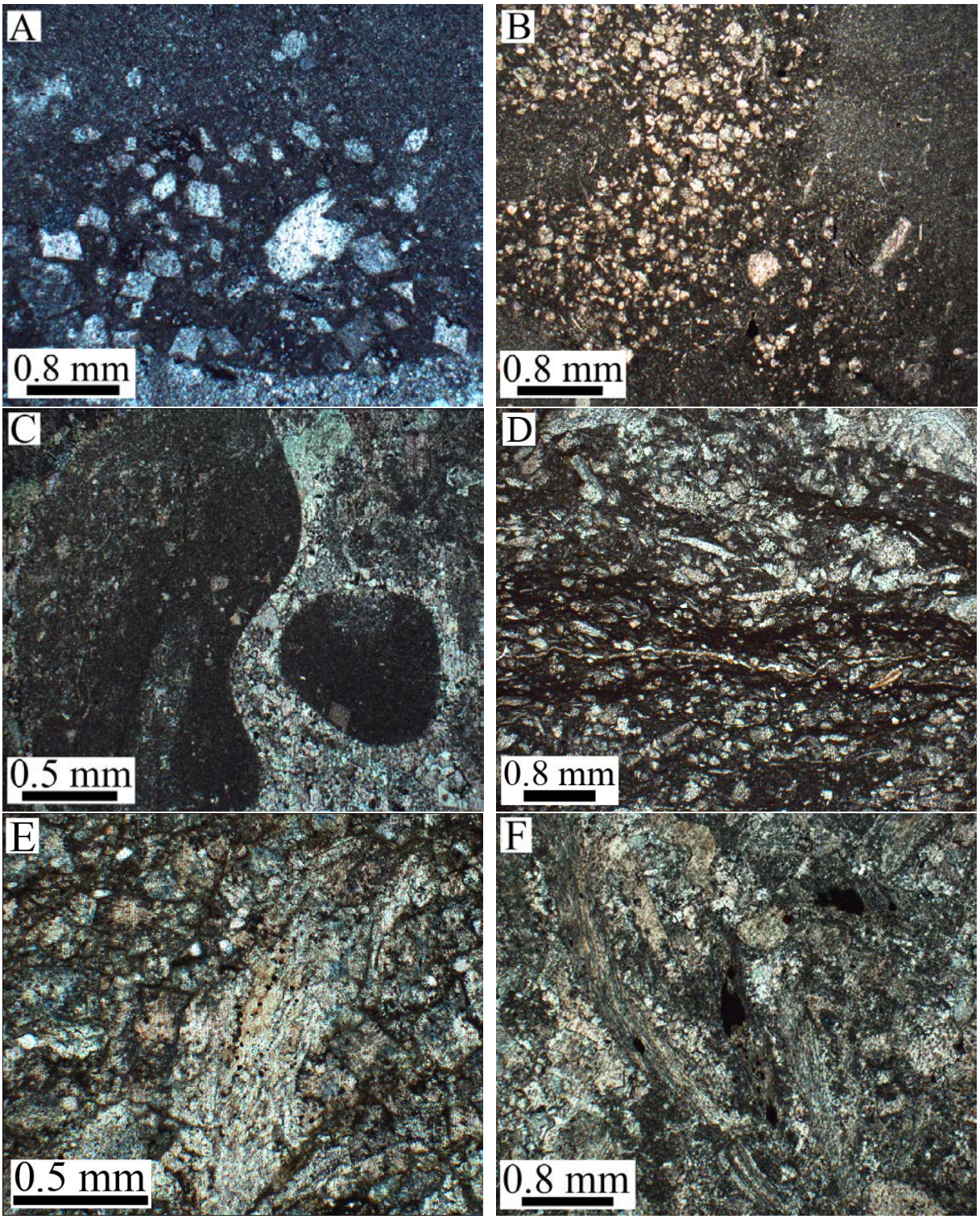

Figure 5- (A) Sample DV P. 5 XPL, (B) Sample DV A. 20 PPL, (C) Sample DV 3.5M XPL, (D) Sample DV 4.2M PPL, (E) Sample DV 5.8M PPL, and (F) Sample DV 5.3M PPL.

4.1.2 Dolomite Petrographic and CL Characterization

Dolomites were divided into four types (Types 1a, 1b, 2, and 3) based on transmitted light and cathodoluminescence analyses. A table with dolomite classification, descriptions, and schematics were compiled in Figure 6. Representative petrographic and CL images for each dolomite type are displayed in Figure 7 (petrographic) and Figure 8 (CL). All samples with dolomite present were recorded and described in Figure 9.

Class.	Dolomite Texture	Dolomite PPL Char.	Dolomite CL Char.	Schematic PPL	Schematic CL
Type 1	often planar-e seldom planar-s, 50-200 µm (1a) <50 µm (1b)	cloudy, inclusion-rich with precursor carbonate, occasionally partially dissolved	no to dull red luminescence, precursor material more brightly luminescent	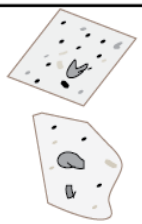	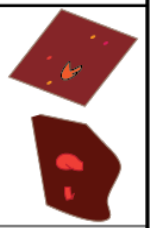
Type 2	very sparse planar-e, most commonly 50-125 µm	clear, few inclusions	no to dull red luminescence		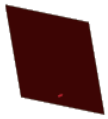
Type 3	packed planar-e to planar-s 75-200 µm	moderately cloudy, occasional inclusions	1. moderate-bright orange with dark inclusions, 2. dull red, 3. moderate orange-red luminescence	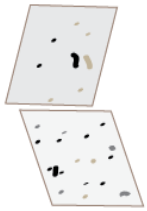	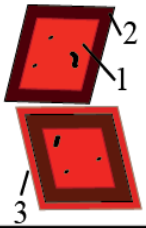

Figure 6- Dolomite classification chart with characteristics (Char.) of each dolomite classification (Class.). Schematic representations represent appearance under plain polar (PPL) and cathodoluminescence (CL) microscopy.

The majority of the dolomite crystals identified in this study are cloudy and inclusion-rich, light grey in color, generally exhibiting a Planar-e (euhedral) and less commonly a Planar-s (subhedral) texture found throughout the sampled length of the outcrop. These dolomites are classified as Type 1 (Figure 7, A and 7, B). In several samples these dolomites appear to have

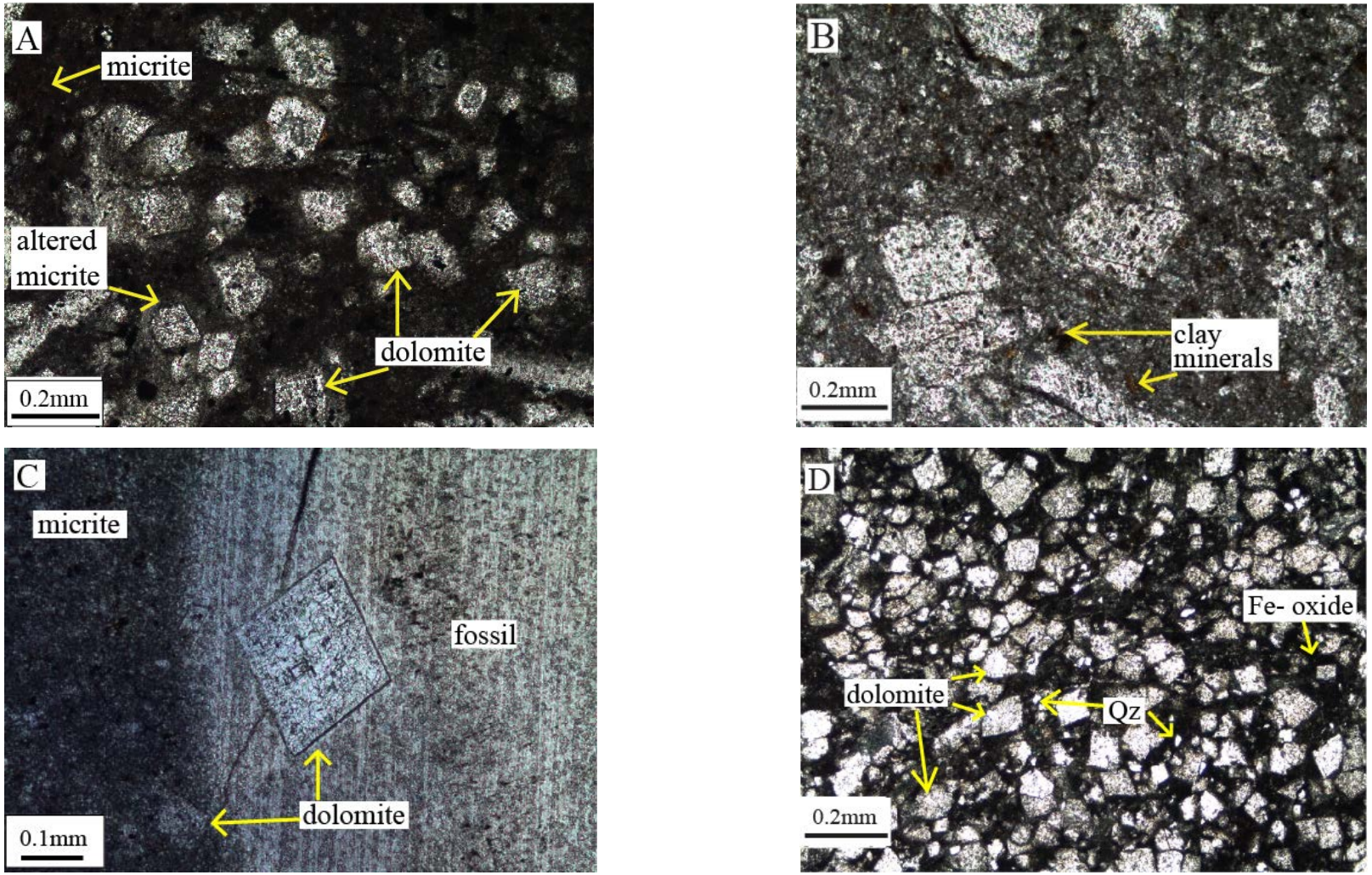

Figure 7, A. Top left image from DV A. 18 (Type 1a) with Planar-e (euhedral) loosely packed, cloudy dolomite with fluid inclusions in a micritic matrix with a lighter colored altered halo around the dolomite. B. Top right sample DV. 2.0M (Type 1a) with several pictured dolomite grains C. Bottom left sample DV 3.5M (Type 2) sample with a dolomite in a trilobite fossil and a smaller dolomite in micrite on the edge of the fossil. D. Bottom right sample DV 4.4M (Type 3) with relatively clear, packed mostly Planar-e dolomite surrounded by Fe-oxides, clays, and interspersed quartz grains.

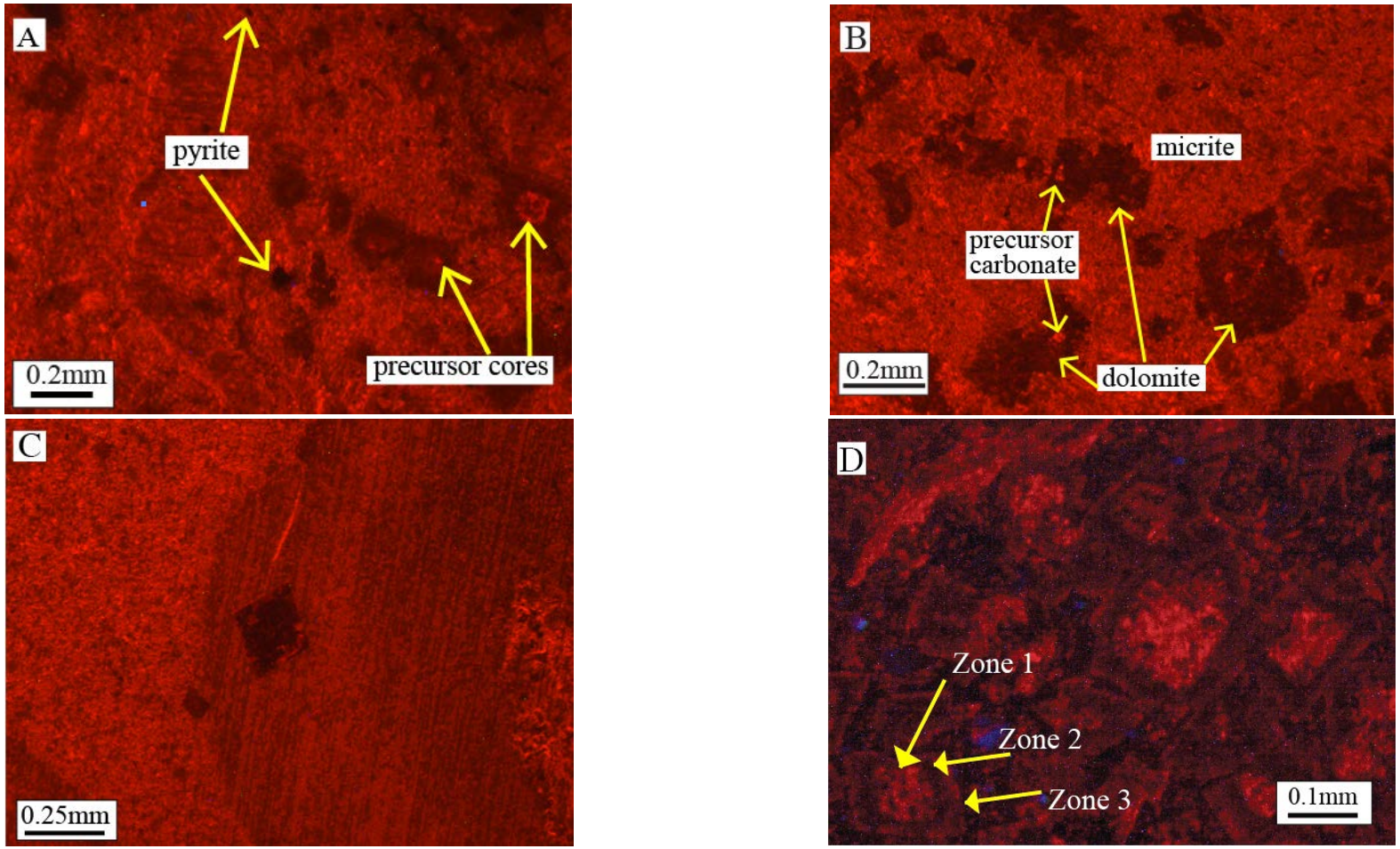

Figure 8, A. Top left image from DV A. 18 (Type 1a) with Planar-e rhombs that are dully luminescent with some examples having a brighter core. B. Top right sample DV. 2.0M CL (Type 1a) sample shows partially dully luminescent dolomite rhombs and fragments with some portions of moderately luminescent precursor material with a similar luminescence to the moderately luminescent micrite matrix C. Bottom left sample DV 3.5M (Type 2) CL exhibiting moderate luminescence of micrite and the trilobite and dull-no luminescence by dolomite. D. Bottom right sample DV 4.4M (Type 3) with zoomed in CL image which shows zoned rhombs with 3 zones, a bright inner zone, dull middle zone, and thin outer zone surrounded by blue luminescent grains that are likely quartz.

Sample	Petrology			Geochemistry		Interpretation
	Class.	Appearance	CL Characteristics	REE Pattern	Ce anomaly	
5.8	3	uncommon, cloudy grey	dull red, thin orange outer rim	flat,contaminants	positive	hydrothermal
5.8	3	clear rim, cloudy inner, inclusion rich	orange inner, dull middle, orange rim	flat,contaminants	positive	hydrothermal
5.3	3	small, relatively clear, surrounded by dark matter	dull- brightly luminescent inner, non- luminescent to dull rim	flat,contaminants	negative La, no Ce	hydrothermal
4.4	3	clear rhombs	bright orange inner, dark middle zone, dull- bright orange rim	flat,contaminants	positive	hydrothermal
4.2	1A	packed, clear- slightly cloudy rhombs	dull red dolomite	flat	none	hydrothermal
4.2	1A	very cloudy rhombs	dull red dolomite	flat	none	hydrothermal
3.5	1A	cloudy, sparse rhombs in micrite	very dark/ no luminescence	LREE enriched	none	early-middle burial
3.5	2	clear rhombs in fossil	very dark/ no luminescence	seawater- like	none	early burial
3	1B	somewhat cloudy with dark inclusions	dull red, lighter red/ orange spots	< 10 grains		early burial
2.5	1B	cloudy grey, burrow infill	dull orange core, non- luminescent rim	< 100 μm		early burial
2.5	1A	cloudy, many inclusions, most partially dissolved	dark core, medium orange ring, dark rim	most dissolved		early-middle burial
2	1A	cloudy, many inclusions, most partially dissolved	no luminescence, few orange cores of previous material	LREE enriched	no La or Ce	early-middle burial
0.5	1B	very small, moderately clear	moderate orange luminescence	< 100 μm		early burial
0.0	1A	partially dissolved, cloudy rhombs	no luminescence, orange cores very seldomly	MREE bulge	negative La, no Ce	early burial, Fe-oxide influence
A. 20	1A	rhombs with precursor cores	very dull small orange cores in some, no luminescence on rim	MREE bulge	none	early burial, Fe-oxide influence
A. 18	1A	rhombs with precursor pieces	no- dull luminescence	MREE bulge	none	early burial, Fe-oxide influence
A. 18	1A	zoned precursor rhomb, clear core and cloudy rim	bright orange luminescent cores, non- luminescent rims	MREE bulge	none	early burial, Fe-oxide influence
A. 13	2	small clear rhomb	no luminescence	< 100 μm		early burial
A. 11	2	clear rhombs with darker rims	very dull orange luminescence	< 100 μm		early burial
A. 11	2	overgrowing grains around it	very dull orange luminescence	< 100 μm		early burial
A. 9	2	small, clear	very dull orange luminescence	< 100 μm		early burial
A. 7	2	small, clear	very dull orange luminescence	< 100 μm		early burial
A. 7 Lower	2	small, clear inside, dark rim	medium orange- red luminescence	< 100 μm		early burial
A. 3	1B	very fine-grained, coarse	medium orange luminescence	< 100 μm		early burial
A. 2.1	1B	mixed cloudy and clear	medium orange luminescence	< 100 μm		early burial
P. 5	1A	semi- cloudy, large, overlapping rhombs	dull orange luminescence	MREE bulge	no La or Ce	early burial, Fe oxide influence
P. 8	1A	grey with dark rim	medium orange luminescence	< 5 grains > 100 μm		

Figure 9- Table of dolomite occurrence petrographic (plain-polar and cathodoluminescence) and geochemical data followed by the diagenetic interpretation for each interval.

been partially dissolved around the rims. These dolomites vary from fine to coarse in nature. The coarser cements range in size from 50-200 μm, Type 1a range from occurrence in concentrated portions to occurring sporadically throughout the slide. Type 1a dolomite occasionally contains small cores or pieces of material that often cannot be distinguished from the surrounding dolomite under plain polar light, but can be differentiated in cross-polar light and CL (Figure 8, A and B). These cores exhibit a brighter, moderate orange-red luminescence compared to the dull red luminescence of the outer portion of the dolomite and the other dolomites of this type. The exception to this is sample DV A. 18. Some of the precursor cores in this sample exhibit some variance in CL luminescence (Figure 8, A). The Type 1b dolomite that is similar in petrographic and CL appearance to 1a dolomite is finer grained, less than 50 μm, making them too small for *in situ* geochemical analysis, which required dolomites greater than 100 μm. These dolomites do exhibit slightly higher moderate red luminescence and are often burrow cements or occur in close proximity to bedding surfaces.

Type 2 dolomite is characterized by clear planar-e rhombs with fewer inclusions than Type 1 and range in size from 50-125 μm, with the exception of DV 3.5M which is ~250 μm in width (Figure 7, C). These dolomites exhibit either no luminescence or dull red luminescence (Figure 8, C). This dolomite occurs uncommonly and very sporadically, usually consisting of only a few Planar-e (euhedral) rhombs in a single slide. Type 2 dolomites are often found in samples that have micritic matrices and occur in these matrices or in association skeletal grains, suggesting that these dolomites did not require massive diagenetic fluid flow for dolomitization.

Type 3 dolomites account for a very small portion of the total dolomite percentage in the study and are grouped as dolomites that exhibit clear CL zoning. Zoned dolomites are more

common in intervals in the upper portion of the sampled intervals among the more heavily dolomitized intervals. These crystals range in size from 75-200 μm. In plain polar petrographic light samples range from clear to cloudy under petrographic analysis (Figure 7, D). Although there are some variations in petrographic appearance, under CL analysis these samples have similar zoning properties. Samples DV 4.4M, and DV 5.8M zonations consist of a large inner zone that is moderate-bright orange luminescence with dark inclusions (Figure 6), a thin middle zone with very dull red luminescence, and an equally thin orange-red, moderately luminescent outer rim (Figure 8, D).

The zoning of DV 5.3M is much less consistent, with inner zone differing between dully luminescent and brightly luminescent, while the outer rim is moderately luminescent. The less consistent zoning in this interval as opposed to the surrounding samples, DV 4.4M and DV 5.8M, potentially indicates inconsistent or incomplete interaction with diagenetic fluids. The outer portions of the samples with three CL zones likely interacted with a diagenetic fluid that was depleted in Fe^{2+} or under more anoxic conditions, as they exhibit brighter luminescence than the dull, middle rim, potentially very late burial or hydrothermal fluid overgrowths.

Each of these three samples exhibit differing petrographic characteristics. Under plain- and cross-polar light in two of the three samples 5.8M) show varying degrees of clarity between their inner and outer rims. The third sample (4.4M) shows no zoning under plain light. Despite their differing appearances in plain light, the CL zoning in each of these samples is consistent. These crystals have a large inner zone or core that is moderate-brightly luminescent, a thin dull- to non-luminescent middle zone, and a dull-bright orange rim.

4.2 DOLOMITE AND STANDARDS GEOCHEMICAL DATA

Total REE abundances (∑REE) range from 7.91-102.45 ppm among interval averages. The average REE data as well as all calculated anomalies for each interval were compiled in Figure 10. Individual dolomite geochemical data were compiled in Appendix 3. REE pattern descriptions were added to Figure 9. Dolomite REE patterns were sorted by stratigraphic location into three intervals and results are presented based on these intervals.

Th values are 0.4 ppm for the SRM 1d standard and 0.11 ppm for the IAEA B7 standard (Appendix 2). Al values are 3050 ppm for the SRM 1d standard and 220 ppm for the IAEA B7 standard. Th values for dolomite range between 0.02-1.14 ppm, and Al values range from 87-6220 ppm (Appendix 3). Binary diagrams of Al vs. ∑REE (Figure 11, A) and Al vs. ∑REE (Figure 11, B) crossplots were made to evaluate contamination effects due to inclusion of terrigenous material in dolomite samples.

4.2.1 Carimona-Lower Guttenberg Interval REE Data

The lowermost set of dolomite REE patterns include samples P. 5, A. 18, A. 20, and DV 0.0M. These samples have REE patterns consistent with MREE enrichment (Figure 12, A and Figure 13), also called a “MREE-bulge” (Johannesson and Zhou, 1999; Haley and Klinkhammer, 2003; Haley et al, 2004; Corlett and Jones, 2012). These samples range in stratigraphic location from below the Deicke to the bed overlying the Elkport K-bentonite. ∑REE values range between 36.33-102.45 ppm, some of the highest values in the study (Figure 10). There is no clear grouping with regard to Ce anomalies (Figure 14). Sample DV 0.0M exhibits a negative La

Sample	La	Ce	Pr	Nd	Sm	Eu	Gd	Tb	Dy	Ho	Er	Tm	Yb	Lu	ΣREE	La_N/Sm_N	Gd_N/Yb_N	Eu/Eu*	Ce/Ce*	Pr/Pr*	*n* =
DV 5.8	4.21	10.06	0.85	3.13	0.59	0.11	0.56	0.09	0.69	0.14	0.52	0.07	0.44	0.07	21.54	1.06	0.73	0.94	1.21	0.86	22
DV 5.3	7.75	17.54	1.77	5.62	1.01	0.22	0.87	0.12	0.81	0.16	0.44	0.06	0.40	0.06	36.83	1.16	1.25	1.19	1.08	1.02	24
DV 4.4	6.05	14.17	1.25	4.39	0.70	0.15	0.72	0.12	0.80	0.17	0.55	0.08	0.46	0.07	29.68	1.29	0.91	1.06	1.17	0.90	20
DV 4.2	3.31	6.27	0.58	2.24	0.37	0.08	0.38	0.05	0.40	0.08	0.26	0.03	0.21	0.03	14.30	1.35	1.02	1.08	1.02	0.89	24
DV 3.5 (1- 4, 7)	1.85	3.33	0.33	0.94	0.18	0.04	0.23	0.04	0.35	0.09	0.30	0.03	0.17	0.02	7.91	1.52	0.80	0.85	0.97	1.06	5
DV 3.5 (5-6, 8-10)	2.60	5.41	0.57	1.68	0.25	0.05	0.28	0.04	0.27	0.06	0.18	0.02	0.14	0.02	11.58	1.59	1.12	1.05	1.03	1.08	5
DV 2.0	2.74	5.80	0.59	2.06	0.34	0.07	0.33	0.05	0.32	0.07	0.19	0.02	0.12	0.02	11.43	1.21	1.54	1.02	1.04	0.98	18
DV 0.0	5.02	18.03	1.90	6.92	1.03	0.22	0.99	0.14	0.92	0.19	0.51	0.06	0.34	0.05	36.33	0.73	1.70	1.09	1.29	0.98	23
A. 20	8.80	30.82	3.64	12.24	2.29	0.42	1.82	0.27	1.57	0.30	0.79	0.10	0.52	0.08	63.66	0.58	2.02	0.99	1.19	1.08	27
A. 18	14.2	44.2	4.96	16.6	2.8	0.59	2.37	0.32	1.9	0.4	0.99	0.13	0.8	0.11	90.27	0.76	1.72	1.15	1.18	1.05	32
P. 5	16.25	41.49	5.58	23.89	4.50	0.76	3.56	0.52	2.91	0.50	1.33	0.15	0.86	0.12	102.45	0.54	2.39	0.92	0.98	1.00	19
Seawater $x10^6{}_N$	0.06	0.01	0.04	0.04	0.05	0.06	0.07	0.07	0.09	0.12	0.14	0.15	0.14	0.16	5.21	1.29	0.52	1.08	0.25	1.45	

Figure 10- *In Situ* rare earth element data collected in this study. Each value is the average of the measured value from the interval. All REE values are in ppm. $_N$ indicates values normalized to Upper Continental Crust values from Taylor and McLennan (1985, 1991) compiled in Rudnick and Gao (2003). Eu, Ce, and Pr anomalies were calculated using the following formulas: $Eu/Eu^* = Eu_N/(0.67Eu_N + 0.33Tb_N)$, $Ce/Ce^* = Ce_N/(0.5La_N + 0.5Pr_N)$, and $Pr/Pr^* = Pr_N/(0.5Ce_N + 0.5Nd_N)$ (Bau and Dulski, 1996; Zhang et al., 2014). Number (n) of dolomite values used in interval averages. REE values for modern seawater (magnified by 106 due to low ΣREE of seawater) were calculated from (Zhang et al., 2014).

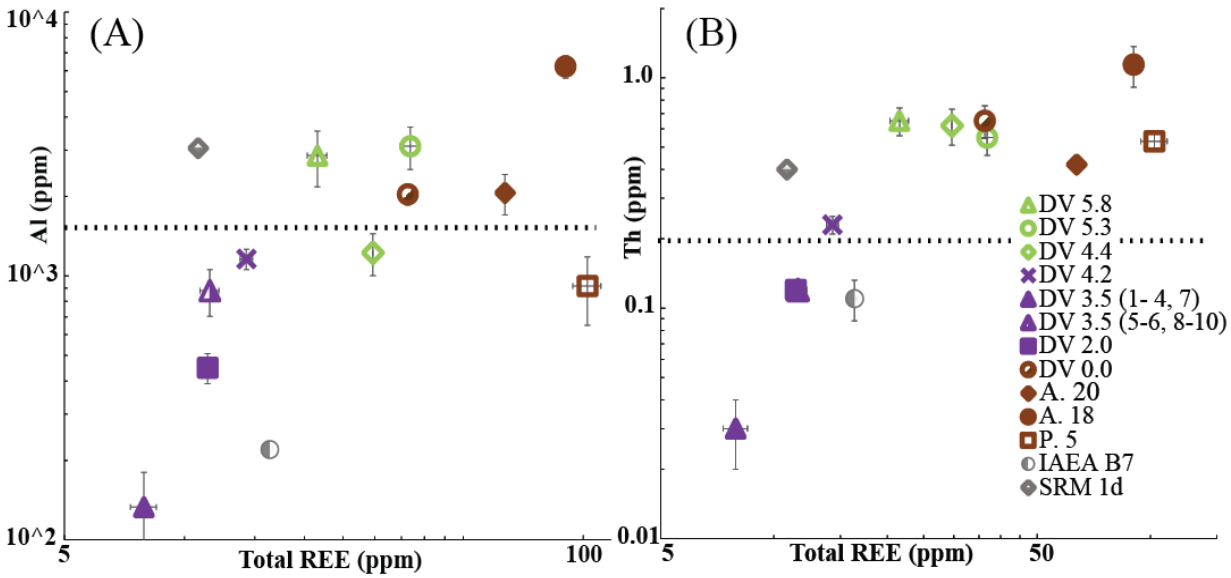

Figure 11-Binary diagrams of Al vs. ∑REE (Figure A) and Th (Figure B) vs. ∑REE are used to evaluate the potential contamination of dolomites. Dotted lines indicate contamination cutoffs equal to greater than 2% of UCC Al and Th concentrations.

anomaly and no Ce anomaly, while sample P. 5 has neither a La nor Ce anomaly. None of the samples exhibit significant Eu anomalies (0.92-1.15) (Figure 15).

4.2.2 Middle-Upper Guttenberg Member Interval REE Data

Three sampled intervals are included in this stratigraphic interval, DV 2.0M, DV 3.5M, and DV 4.2M. The samples from DV 3.5M were divided based on two different REE patterns. This first REE pattern includes sample spots sample spots 1-4 and 7 from dolomite formed in a trilobite fossil. The second pattern type came from sample spots 5, 6, and 8-10 formed in the micritic matrix filling the inside of the fossil cavity. This interval includes several REE patterns; the first is a very slight LREE enrichment trend exhibited by DV 2.0M and several dolomites from DV 3.5M (sample spots 5, 6, 8-10) (Figure 12, B and Figure 13). These samples have the lowest ∑REE values of the sampled intervals, 11.43 ppm and 11.58 ppm, with the exception of the other DV 3.5M ablation spots within the fossil (sample spots 1-4, 7) (7.91 ppm). Neither sample has a Ce anomaly, and plots on the line between no La anomaly and a negative La

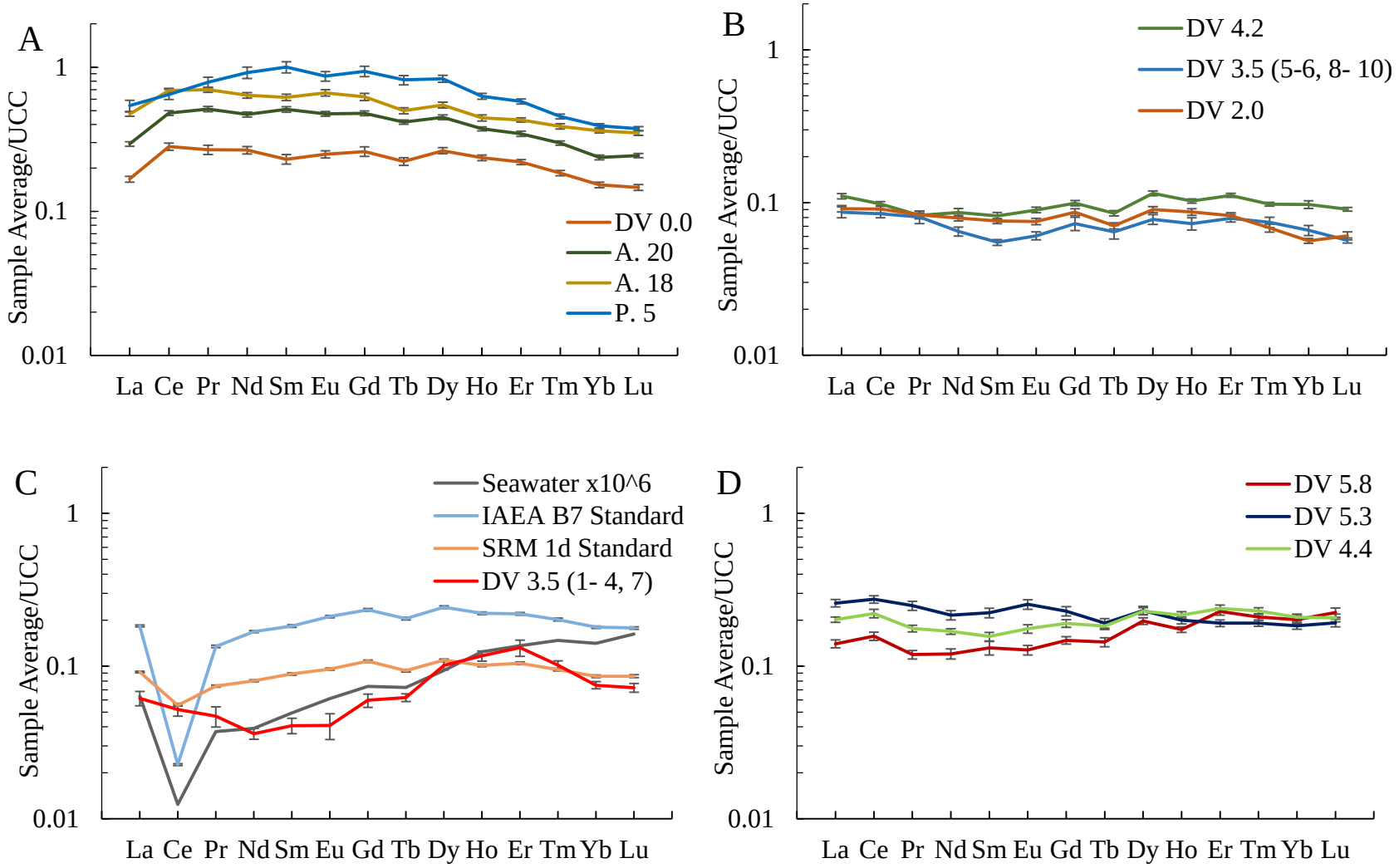

Figure 12-REE patterns (average for each dataset) for intervals and standards. (A) Samples from the Carimona-Lower Guttenberg Interval. (B) Samples from the Middle-Upper Guttenberg Interval. (C) Seawater and standards included for basis of comparison to a middle Guttenberg sample. (D) Samples from the Ion Member Interval.

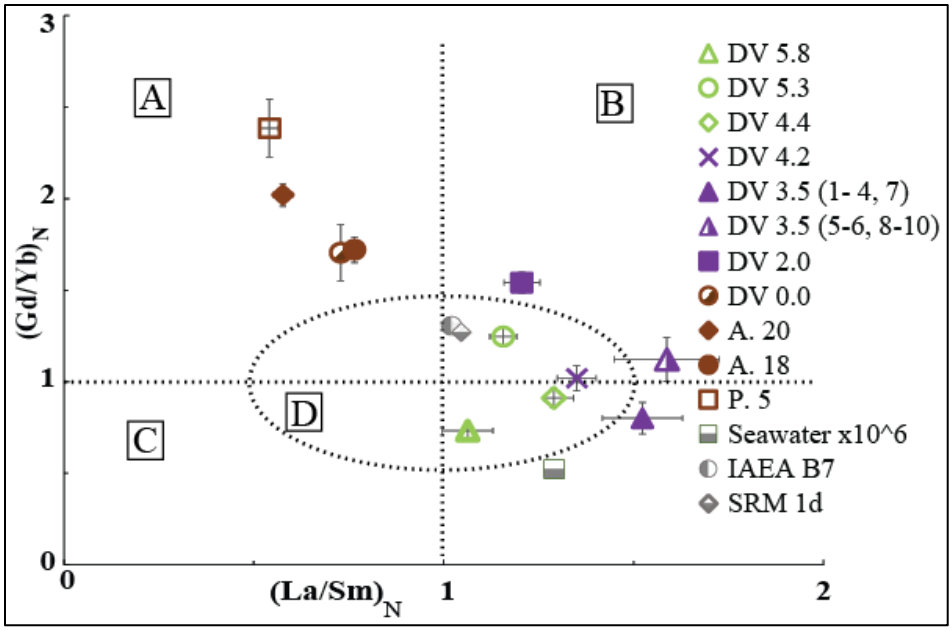

Figure 13-Binary diagram of UCC normalized (N) La/Sm vs. Gd/Yb, which are useful in determining REE distribution patterns. Field a: MREE enrichment; Field b: LREE enrichment; Field c: HREE enrichment; Field d (oval): flat REE pattern.

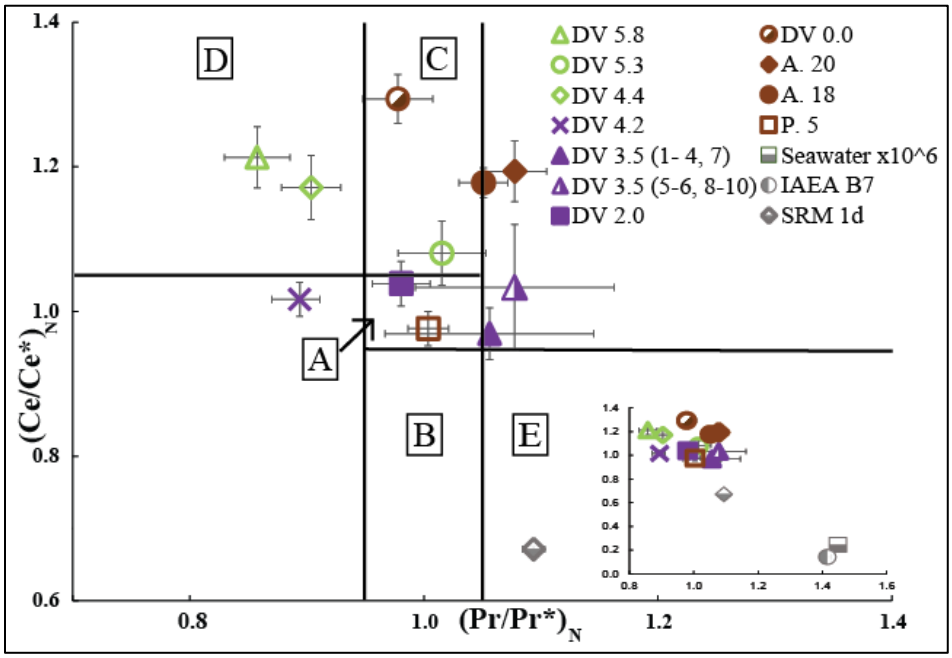

Figure 14-Binary diagram of UCC normalized (N) values showing Ce/Ce* and Pr/Pr* relationship after Bau and Dulski (1996) and Zhang et al. (2014). Field a: neither Ce nor La anomaly; Field b: positive La anomaly, no Ce anomaly; Field c: negative La anomaly, no Ce anomaly; Field d: true positive Ce anomaly; Field e: true negative Ce anomaly. Inset diagram in the bottom right shows the large negative anomaly exhibited by seawater and reference material IAEA B7.

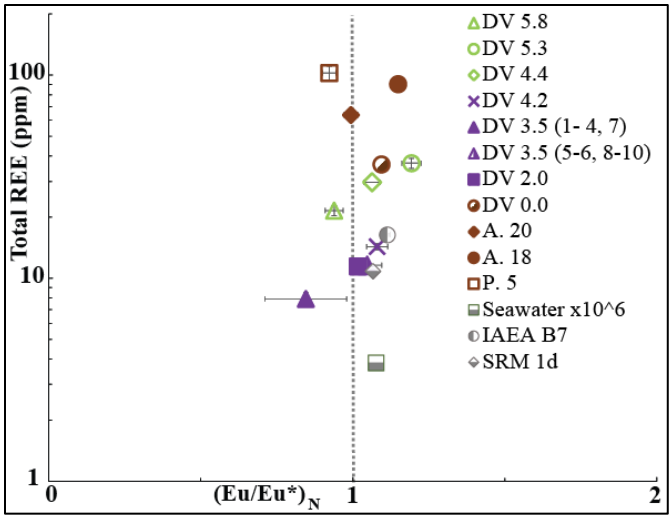

Figure 15-Total REE vs Eu anomaly binary diagram of sample intervals. Seawater value calculated from Zhang et al., 2014. Eu/Eu* values are normalized to UCC. Error bars are standard error calculated for each both total concentration and the Eu anomaly.

anomaly (Figure 13). These samples also have neutral Eu anomaly values of 1.02 and 1.05 (Figure 15). DV 4.2M, the highest sample in this stratigraphic interval, is plotted alongside these samples. This sample exhibits a flat pattern (Figure 12, C and Figure 13). This sample also has a relatively low ∑REE values of 14.30 ppm (Figure 10). This sample plots within the field of neither Ce nor La anomalies (Figure 14).

The other pattern in this stratigraphic interval is one of higher HREE values compared to LREE, or HREE enrichment, from laser ablation of two dolomites within a skeletal grain from DV 3.5M (sample spots 1-4, 7) (Figure 12, C and Figure 13). These samples have the lowest average ∑REE value, 7.91 ppm. These dolomites exhibit no true positive or negative Ce anomalies (Figure 14). With the exception of a lack of Ce anomaly and lower HREE Tm, Yb, and Lu values, this REE trend is very similar to that of modern seawater (Figure 12, C). This trend was plotted with the modern seawater, IAEA B7 standard, and NIST SRM 1d standard for comparison of seawater and seawater-like signatures from other carbonates.

4.2.3 Ion Member Interval REE Data

The third interval samples, DV 4.4M, DV 5.3M, and DV 5.8M, are overprinted by terrigenous contaminants, thus REE patterns and ∑REE values cannot be used. Dolomites DV 4.4M and DV 5.8M exhibit similar geochemical properties of true positive Ce anomalies (Figure 14) while a positive Ce anomaly is not exhibited by DV 5.3M. Sample DV 5.3M has the highest recorded Eu anomaly value of 1.19, while DV 4.4M and DV 5.8M have moderate values of 1.06 and 0.94 (Figure 15).

5. INTERPRETATIONS AND DISCUSSION

5.1 REE PATTERNS AND EVALUATING CONTAMINATION EFFECTS BY TERRIGENOUS MATERIAL

Due to the low ∑REE concentrations of carbonate relative to other signal sources, signatures of carbonates are extremely susceptible to contamination, or overprinting, by other sources of REE such as terrigenous clays or Fe-oxides. This results in any primary seawater or secondary diagenetic fluid signature to be overprinted (Bolhar et al., 2004; Nothdurft et al., 2004; Zhang et al., 2014). Thus, the evaluation and recognition of contaminated samples is critical to the accurate evaluation of REE patterns in carbonates. Nothdurft et al. (2004) effectively illustrated that even 2% contamination by shale can obliterate the elemental anomalies and result in relatively flat REE patterns.

Incompatible elements (e.g., Al and Th) that are often concentrated in terrigenous sediments were used to evaluate this contamination potential as has been done in previous limestone and dolomite studies (Bau and Alexander, 2006; Frimmel, 2009; Zhang et al., 2014). Due to the high REE concentration of shales and clays, a positive correlation between these incompatible elements and ∑REE should be present if contamination has occurred (Bolhar et al., 2004; Frimmel, 2009; Zhang et al., 2014). Reference material SRM 1d exceeds the 2% cutoff . Higher Al and Th values in SRM 1d are unsurprising as this sample is described as an argillaceous limestone indicating a clay component in the sample (“Certificate of Analysis”, 2005). This is a possible explanation why the REE pattern of SRM 1d is more flat and exhibits a less significant Ce anomaly with respect to the REE patterns of IAEA B7 and modern seawater.

Th values for dolomite range between 0.02-1.14 ppm, and Al values range from 87-6220 ppm (Appendix 3). From a graphical standpoint there appears to be a positive relationship

between both Al and Th and ∑REE concentration among the dolomite samples (Figure 11). Statistical analysis using linear regression yielded values of R^2= 0.27 for the Al crossplot and R^2= 0.44 for the Th crossplot. This indicates at least a moderate positive correlation between REE concentrations and Al/ Th concentrations (Figure 11) for the studied dolomite samples.

Carimona-Lower Guttenberg samples DV P. 5, A. 18, A. 20, and 0.0M have the highest ∑REE, Al, and Th values of any stratigraphic interval. The role of terrigenous sediment contaminants affecting the REE patterns is difficult to argue, but REE patterns for this interval are distinctly non-linear. Thus, despite incorporation of siliciclastic material, the expected linear REE pattern from siliciclastic material has been overprinted by a stronger signal source.

Samples from the Middle Guttenberg to Upper Guttenberg exhibit percentages at (DV 4.2M) or below (DV 2.0M and DV 3.5M) cutoff values for both elements. It should be noted that ∑REE concentrations and the shape of the curves of this interval are not greatly different despite DV 4.2M samples being closer to the contamination cutoff. REE patterns for this interval are interpreted as being the result of diagenetic fluids instead of contamination.

The Ion Member samples (DV 4.4M, 5.3M, and 5.8M) plot near or above the contamination cutoff for Al and above the cutoff for Th (5.2-6.2%). As mentioned previously in the results, these REE patterns are interpreted as the result of contamination and the geochemical data must be interpreted with this in mind. This enrichment could be the result of hydrothermal fluids (Read et al., 2002).

5.2 MODERN SEAWATER REE PATTERNS COMPARED TO DOLOMITE OF THIS STUDY

The geochemical characteristics of modern seawater include: low ∑REE, HREE enrichment, positive La and slightly positive Gd anomalies, and a distinctive negative Ce

anomaly (McLennan, 1989). Until recently, limestones were thought to be poor REE proxies for seawater due to the higher ∑REE concentrations relative to modern skeletal carbonates and were thought to be diagenetically overprinted (Nothdurft et al., 2004). Recent studies have proven that even ancient carbonates through the Phanerozoic can retain seawater-like REE patterns (Shields and Webb, 2004; Zhang et al., 2008; Zhao and Jones, 2013). This indicates that the REE geochemistry of modern seawater and ancient seawater, at least through the Phanerozoic, has remained very similar. Banner et al. (1988) further argued that diagenetic fluid of a seawater-like nature mediating dolomitization would result in maintaining the seawater-like REE pattern of precursor carbonate material. This argument has been proven in later studies (Qing and Mountjoy, 1994; Bau and Alexander, 2006; Zhao and Jones, 2013). In comparison of the modern seawater REE patterns to the dolomite and carbonate standard REE patterns of this study, it is apparent that only one set of dolomite in this study exhibit seawater-like REE patterns (Figure 12, C). These dolomites came from Sample DV 3.5M. The REE patterns of all other dolomites in this study were formed by non-seawater diagenetic fluids or were overprinted by incorporation of contaminants such as Fe-oxides and siliciclastic material.

5.3 CE AND EU ANOMALIES AS REDOX AND TEMPERATURE INDICATORS

Cerium and europium can provide valuable information about the diagenetic fluid that mediated deposition. Cerium is a redox-sensitive element, causing it to act differently than the rest of the REEs. Ce^{3+} in a dissolved state can be oxidized to Ce^{4+} in particulate form, which preferentially takes place in shallow water (Alibo and Nozaki, 1999; Zhao and Jones, 2013) and results in the negative Ce anomaly ($Ce/Ce^{*}<1$) of oxygenated seawater, an indicator of oxygenation state of fluids. Cerium oxidation is affected more heavily by pH than by oxygen fugacity and oxidation is favored by alkaline fluids (Elderfield and Sholkovitz, 1987).

Temperatures also affect oxygen fugacity, as the Ce^{4+}/ Ce^{3+} equilibrium state shifts toward higher fugacity as temperature increases. This means that negative Ce anomalies can erased by low-pH or high temperature hydrothermal or basinal diagenetic fluids (Frimmel, 2009). Negative Ce anomalies are absent in all of the tested samples (Figure 14, Field C), indicating that either none of these dolomites were formed in oxic conditions, or that the contamination overprinted these signatures. Contaminated dolomites DV 4.4M and DV 5.8M are the only samples that have positive Ce anomalies (Figure 14, Field D). Despite overprinting by siliciclastic contamination, this anomaly potentially indicates anoxic conditions or warm temperatures of diagenetic fluids because contamination should flatten the pattern and not result in anomalies.

Eu^{3+}/ Eu^{2+} redox potential is highly dependent on temperature, thus high temperature hydrothermal or basinal diagenetic fluid results in Eu anomalies (Frimmel, 2009). Positive Eu anomalies are associated with pyrite-bearing carbonates and acidic, reducing hydrothermal fluids, while negative Eu anomalies occur in Fe-oxide rich carbonates. The lack of significant positive Eu anomalies (Figure 15) in any samples can either be attributed to these dolomites having no interaction with high temperature hydrothermal fluids (>200-250^{o} C) (Bau and Dulski, 1996; Azomani et al., 2013) or terrigenous overprinting from contamination. Assuming that this anomaly is still indicative of diagenetic fluids, it is still possible that heated diagenetic fluids, either basinal or hydrothermal brines, could have interacted with these rocks assuming they were no warmer than 90-130^{o} C, as positive Eu anomalies require higher temperature (Zhang et al., 2014). This is consistent with UMV mineralization studies: 50-121^{o} C of liquid inclusions in sphalerite and calcite by Bailey and Cameron (1951) and 50-120 ^{o} C by Heyl et al. (1974).

5.4 GEOCHEMISTRY AND PETROGRAPHY: INTERPRETATIONS BY STRATIGRAPHIC INTERVAL

5.4.1-Carimona-Lower Guttenberg Interval

The association of dolomites with burrows in this interval is likely the result of the higher permeability created by the burrowing effect, allowing greater water/sediment interaction, and also acting as a sink for organic matter, clays, and Fe-oxides (Gingras et al., 2004; Freiburg et al., 2012 Baniak et al., 2013). It was also previously noted that samples are within close proximity to K-bentonite beds (Figure 17). This relationship between greater dolomite occurrence, burrows, and K-bentonites is potentially due to weathering of volcanic ash and conversion to K-bentonite, providing diagenetic fluids Mg^{2+} ions that could promote dolomitization. In a review of 55 previous studies of ash water leachates Witham et al. (2004) summarized that Mg^{2+} and, amongst others ions including Ca^{2+}, Na^{+}, SO_4^{2-}, and Cl^{-} are prominent species released upon exposure to and interaction with water (Witham et al., 2005). In the most direct manner, the volcanic ash was potentially a source of Mg^{2+} to the pore fluids, resulting in supersaturation of fluid with respect to dolomite, and promoting dolomitization (Figure 18). Another possible cause is that SO_4^{2-} released from the K-bentonites bound to free Mg^{2+} and later interacted with sulfate-reducing bacteria (SRB), resulting in the release of Mg^{2+}. This interaction has been attributed to the promotion of dolomitization, particularly in burrows, and the reaction is represented by the following formula (Wright, 2000; Corlett and Jones, 2012):

$$2CH_2O + MgSO_4 \rightarrow 2HCO_3 + H_2S + Mg^{2+}$$

Although this interval does exhibit geochemical evidence of siliciclastic material, this contamination appears to be overprinted by Fe-oxide signal contamination. This signal could be the result of Fe-oxides contained inside the dolomite, however Fe-oxide contaminated carbonates

in another study exhibited a flatter REE pattern than the samples of this interval (Frimmel, 2009). Therefore, this pattern is interpreted as Fe-oxides becoming reduced under anoxic porewater conditions causing them to release their preferentially scavenged REEs, as similarly demonstrated by Corlett and Jones (2012) (Figure 18).

These samples exhibit what has been called the "MREE" bulge (Figure 12, A) (Johannesson and Zhou, 1999; Haley et al., 2004). Haley et al. (2004) attributed this pattern found in porewaters to the presence of Fe-oxides in the porewaters. This pattern has been recorded in previous studies of dolomite filled burrows from a Devonian ramp setting in the Northwest Territory, Canada (Corlett and Jones, 2012). In this study the MREE bulge was interpreted as a sign of fully anoxic conditions below the sediment-water interface where Fe-oxides, which preferentially scavenge MREEs in the water column, are reduced and release MREEs causing enrichment in carbonates forming in this condition (Haley et al., 2004). In these samples, fully anoxic conditions in which Fe-oxides could be reduced and release MREE are supported by the very dull, quenched luminescence exhibited by these dolomites under CL. The seldom occurrence of more moderately luminescent non-zoned cores are likely remnants of previous carbonate material that were largely replaced when dolomitization occurred, similar to Smith and Simo (1997).

The lower MREE enrichment in sample DV 0.0M is potentially indicative of lower Fe-oxide concentrations in the water column and in porewaters. There exist two possibilities for lower Fe-oxide concentrations. Sediment input into the midcontinent sea slowed, indicated by the shift in lithologies from shale facies of the Specht's Ferry (DV P. 5, DV A. 18, DV A. 20) to carbonate facies in the overlying Guttenberg Member (DV 0.0M). This would cause fewer terrigenous grains for Fe-oxides to coat and could potentially result in lower MREE enrichment. Alternatively, subduction related volcanic ash has proven capable of quickly releasing large

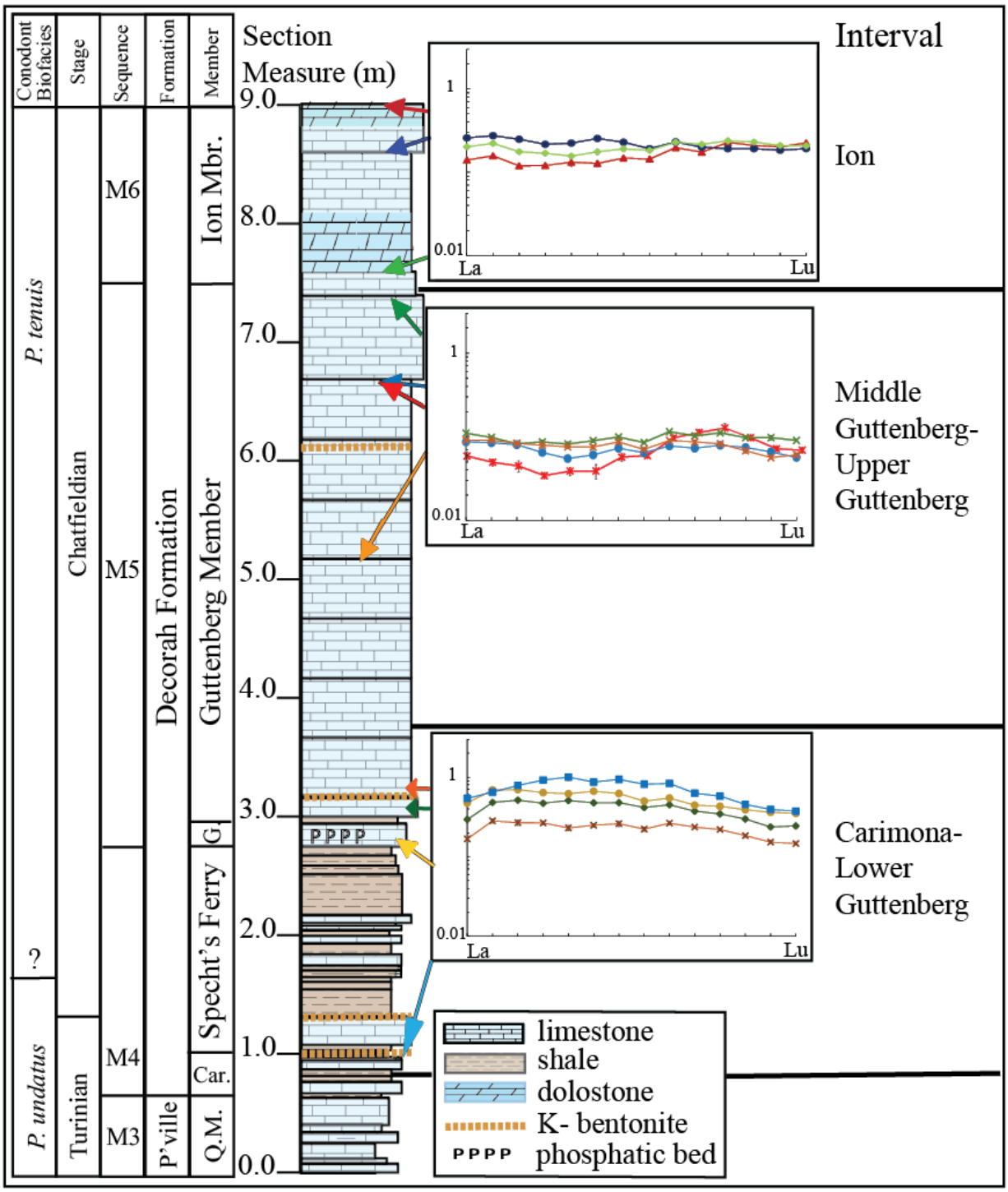

Figure 17-Combined stratigraphic column and dolomite REE patterns by interval demonstrating the stratigraphic relationship between dolomite and shales, K-bentonites, and the spatial variability of these patterns. Arrow colors correspond to REE pattern colors. The seawater-like signature in DV 3.5M (red pattern) is included in the other samples of the same interval.

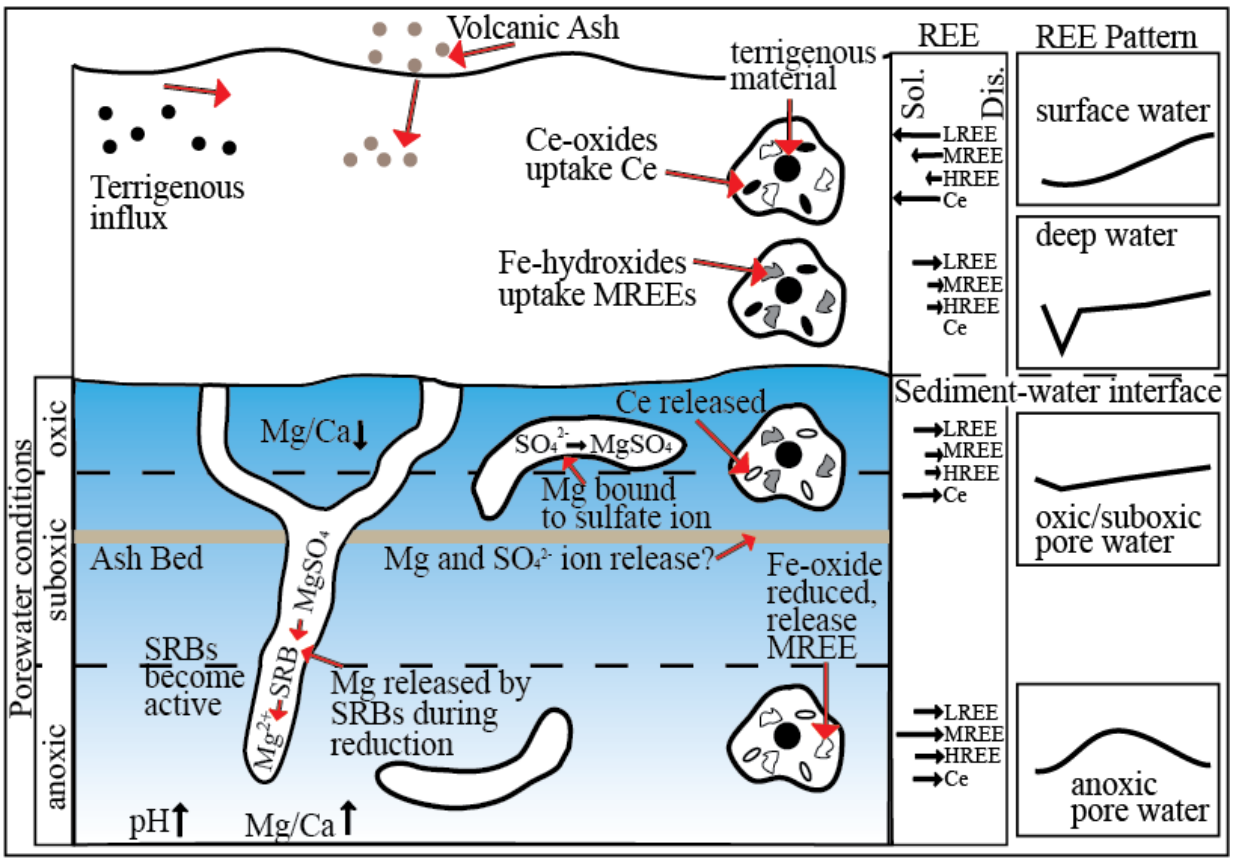

Figure 18- Schematic diagram that illustrates the early burial geochemical conditions that likely contributed to dolomitization inside of burrows. Modified from Corlett and Jones (2012). Left panel shows interaction between porewater and sediments in the water column and in the shallow burial environments. SRBs indicate sulfate reducing bacteria. The middle column reveals the net movement of REE between solid (Sol.) material and dissolved (Dis.) in porewater during burial. The far right column (modified from Haley et al., 2004) is the REE pattern expected in the water mass.

amounts of adsorbed Fe into seawater (Frogner et al., 2001; Duggen et al., 2007). Fe released can be on the order of 0.01-91 mg/kg ash based on a compilation of 22 volcanic-ash water-leachate studies in Witham et al. (2005). If Fe concentrations contributing to the formation of Fe-oxides in seawater were controlled by immediate leaching from volcanic ash, the fact that this sample was deposited after the ash makes it likely that any Fe-oxide enrichment of diagenetic fluids due to ash-water interaction would have been less likely.

The shallow burial model of dolomitization in this interval matches interpretations from only one other regional study (Smith and Simo, 1997). This study revealed that these dolomites occasionally nucleated on precursor protodolomite seed crystals. These cores are not always present or are unidentifiable in many of the dolomites of this study, however. The zoned nature of precursor material in Although the dolomitization realms and some characteristics of the dolomites in these studies are the same, the mechanisms for dolomitization are different. We must look at other studies to find similar traits. The burrow or bioturbation related nature of these dolomites, as well as the Fe-oxide influenced REE pattern have been identified in other studies oxides (Gingras et al., 2004; Haley et al., 2004; Corlett and Jones, 2012; Freiburg et al., 2012 Baniak et al., 2013). A novel finding from this interval is the association of larger burrow-related dolomite in this interval with K-bentonites, and a potential cause could be Mg^{2+} leached from K-bentonites which promoted dolomite growth. No previous regional dolomitization studies have been conducted on these Carimona-Lower Guttenberg strata to compare these findings to though.

5.4.2 Middle to Upper Guttenberg Interval

The only dolomites in this study that exhibit seawater-like REE patterns are found in a portion of the dolomites from DV 3.5M (1-4, 7) (Figure 12, C). It is not surprising that these dolomites also have the lowest ∑REE values and Al and Th concentrations, indicators of contamination (Figure 11). The HREE enrichment pattern of seawater is tracked well by this sample until the HREE Tm, Yb, and Lu. Thus this deviation from commonly applied seawater patterns is interpreted as being indicative of a shallow water seawater REE pattern consistent with the shallowing upward interpretation of Guttenberg Member deposition (Ludvigson et al., 1996; Ludvigson et al., 2004).

These samples do not exhibit the negative Ce anomaly that should be present for normal seawater-derived carbonates (Figure 12 C and Figure 14). This means that diagenetic fluid conditions were likely less oxic, sub-oxic to anoxic, than that of modern seawater, as indicated by the neutral Ce anomaly. Similar REE patterns without a Ce anomaly are recorded by Bau and Alexander (2006) in Mid-Paleoproterozoic dolomites and are interpreted as an anoxic seawater signature. The dark nature of luminescence in this sample supports that this dolomite was likely formed under anoxic conditions, supporting the Ce anomaly data (Hiatt and Pufahl, 2014). Trace element Mn vs Fe plots record the most oxidizing signature of samples for which trace elements were analyzed, however. In this case REE and trace element data are potentially contradicting regarding the redox nature of the diagenetic fluid. Other studies support periodic dysoxia or anoxia of seawater during this time period (Ludvigson, 1996; Ludvigson et al., 2004; McLaughlin et al., 2011). Mg sourcing for the formation of this dolomite remains an issue, however. Dolomitized fossils in UMV strata were also identified by Van Tuyl (1914) and were likewise attributed to burial dolomitization. Selective and complete dolomitization of fossils is not uncommon under natural conditions or experimental conditions (Bullen and Sibley, 1984; Gregg and Sibley, 1984), but the unique texture, single planar euhedral rhombs, is different than has been observed in other studies. It is possible that Mg necessary for the formation of this dolomite was caused by the remobilization of Mg due to leaching surrounding high Mg fossils and carbonate grains, as Van Tuyl proposed. Grain and matrix replacement was discussed in the results presented for this slide, making this source of Mg reasonable.

Samples DV 2.0M and DV 3.5M (5-6, 8-10) exhibit LREE enrichment patterns (Figure 12, B and Figure 13). LREE enrichment in dolomite has been attributed to dolomitization by hydrothermal fluids, however in many cases when LREE is present there is also a strong positive

Eu anomaly due to the temperature of the hydrothermal fluids (Bolhar and Van Kranendonk, 2007; Zhang et al., 2014). Low Ba values (Figure 16) in DV 3.5 preclude hydrothermal diagenetic fluid interaction. Hydrothermal fluids also generally exhibit high ∑REE values, but these samples exhibit very low values. Furthermore, these samples also lack any other petrographic evidence of hydrothermal diagenesis associated with UMV-type mineralization. These samples are also in micrite of low porosity and permeability where hydrothermal fluid is unlikely to have been able to penetrate the samples effectively. Thus hydrothermal fluid seems unlikely to be the diagenetic mediating fluid. High Mn-Sr ratios (Figure 16) indicate recrystallization as opposed to direct precipitation, ruling out any syndepositional dolomitization. Ferroan dolomite, which these samples exhibit with high Fe concentrations (DV 3.5M 5-6, 8-10) and dull CL luminescence (all samples of this interval), has been interpreted to have been of burial origin (McHargue and Price, 1982; Yoo et al., 2000). Having ruled out syndepositional and hydrothermal dolomitization, the diagenetic realm for these dolomites must be burial. Due to their close proximity to the dolomite formed by seawater-like conditions in shallow burial conditions, it is likely that these dolomites were also formed in similar shallow burial conditions. These dolomites from DV 3.5M in micritic matrices are most closely related to what Asquith (1967) considered to be shallow burial dolomite often protected in fossils. The samples from DV 2.0M with precursor cores are more closely related to the shallow burial dolomite described by Smith and Simo (1997). The question that remains is why are the REE patterns for these dolomites much different than for the previously discussed sample with a seawater-like signature?

A modest LREE enrichment and lack of Ce anomaly of carbonates has been identified in other studies (Nothdurft et al., 2004; Azmy et al., 2011). It has been shown that suspended ocean

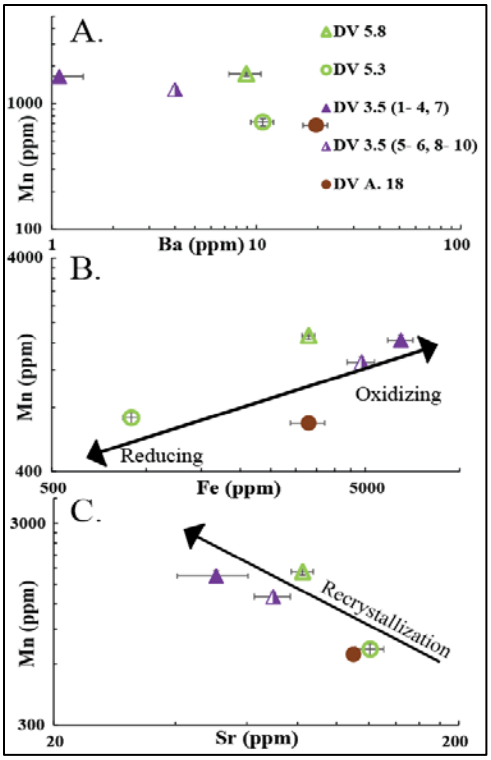

Figure 16-Binary diagrams of Mn versus Ba (A), Mn vs. Fe (B), and Mn vs. Sr (C) for selected intervals. These plots can be used to aid in the characterization of diagenetic fluids. Mn vs. Ba indicates hydrothermal influence. Mn vs. Fe reveal the redox conditions during diagenesis. Sr vs. Mn can reflect the degree of diagenetic recrystallization.

particles and estuarine colloids preferentially uptake LREE (Sholkovitz et al., 1993; Sholkovitz et al., 1994) resulting in the relative HREE enrichment of seawater. Nothdurft et al. (2004) claimed that these samples had incorporated estuarine colloids, resulting in a pattern that displayed LREE enrichment. Furthermore, Nothdurft et al. (2004) showed that contamination evaluations did not reveal contamination, as those samples exhibited low ∑REE and Al concentrations, even given colloidal incorporation that affected the REE pattern. If these dolomites were formed contemporaneously to the dolomites inside the fossil in DV 3.5M (1-4, 7), incorporation of colloidal material in the dolomite during recrystallization of the micrite is the cause of their differing REE signatures. However, if these dolomites formed during slightly later

burial than those from DV 3.5M (1-4, 7), the diagenetic fluids could have been different, resulting in a different REE pattern.

Studies have shown that porewaters only require several 10s of cm below the sediment-water interface can lose a seawater-like signature (Elderfield and Sholkovitz, 1987), and porewaters can exhibit flat or more linear patterns as POC (particulate organic carbons) remineralizes (Haley et al,. 2004). Azmy et al. (2011) found Ordovician lime mudstones and burial cements in with similar modest LREE enrichment. Dolomites with similar REE concentrations and patterns were also interpreted as having been early burial and replacement in nature (Zhang et al., 2008; Azmy et al., 2013; Azomani et al., 2013; Zhang et al., 2014). Nonmarine Ce signatures of subsurface fluids have been proven to be obtained from interaction with detrital sediments, which would also erase any negative Ce anomaly because in the subsurface Ce is more likely to remain in its trivalent state due to anoxic conditions (Banner et al., 1988 and references there-in, pg. 427). Although the exact reason for the REE pattern exhibited by these samples is unclear, it is likely that these dolomites formed in a relatively early burial environment.

DV 4.2M with the "flat" REE pattern (Figure 12, B) is interpreted as having been the result of later stage burial fluids, more specifically hydrothermal fluids, as will be explained. Pressure solution seams have been tied to dolomitization previously (Wanless, 1979). This study claimed that the dissolution of limestone provides sufficient Mg^{2+} to promote dolomitization in proximal strata. A solution seam above this dolomite in this thin section are thus proposed as a source of Mg^{2+} for the formation of dolomite (Wanless, 1979). More recently, a new dolomitization model linking pressure solution, dolomitization, and MVT-type mineralization was proposed by Merino and Canals (2011). In this model, calcite dissolution supersaturates

these brines with respect to dolomite. These brines then further infiltrate the calcite and pressure dissolve this calcite, forming dolomite. This reaction forms a positive feedback loop and causes self-acceleration until the available Mg is scavenged too quickly, resulting in the process shutting down. This results in abrupt contacts between limestone and dolomite. The abrupt transition (0.2m) between this less altered portion and the heavily dolomitized sample DV 4.4M, which is attributed to hydrothermal interaction, serves to act as evidence that this process has occurred at least at this outcrop if not regionally. The prevailing theory of calcite to dolomite replacement invokes dissolution of calcite followed by the precipitation of dolomite. Merino and Canals (2011) note that many petrographic analyses reveal that replacement cannot occur by dissolution-precipitation. In this study, the petrographic evidence of these samples and those of the overlying Ion Member interval seem to fit the Merino and Canals (2011) model.

The application of this model and its mechanics of abrupt limestone-dolostone transitions serves to act as an argument against Badiozamani's (1973) distinct limestone-dolomite transitions argument necessarily being indicative of Dorag dolomitization. The application of this mechanic to the hydrothermal dolomitization model at this outcrop may serve to provide greater insight into dolomite-limestone contacts and their formation in the UMV given more study.

5.4.3 Ion Member

Samples DV 4.4M, DV 5.3M, and DV 5.8M exhibit high Al, Th, and ∑REE consistent with contamination, therefore the REE patterns of these samples cannot be trusted as reliable indicators of diagenetic fluids (Figure 11). Some useful features are still evident in these patterns however. Petrographic evidence combined with information from previous literature and studies can still be used to make inferences regarding the nature and origin of this dolomite.

Based on petrographic analysis, the Ion interval samples DV 4.4M and DV 5.8M are extensively dolomitized, suggesting large volumes of fluid flow to support such extensive alteration. Within the REE suite, samples DV 4.4M and DV 5.8M are the only samples with a positive Ce anomaly (Figure 14). There exists no cause for Ce fractionation in siliciclastic contaminants, therefore this positive anomaly is likely not the result of contamination (Bayon et al., 2015). A positive Ce anomaly is indicative of heavily reducing conditions, which can occur as the result of a shift from Ce^{4+}/ Ce^{3+} redox equilibrium toward higher oxygen fugacity with warmer diagenetic fluid temperatures (Frimmel, 2009). The moderate to brightly luminescent inner zones of the dolomite in these samples are caused by high Mn^{2+} and low Fe^{2+} with respect to each other, indicative of low oxygen levels (Hiatt and Pufahl, 2014). CL patterns of these samples are similar to the dolomite patterns of type 1 (dull orange) and type 3 (red/ no luminescence) of the hydrothermal dolomite identified by Smith and Simo (1997) in the Prairie du Chien Group. In this study however, these samples occasionally exhibit a third outer zone of orange luminescence (Figure 6 and Figure 8, D). Petrographic analysis of these thin sections shows sulfide mineral replacement of many skeletal grains in these thin sections. Pyrite and marcasite are identified as minerals commonly precipitated by regional hydrothermal fluids (Tupas, 1950; Van Heyl et al., 1959), and the dark matter filling the intercrystalline pore space is potentially hydrothermally precipitated Fe-oxide, a feature noted in the overlying Galena Group (Gregg and Sibley, 1984). Furthermore, Ion Member strata have been shown to be influenced by hydrothermal fluids in many parts of the UMV (Agnew et al., 1956). These lines of evidence lend to the interpretation that these dolomites are hydrothermal in nature.

The sample between these two, DV 5.3M, is not as extensively dolomitized. Once again, the work by Merino and Canals (2011) which was explained earlier can be applied to this

sample. Dolomites in this sample are largely concentrated toward the upper portion of the sample. Thus, hydrothermal fluids were likely flowing through the rock directly overlying this sample, and this sample is the lower edge of the limestone-dolomite replacement front. These differing characteristics and the extent of dolomitization were likely controlled by the lithology and the extent and speed to which diagenetic fluids could penetrate due to permeability differences in the original rock (Deininger, 1964). Alternatively, the hydrothermal fluids could have followed higher permeability fractures or seams, leading to this interbedding of heavily dolomitized samples with samples not completely dolomitized.

Although the overwhelming evidence suggests that hydrothermal fluids affected dolomitization of at least some of the strata in this interval, several questions remain. What was the nature of the pre-existing carbonate material? This is difficult to accurately evaluate due to the extent of alteration of DV 4.4 and DV 5.8, effectively erasing the original texture and characteristics of the rocks. Smith and Simo (1997) noted that some of the precursor dolomite phases were overgrown, in the event that they were not replaced, by later hydrothermal dolomite. Gregg and Sibley (1984) identified Galena Group dolomites as hydrothermal in nature having partially neomorphosed precursor dolomite. It is possible that the inner zone of this dolomite was neomorphosed or replaced by later hydrothermal fluids. Hydrothermal replacement of non-dolomite precursor carbonate material is the preferred for several reasons. First, the inner zones of these dolomites responsible for the REE signature exhibit a positive Ce anomaly that could be the temperature controlled and related to warmer diagenetic fluids. The surrounding samples (DV 4.2M and DV 5.3M) do not exhibit a high degree of dolomitization. It seems unlikely that such high dolomite-limestone interbedding of precursor carbonate in such close stratigraphic proximity by any other depositional model than the hydrothermal mechanism applied.

The CL zonation of overgrowths creating the dully luminescent middle zonation and the occasionally occurring, more brightly luminescent outer zone are likely the result of the evolution of the hydrothermal fluid as dolomite overgrowth occurred. The dull/dark middle zone to moderately luminescent outer zone could be caused by the Fe^{2+} removal from the hydrothermal fluids before this zone. This could be the result of sulfide mineral precipitation or replacement, either marcasite or pyrite, removing Fe^{2+} from the fluids and shifting zoning characteristics from quenched luminescence to moderate luminescence (Hiatt and Pufahl, 2014). Deininger (1964) also found Fe zoning in hydrothermal dolomite of southwest Wisconsin in the Platteville Formation, stratigraphically lower than these samples.

Several studies have attributed the Ion Member and overlying Galena Group strata to hydrothermal dolomitization (Agnew et al., 1956; Gregg and Sibley, 1984; Sibley and Gregg, 1987). It is likely that these hydrothermal fluids flowed from the Illinois Basin in the south updip into the Wisconsin strata (Hall and Friedman, 1963; Heyl, 1969). These fluids were likely a mixture of high salinity basinal brines (Van Heyl et al., 1974). Timing can be constrained by Rb-Sr dating to Early Permian hydrothermal mineralization (270 Ma) associated with the Alleghenian/Ouachita orogeny (Brannon et al., 1992; Rowan et al., 1995).

5.5 INSIGHTS INTO DOLOMITIZATION AND RELATION TO PREVIOUS STUDIES

Petrographic and geochemical evidence from this study points to two depositional realms with dolomitization driven by several different mechanisms in the shallow burial realm (Figure 19). The second dolomitization model is that of hydrothermal dolomite.

The first stage, early burial dolomite, can be divided into several categories. Dolomites in the Carimona-Lower Guttenberg interval are burrow-associated and occur in greater size near K-

bentonite beds. This study argues that the K-bentonites provided a potential source of Mg from water-ash interaction to aid in dolomitization, and that burrow conditions, specifically SRBs, likely contributed to the formation of these dolomites. REE released from Fe-oxides during changing porewater redox conditions from oxic to anoxic, occurred in the shallow burial realm. This dolomitization model is consistent with burrow-related dolomitization presented by Corlett and Jones (2012) as well as the Fe-oxide associated REE pattern presented by (Gingras et al., 2004; Haley et al., 2004; Corlett and Jones, 2012; Freiburg et al., 2012 Baniak et al., 2013). The early burial dolomitization model, including precursor carbonate cores, is consistent with the interpretation of Smith and Simo (1997).

A similar early burial depositional model was applied to the two lower Guttenberg sample DV 2.0M and DV 3.5M. A portion of the dolomite inside a fossil in DV 3.5M likely formed very near the sediment-water interface, as indicated by the REE pattern. It also seems likely that this REE pattern is consistent with relatively shallow water that was potentially anoxic, seawater conditions supported by paleoceanographic and sequence stratigraphic studies (Ludvigson et a., 1996; Ludvigson et al., 2004). The sourcing of Mg and the nature of the water is problematic however. Dolomite in fossils was recognized by Van Tuyl (1914) who also attributed this dolomitization to a burial realm. The remaining dolomites of this interval, which are found in micritic matrices, were also attributed to a relatively early burial origin, matching the burial interpretation and petrographic and CL appearances of Platteville Formation dolomites from Asquith (1967) and Smith and Simo (1997).

Hydrothermal dolomitization, is exhibited in the upper portion of the sampled interval, upper portion of the Guttenberg Member and the sampled portion of the Ion Member. Hydrothermal dolomitization of these strata has been discussed previously (Agnew et al., 1956;

REE Patterns	Major and trace elements	Intervals	Diagenetic event
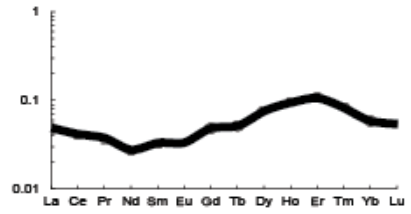	High Mn Low Ba High Fe Moderate Sr	DV 3.5 (1- 4, 7)	Early burial recrystallization of fossil
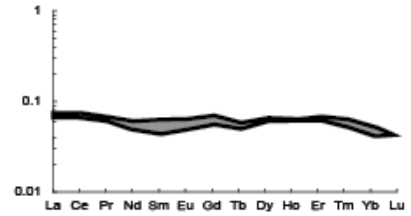	High Mn (DV 3.5) Moderate Ba High Fe Moderate Sr	DV 3.5 (5, 6, 8- 10) DV 2.0	Early burial micritic recrystallization
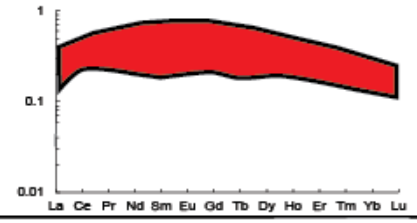	Moderate Mn (A.18) High Ba Moderate Fe High Sr	DV 0.0 DV A. 20 DV A. 18 DV P. 5	Early burial dolomitization in/around burrows, Fe-oxides influence of REE
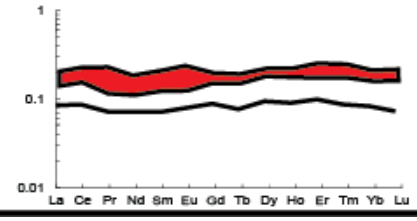	High Mn High Ba Low/Moderate Fe High Sr	DV 4.2 DV 4.4 DV 5.3 DV 5.8	Hydrothermal dolomitization of limestone

Figure 19- REE patterns and geochemical results compiled by specific interpretations associated with dolomite formation. Red REE patterns indicate samples that were above the 2% terrigenous contamination cutoff limit applied to data.

Smith and Simo, 1997). These portions are unique in that it seems that hydrothermal fluid selectively penetrated layers. Unlike the overlying Galena Group hydrothermal dolomite (Gregg and Sibley, 1984), this dolomite is interpreted as having replaced carbonates and not overgrowing or neomorphosing precursor dolomite. Furthermore, these samples exhibit evidence supporting a new hydrothermal dolomitization model (Merino and Canals, 2011) that invokes pressure solution-replacement rather than dissolution-precipitation.

Due to the location of this outcrop in relation to the Wisconsin Arch, this study cannot directly disprove that dolomitization on the Wisconsin Arch is not the result of Badiozamani's Dorag dolomitization. Based on Badiozamani's limestone-dolostone transition argument and the stratal geometries he used, if Dorag-type dolomitization were to have occurred at this outcrop, it would likely have been below the contact between the Quimby's Mill Formation and the Carimona Member or the Specht's Ferry Formation and the Guttenberg Formation. There is no large-scale dolomitization of the lower interval, however, and the occurrence of the burrow-associated dolomite is primarily above the Specht's Ferry-Guttenberg contact. Although, this could be because the location of this outcrop was too distal to the Wisconsin Arch to have experienced extensive dolomitization by mixing zone diagenesis. Furthermore, this study has found evidence of hydrothermal alteration by pressure-solution replacement which potentially overcomes Badiozamani's argument that distinct limestone-dolomite boundaries are only indicative of mixing zone dolomitization. More work regarding the importance and application of this recent dolomitization model is necessary. We can say, however, that there exists no dolomite formed at this outcrop that was interpreted as having formed by Dorag-type dolomitization. Thus Luczaj's argument that the Dorag model should not have been widely applied to dolomites of the southern Wisconsin area seems appropriate.

6. CONCLUSIONS

The petrographic and geochemical study of dolomites from the upper portion of the Platteville Formation and the Decorah of the Upper Mississippi Valley in southwestern Wisconsin has yielded additional evidence to support multiple phases of dolomitization in the studied strata. Petrographic and cathodoluminescence characteristics were combined with *in situ* geochemical REE analysis techniques of LA-ICP-MS on these dolomites to provide a new means of interpreting the history of dolomitization.

Although REE data can be a powerful tool in the analysis of paleoceanographic and diagenetic conditions in carbonates, this study had issues similar to other studies revealing that even minor contamination can greatly hinder the utility of the geochemical data toward providing evidence for interpretations. Despite this issue, petrographic and geochemical results were combined to reveal that the dolomite in the Carimona Member, Specht's Ferry Formation, and Guttenberg Formation, and Ion Member were largely formed in two realms, shallow burial and hydrothermal. These interpretations are similar to other studies of overlying and underlying Ordovician strata in the southern Wisconsin region.

The application of new analytical techniques and the evaluation of dolomitization in formations that had not previously been extensively studied have provided new insight into dolomitization, and particularly some mechanisms for dolomitization, that had not previously been applied. The findings of greatest note are the apparent link between dolomitization, particularly larger and greater numbers of dolomites than surrounding strata, and K-bentonites in the studied samples. This paper argues for a genetic link due to Mg release into water by ash-water leaching. These dolomites also exhibit "MREE" typical of Fe-oxide desorption in anoxic

porewater. Furthermore, evidence for a relatively new model for hydrothermal alteration seems to be applicable here. This pressure solution-replacement model of hydrothermal dolomitization will need more work in order to be applied to this outcrop or the region. Although it is impossible to disprove the Badiozamani “Dorag” model of dolomitization for all dolomites in the area given the distance of this outcrop from the Wisconsin Arch, none of these dolomites were attributed to a mixing zone diagenetic realm. Thus Luczaj’s argument that the “Dorag” model of deposition should not be widely applied to the majority of Lower and Middle Ordovician dolomites seems fair.

REFERENCES

Agnew, A. F., & Heyl Jr, A. V. (1946). Quimbys Mill, New Member of Platteville Formation, Upper Mississippi Valley: GEOLOGICAL NOTES. *American Association of Petroleum Geologists Bulletin, 30*(9), 1585-1587.

Agnew, A. F., Heyl, A. V., Behre, C. H., & Lyons, E. J. (1956). Stratigraphy of Middle Ordovician rocks in the zinc–lead district of Wisconsin, Illinois, and Iowa. *United States Geological Survey Professional Paper*, 274(K), 248-312.

Alibo, D. S., & Nozaki, Y. (1999). Rare earth elements in seawater: particle association, shale-normalization, and Ce oxidation. *Geochimica et Cosmochimica Acta, 63*(3), 363-372.

Asquith, G. B. (1967). The marine dolomitization of the Mifflin Member Platteville Limestone in southwest Wisconsin. *Journal of Sedimentary Research*, *37*(2), 311-326.

Azmy, K., Brand, U., Sylvester, P., Gleeson, S. A., Logan, A., & Bitner, M. A. (2011). Biogenic and abiogenic low-Mg calcite (bLMC and aLMC): Evaluation of seawater-REE composition, water masses and carbonate diagenesis. *Chemical Geology*, *280*(1), 180-190.

Azmy, K., Lavoie, D., Wang, Z., Brand, U., Al-Aasm, I., Jackson, S., & Girard, I. (2013). Magnesium-isotope and REE compositions of Lower Ordovician carbonates from eastern Laurentia: implications for the origin of dolomites and limestones. *Chemical Geology, 356* (2013), 64-75.

Azomani, E., Azmy, K., Blamey, N., Brand, U., & Al-Aasm, I. (2013). Origin of Lower Ordovician dolomites in eastern Laurentia: Controls on porosity and implications from geochemistry. *Marine and Petroleum Geology, 40*, 99-114.

Badiozamani, K. (1973). The Dorag dolomitization model--application to the Middle Ordovician of Wisconsin. *Journal of Sedimentary Research, 43*(4), 965-984.

Baniak, G. M., Gingras, M. K., & Pemberton, S. G. (2013). Reservoir characterization of burrow-associated dolomites in the Upper Devonian Wabamun Group, Pine Creek gas field, central Alberta, Canada. *Marine and Petroleum Geology, 48*, 275-292.

Banner, J. L., Hanson, G., & Meyers, W. (1988). Rare earth element and Nd isotopic variations in regionally extensive dolomites from the Burlington-Keokuk Formation (Mississippian): Implications for REE mobility during carbonate diagenesis. *Journal of Sedimentary Research, 58*(3), 415-432.

Barca, D., Belfiore, C. M., Crisci, G. M., La Russa, M. F., Pezzino, A., & Ruffolo, S. A. (2011). A new methodological approach for the chemical characterization of black crusts on building stones: a case study from the Catania city centre (Sicily, Italy). *Journal of Analytical Atomic Spectrometry, 26*(5), 1000-1011.

Bau, M. (1991). Rare-earth element mobility during hydrothermal and metamorphic fluid-rock interaction and the significance of the oxidation state of europium. *Chemical Geology, 93*(3), 219-230.

Bau, M., & Alexander, B. (2006). Preservation of primary REE patterns without Ce anomaly during dolomitization of Mid-Paleoproterozoic limestone and the potential re-establishment of marine anoxia immediately after the "Great Oxidation Event". *South African Journal of Geology*, *109*(1-2), 81-86.

Bau, M., Koschinsky, A., Dulski, P., & Hein, J. R. (1996). Comparison of the partitioning behaviours of yttrium, rare earth elements, and titanium between hydrogenetic marine ferromanganese crusts and seawater. *Geochimica et Cosmochimica Acta*, *60*(10), 1709-1725.

Bau, M., Möller, P., & Dulski, P. (1997). Yttrium and lanthanides in eastern Mediterranean seawater and their fractionation during redox-cycling. *Marine Chemistry, 56*(1), 123-131.

Bolhar, R., Kamber, B. S., Moorbath, S., Fedo, C. M., & Whitehouse, M. J. (2004). Characterisation of early Archaean chemical sediments by trace element signatures. *Earth and Planetary Science Letters, 222*(1), 43-60.

Bolhar, R., & Van Kranendonk, M. J. (2007). A non-marine depositional setting for the northern Fortescue Group, Pilbara Craton, inferred from trace element geochemistry of stromatolitic carbonates. *Precambrian Research, 155*(3), 229-250.

Brannon, J. C., Podosek, F. A., & McLimans, R. K. (1992). Alleghenian age of the Upper Mississippi Valley zinc–lead deposit determined by Rb–Sr dating of sphalerite. *Nature, 356*, 509-511.

Bullen, S. B., & Sibley, D. F. (1984). Dolomite selectivity and mimic replacement. *Geology, 12*(11), 655-658.

Carmichael, S. K., Ferry, J. M., & McDonough, W. F. (2008). Formation of replacement dolomite in the Latemar carbonate buildup, Dolomites, northern Italy: Part 1. Field relations, mineralogy, and geochemistry. *American Journal of Science, 308*(7), 851-884.

Certificate of Analysis: Standard Reference Material 1d. (2005, February 18). Retrieved January 4, 2016, from https://www-s.nist.gov/srmors/certificates/1D.pdf?CFID=36997806&CFTOKEN=8b8903d67739486-7364A516-CFFD-E7BD-3AA4E42FC3E8A169 .

Choi, Y. S. (1999). Sedimentologic and Sequence Stratigraphic Interpretation of a Mixed Carbon-Ate-Siliciclastic Ramp, Midcontinent Epeiric Sea, Middle to Upper Ordovician Decorah and Galena Formations, Wisconsin. *Society for Sedimentary Geology (SEPM), Special Publications of SEPM, 63,* 275-289.

Choi, Y. S., & Simo, J. (1998). Ramp facies and sequence stratigraphic models in an epeiric sea: the Upper Ordovician mixed carbonate-siliciclastic Glenwood and Platteville Formations, Wisconsin, USA. *Geological Society, London, Special Publications, 149*(1), 437-456.

Cocks, L. R. M., & Torsvik, T. H. (2011). The Palaeozoic geography of Laurentia and western Laurussia: a stable craton with mobile margins. *Earth-Science Reviews, 106*(1), 1-51.

Corlett, H. J., & Jones, B. (2012). Petrographic and geochemical contrasts between calcite-and dolomite-filled burrows in the Middle Devonian Lonely Bay Formation, Northwest Territories, Canada: Implications for dolomite formation in Paleozoic burrows. *Journal of Sedimentary Research, 82*(9), 648-663.

Deininger, R. W. (1964). Limestone-dolomite transition in the Ordovician Platteville Formation in Wisconsin. *Journal of Sedimentary Research, 34*(2), 281-288.

Duggen, S., Croot, P., Schacht, U., & Hoffmann, L. (2007). Subduction zone volcanic ash can fertilize the surface ocean and stimulate phytoplankton growth: Evidence from biogeochemical experiments and satellite data. *Geophysical Research Letters, 34*(1), 1-5.

Dunham, R. J. (1962). Classification of carbonate rocks according to depositional textures. *American Association of Petroleum Geologists Special Volumes, A038*(1962), 108-121.

Elderfield, H., & Sholkovitz, E. (1987). Rare earth elements in the pore waters of reducing nearshore sediments. *Earth and Planetary Science Letters, 82*(3), 280-288.

Fanton, K., & Holmden, C. (2007). Sea-level forcing of carbon isotope excursions in epeiric seas: implications for chemostratigraphy. *Canadian Journal of Earth Sciences, 44*(6), 807-818.

Flügel, E. (2004). *Microfacies of carbonate rocks: analysis, interpretation and application*. Berlin: Springer.

Freiburg, J. T., Fouke, B. W., & Lasemi, Z. (2012). *New Insights on Upper Mississippi Valley Mineralization based on Solution Cavities in the Ordovician Galena Group at the Conco Mine, North Aurora, Illinois, USA*. Illinois State Geological Survey, Prairie Research Institute., 2012.

Frimmel, H. E. (2009). Trace element distribution in Neoproterozoic carbonates as palaeoenvironmental indicator. *Chemical Geology*, *258*(3), 338-353.

Frogner, P., Gíslason, S. R., & Óskarsson, N. (2001). Fertilizing potential of volcanic ash in ocean surface water. *Geology*, *29*(6), 487-490.

Gingras, M. K., Pemberton, S. G., Muelenbachs, K., & Machel, H. (2004). Conceptual models for burrow-related, selective dolomitization with textural and isotopic evidence from the Tyndall Stone, Canada. *Geobiology*, *2*(1), 21-30.

Gromek, P., Gleeson, S. A., & Simonetti, A. (2012). A basement-interacted fluid in the N81 deposit, Pine Point Pb-Zn District, Canada: Sr isotopic analyses of single dolomite crystals. *Mineralium Deposita*, *47*(7), 749-754.

Haley, B. A., & Klinkhammer, G. P. (2003). Complete separation of rare earth elements from small volume seawater samples by automated ion chromatography: method development and application to benthic flux. *Marine Chemistry*, *82*(3), 197-220.

Haley, B. A., Klinkhammer, G. P., & McManus, J. (2004). Rare earth elements in pore waters of marine sediments. *Geochimica et Cosmochimica Acta*, *68*(6), 1265-1279.

Hall, W. E., & Friedman, I. (1963). Composition of fluid inclusions, Cave-in-Rock fluorite district, Illinois, and Upper Mississippi Valley zinc-lead district. *Economic Geology*, *58*(6), 886-911.

Hardie, L. A. (1987). PERSPECTIVES Dolomitization: A Critical View of some Current Views. *Journal of Sedimentary Research*, *57*(1), 166-183.

Hecht, L., Freiberger, R., Gilg, H. A., Grundmann, G., & Kostitsyn, Y. A. (1999). Rare earth element and isotope (C, O, Sr) characteristics of hydrothermal carbonates: genetic implications for dolomite-hosted talc mineralization at Göpfersgrün (Fichtelgebirge, Germany). *Chemical Geology*, *155*(1), 115-130.

Hellstrom, J., Paton, C., Woodhead, J., & Hergt, J. (2008). Iolite: software for spatially resolved LA-(quad and MC) ICPMS analysis. *Mineralogical Association of Canada short course series*, *40*, 343-348.

Heyl, A. (1969). Some aspects of genesis of zinc-lead-barite-fluorite deposits in the Mississippi Valley, USA. *Transactions of the Institution of Mining and Metallurgy. Section B–Applied Earth Science, 78*, 148-160.

Heyl, A., Landis, G., & Zartman, R. (1974). Isotopic evidence for the origin of Mississippi Valley-type mineral deposits: A review. *Economic Geology, 69*(6), 992-1006.

Heyl, A. V., & West, W. S. (1982). Outlying mineral occurrences related to the Upper Mississippi Valley mineral district, Wisconsin, Iowa, Illinois, and Minnesota. *Economic Geology, 77*(8), 1803-1817.

Hiatt, E., & Pufahl, P. Cathodoluminescence petrography of carbonate rocks: A review of applications for understanding diagenesis, reservoir quality, and pore system evolution. In Coulson, I. (ed.) Cathodoluminescence and its application to geoscience: *Mineralogical Association of Canada, Short Course Series, 45*, 75-96.

Holland, H. D., & Zimmermann, H. (2000). The Dolomite Problem Revisited1. *International Geology Review, 42*(6), 481-490.

Holland, S. M., & Patzkowsky, M. E. (1997). Distal orogenic effects on peripheral bulge sedimentation: Middle and Upper Ordovician of the Nashville Dome. *Journal of Sedimentary Research, 67*(2), 250-263.

Huff, W. D., Kolata, D. R., Bergström, S. M., & Zhang, Y. S. (1996). Large-magnitude Middle Ordovician volcanic ash falls in North America and Europe: dimensions, emplacement and post-emplacement characteristics. *Journal of Volcanology and Geothermal Research,73*(3), 285-301.

Jochum, K. P., Scholz, D., Stoll, B., Weis, U., Wilson, S. A., Yang, Q., . . . Andreae, M. O. (2012). Accurate trace element analysis of speleothems and biogenic calcium carbonates by LA-ICP-MS. *Chemical Geology, 318*, 31-44.

Johannesson, K. H., & Zhou, X. (1999). Origin of middle rare earth element enrichments in acid waters of a Canadian High Arctic lake. *Geochimica et Cosmochimica Acta, 63*(1), 153-165.

Kolata, D. R., Frost, J. K., & Huff, W. D. (1987). Chemical correlation of K-bentonite beds in the Middle Ordovician Decorah Subgroup, upper Mississippi Valley. *Geology, 15*(3), 208-211.

Kolata, D. R., Huff, W. D., & Bergström, S. M. (2001). The Ordovician Sebree Trough: An oceanic passage to the Midcontinent United States. *Geological Society of America Bulletin, 113*(8), 1067-1078.

Kučera, J., Cempírek, J., Dolníček, Z., Muchez, P., & Prochaska, W. (2009). Rare earth elements and yttrium geochemistry of dolomite from post-Variscan vein-type mineralization of the Nízký Jeseník and Upper Silesian Basins, Czech Republic. *Journal of Geochemical Exploration, 103*(2), 69-79.

Leonard, A. (1906). Geology of Clayton County. *Iowa Geological Survey Annual Report, 16*(1), 213-318.

Li, J., Jiang, X. Y., Xu, J. F., Zhong, L. F., Wang, X. C., Wang, G. Q., & Zhao, P. P. (2014). Determination of Platinum-Group Elements and Re-Os Isotopes using ID-ICP-MS and N-TIMS from a Single Digestion after Two-Stage Column Separation. *Geostandards and Geoanalytical Research, 38*(1), 37-50.

Luczaj, J. A. (2006). Evidence against the Dorag (mixing-zone) model for dolomitization along the Wisconsin arch: A case for hydrothermal diagenesis. *AAPG Bulletin, 90*(11), 1719-1738.

Lüders, V., Möller, P., & Dulski, P. (1993). REE fractionation in carbonates and fluorite. *Monograph series on mineral deposits, 30*(9), 133-150.

Ludvigson, G. A., Bunker, B. J., & Section, S. G. L. (2005). *Facets of the Ordovician Geology of the Upper Mississippi Valley Region: Guidebook for the 35th Annual Field Conference of the Great Lakes Section, Society for Sedimentary Geology (SEPM) September 23-25, 2005*: Iowa Department of Natural Resources Geological Survey.

Ludvigson, G. A., Jacobson, S. R., Witzke, B. J., & González, L. A. (1996). Carbonate component chemostratigraphy and depositional history of the Ordovician Decorah Formation, Upper Mississippi Valley. *Geological Society of America, Special Papers, 306*, 67-86.

Ludvigson, G. A., Witzke, B. J., González, L. A., Carpenter, S. J., Schneider, C. L., & Hasiuk, F. (2004). Late Ordovician (Turinian–Chatfieldian) carbon isotope excursions and their stratigraphic and paleoceanographic significance. *Palaeogeography, Palaeoclimatology, Palaeoecology, 210*(2), 187-214.

McHargue, T. R., & Price, R. C. (1982). Dolomite from clay in argillaceous or shale-associated marine carbonates. *Journal of Sedimentary Research, 52*(3), 873-886.

McKenzie, J. A., & Vasconcelos, C. (2009). Dolomite Mountains and the origin of the dolomite rock of which they mainly consist: historical developments and new perspectives. *Sedimentology, 56*(1), 205-219.

McLaughlin, P. I., Emerson, N., Witzke, B., Sell, B., & Emsbo, P. (2011). Distal signatures of Late Ordovician oceanic anoxia—New data from a classic epeiric ramp transect. *Field Guides, 24*, 259-284.

McLennan, S. (1989). Rare earth elements in sedimentary rocks; influence of provenance and sedimentary processes. *Reviews in Mineralogy and Geochemistry, 21*(1), 169-200.

Merino, E., & Canals, À. (2011). Self-accelerating dolomite-for-calcite replacement: Self-organized dynamics of burial dolomitization and associated mineralization. *American Journal of Science, 311*(7), 573-607.

Nothdurft, L. D., Webb, G. E., & Kamber, B. S. (2004). Rare earth element geochemistry of Late Devonian reefal carbonates, Canning Basin, Western Australia: confirmation of a seawater REE proxy in ancient limestones. *Geochimica et Cosmochimica Acta, 68*(2), 263-283.

Panchuk, K. M., Holmden, C. E., & Leslie, S. A. (2006). Local controls on carbon cycling in the Ordovician midcontinent region of North America, with implications for carbon isotope secular curves. *Journal of Sedimentary Research, 76*(2), 200-211.

Paton, C., Hellstrom, J., Paul, B., Woodhead, J., & Hergt, J. (2011). Iolite: Freeware for the visualisation and processing of mass spectrometric data. *Journal of Analytical Atomic Spectrometry, 26*(12), 2508-2518.

Qing, H., & Mountjoy, E. W. (1994). Formation of coarsely crystalline, hydrothermal dolomite reservoirs in the Presqu'ile Barrier, Western Canada Sedimentary Basin. *AAPG Bulletin, 78*(1), 55-77.

Quinton, P. C., Herrmann, A. D., Leslie, S. A., & MacLeod, K. G. (2015). Carbon cycling across the southern margin of Laurentia during the Late Ordovician. *Palaeogeography, Palaeoclimatology, Palaeoecology*. (In Press).

Read, David, Andreoli, M. A., Knoper, M., Williams, C. T., & Jarvis, N. (2002). The degradation of monazite Implications for the mobility of rare-earth and actinide elements during low-temperature alteration. *European Journal of Mineralogy, 14*(3), 487-498.

Rowan, E., & Goldhaber, M. (1995). Duration of mineralization and fluid-flow history of the Upper Mississippi Valley zinc-lead district. *Geology, 23*(7), 609-612.

Scotese, C. R. (2004). A continental drift flipbook. *The Journal of Geology, 112*(6), 729-741.

Scotese, C. R. and McKerrow, W.S. (1990). Revised World maps and introduction. *Geological Society, London, Memoirs, 12*, 1-21.

Sell, B., Ainsaar, L., & Leslie, S. (2013). Precise timing of the Late Ordovician (Sandbian) super-eruptions and associated environmental, biological, and climatological events. *Journal of the Geological Society,170*(5), 711-714.

Sell, B. K., Samson, S. D., Mitchell, C. E., McLaughlin, P. I., Koenig, A. E., & Leslie, S. A. (2015). Stratigraphic correlations using trace elements in apatite from Late Ordovician (Sandbian-Katian) K-bentonites of eastern North America. *Geological Society of America Bulletin*, B31194-1.

Shields, G. A., & Webb, G. E. (2004). Has the REE composition of seawater changed over geological time? *Chemical Geology, 204*(1), 103-107.

Sholkovitz, E., & Shen, G. T. (1995). The incorporation of rare earth elements in modern coral. *Geochimica et Cosmochimica Acta, 59*(13), 2749-2756.

Sholkovitz, E. R. (1993). The geochemistry of rare earth elements in the Amazon River estuary. *Geochimica et Cosmochimica Acta, 57*(10), 2181-2190.

Sholkovitz, E. R., Landing, W. M., & Lewis, B. L. (1994). Ocean particle chemistry: the fractionation of rare earth elements between suspended particles and seawater. *Geochimica et Cosmochimica Acta, 58*(6), 1567-1579.

Sibley, D. F., & Gregg, J. M. (1987). Classification of dolomite rock textures. *Journal of Sedimentary Research, 57*(6), 967-975.

Simo, J. T., Emerson, N. R., Byers, C. W., & Ludvigson, G. A. (2003). Anatomy of an embayment in an Ordovician epeiric sea, Upper Mississippi Valley, USA. *Geology, 31*(6), 545-548.

Smith, G. L. (1991). *Sequence stratigraphy and diagenesis of the Lower Ordovician Prairie du Chien Group on the Wisconsin arch and in the Michigan Basin*: University of Wisconsin—Madison, 265.

Smith, G. L., & Simo, J. A. (1997). Carbonate diagenesis and dolomitization of the lower Ordovician Prairie du Chien Group. *Geoscience Wisconsin, 16*, 1-16.

Tonarini, S., Pennisi, M., Adorni-Braccesi, A., Dini, A., Ferrara, G., Gonfiantini, R., . . . Gröning, M. (2003). Intercomparison of boron isotope and concentration measurements. Part I: Selection, preparation and homogeneity tests of the intercomparison materials. *Geostandards Newsletter, 27*(1), 21-39.

Torsvik, T. H., & Cocks, L. R. M. (2009). The Lower Palaeozoic palaeogeographical evolution of the northeastern and eastern peri-Gondwanan margin from Turkey to New Zealand. *Geological Society, London, Special Publications, 325*(1), 3-21.

Tupas, M. H. (1950). *The significance of mineral relationships in the Upper Mississippi Valley lead-zinc ores*. University of Wisconsin-Madison.

Van Heyl, A. (1959). *The geology of the Upper Mississippi Valley zinc-lead district* (Vol. 309): US Government Printing Office.

Van Tuyl, F. (1914). The Origin of Dolomite; Iowa Geological Survey, Vol. *XXV, Annual Report*, 251-422.

Wang, L., Hu, W., Wang, X., Cao, J., & Chen, Q. (2014). Seawater normalized REE patterns of dolomites in Geshan and Panlongdong sections, China: Implications for tracing dolomitization and diagenetic fluids. *Marine and Petroleum Geology, 56*, 63-73.

Wang, X., Jin, Z., Hu, W., Zhang, J., Qian, Y., Zhu, J., & Li, Q. (2009). Using in situ REE analysis to study the origin and diagenesis of dolomite of Lower Paleozoic, Tarim Basin. *Science in China Series D: Earth Sciences, 52*(5), 681-693.

Wanless, H. R. (1979). Limestone response to stress: pressure solution and dolomitization. *Journal of Sedimentary Research, 49*(2), 437-462.

Warren, J. (2000). Dolomite: occurrence, evolution and economically important associations. *Earth-Science Reviews, 52*(1), 1-81.

Whitaker, F. F., Smart, P. L., & Jones, G. D. (2004). Dolomitization: from conceptual to numerical models. *Geological Society, London, Special Publications, 235*(1), 99-139.

Witham, C. S., Oppenheimer, C., & Horwell, C. J. (2005). Volcanic ash-leachates: a review and recommendations for sampling methods. *Journal of Volcanology and Geothermal Research, 141*(3), 299-326.

Witzke, B., & Ludvigson, G. (2005). The Ordovician Galena Group in Iowa and its regional stratigraphic relationships. *Facets of Ordovician geology of the Upper Mississippi Valley region. Edited by G. Ludvigson and B. Bunker. Iowa Geological Survey, Guidebook Series*(24).

Xuefeng, Z., Wenxuan, H., Zhijun, J., Juntao, Z., Yixiong, Q., Jingquan, Z., . . . Xiaomin, X. (2008). REE compositions of Lower Ordovician dolomites in Central and North Tarim Basin, NW China: A potential REE proxy for ancient seawater. *Acta Geologica Sinica (English edition), 82*(3), 610-621.

Yoo, C. M., Gregg, J. M., & Shelton, K. L. (2000). Dolomitization and dolomite neomorphism: Trenton and Black River limestones (middle Ordovician) northern Indiana, USA. *Journal of Sedimentary Research, 70*(1), 265-274.

Young, S. A., Saltzman, M. R., & Bergström, S. M. (2005). Upper Ordovician (Mohawkian) carbon isotope (δ13C) stratigraphy in eastern and central North America: Regional expression of a perturbation of the global carbon cycle. *Palaeogeography, Palaeoclimatology, Palaeoecology, 222*(1-2), 53-76.

Zhang, W., Guan, P., Jian, X., Feng, F., & Zou, C. (2014). In situ geochemistry of Lower Paleozoic dolomites in the northwestern Tarim basin: Implications for the nature, origin, and evolution of diagenetic fluids. *Geochemistry, Geophysics, Geosystems., 15*, 2744-2764.

Zhao, H., & Jones, B. (2012). Distribution and interpretation of rare earth elements and yttrium in Cenozoic dolostones and limestones on Cayman Brac, British West Indies. Sedimentary Geology, *284*, 26-38.

APPENDIX 1: LITHOLOGICAL CLASSIFICATIONS AND CL PARAMETERS

Sample #	cm from Deicke	Classification	CL Pressure (mTorr)	CL Current (mA)	CL Voltage (kV)
5.8	787.7	dolostone	34	0.67	-4.9
5.3	747.7	grainstone	34	0.68	-4.9
4.4	657.7	dolostone	32	0.563	-5.0
4.2	637.7	wackestone	33	0.59	-5.0
3.5	567.7	wackestone (floatstone)	35	0.64	-4.8
2.0	417.7	wackestone	32	0.60	-5.2
0.0	217.7	mudstone	36	0.65	-4.9
A. 20	204.6	wackestone	36	0.67	-4.9
A. 18	183.2	wackestone	36	0.66	-4.8
P. 5	-15.9	packstone	37	0.486	-5.5

APPENDIX 2: NIST SRM 1D AND IAEA B7 EXPERIMENT AND REFERENCE DATA

	NIST SRM 612		NIST SRM 1d				IAEA B7		
	Reference Value	Reference value	Measured			Reference value	Measured		
Element			N= 77	%RSD	%RD		N= 75	%RSD	%RD
Mg	77	1815*	2049	10.39	12.87	1845	1837	14.58	0.45
Al	11167	2784*	3049	17.12	9.53		220	34.82	
Sr	78.4*	273*	273	10.53	0.13	224	220	12.05	1.62
Y	38	4.18	3.62	18.25	13.41	7.2	6.4	16.03	11.57
Ba	39.7	29.2	29.2	30.70	0.16	6.7	7.1	16.25	5.73
La	35.8	3.57	2.75	10.37	23.01	4.7	5.5	11.17	17.00
Ce	38.7	4.03	3.56	12.21	11.78	1.44	1.45	13.76	0.61
Pr	37.2	0.54	0.53	13.83	2.60	0.9	0.96	14.64	6.22
Nd	35.9	2.62	2.09	15.34	20.35	3.9	4.37	14.88	12.10
Sm	38.1	0.51	0.40	15.40	21.46	0.75	0.82	16.65	9.73
Eu	35	0.1	0.08	13.35	15.81	0.18	0.19	16.25	3.21
Gd	36.7	0.43	0.41	15.11	4.74	0.84	0.89	17.36	5.89
Tb	36	0.08	0.06	16.71	25.20	0.13	0.13	17.47	0.87
Dy	36	0.52	0.38	16.49	26.28	0.83	0.85	17.56	2.46
Ho	38	0.09	0.08	17.45	9.96	0.18	0.18	16.69	1.26
Er	38	0.34	0.24	16.25	29.21	0.49	0.51	16.20	3.37
Tm	38	0.04	0.03	16.48	21.53	0.07	0.07	18.97	4.93
Yb	39.2	0.31	0.19	17.52	38.92	0.38	0.40	16.26	4.15
Lu	36.9	0.04	0.03	18.84	31.20	0.07	0.06	17.07	18.77
Th	37.79*	0.46	0.40	17.95	13.91	0.1	0.11	20.66	7.73

All values listed are in ppm. NIST SRM 612 and NIST SRM 1d reference values with * are from NIST Certificates. denote certified values. All other SRM 1d values are from LA-ICP-MS analysis results (Barca, 2011), and all other SRM 612 values are from GEOREM database. These values are informational only. IAEA B7 reference values are from EPMA (Mg, Sr, Ba) and LA-ICP-MS (trace elements) analysis results in Tonarini et al. (2003). IAEA B7 is not a certified standard. All values are informational only. Measured values are an average of all ablation runs. "N" indicates the number of ablations. %RSD, indicating variance within experimental data, was calculated using the formula %RSD=(Average / Standard Deviation) x 100. %RD, indicating accuracy relative to reference values, was calculated using the formula %RD=(Average - Reference Value / Reference Value) x 100.

APPENDIX 3: INDIVIDUAL DOLOMITE GEOCHEMICAL DATA

Sample Interval	Dolomite Number	Measured Isotope																				
		^{27}Al	^{55}Mn	^{57}Fe	^{88}Sr	^{90}Zr	^{137}Ba	^{139}La	^{140}Ce	^{141}Pr	^{146}Nd	^{147}Sm	^{153}Eu	^{157}Gd	^{159}Tb	^{163}Dy	^{165}Ho	^{166}Er	^{169}Tm	^{172}Yb	^{175}Lu	^{232}Th
DV 5.8	Dolomite 1	1380	1430	3200	88	4.4	6.4	3.75	9.2	0.61	2.7	0.437	0.085	0.52	0.073	0.58	0.125	0.48	0.058	0.298	0.061	0.367
	Dolomite 6	860	1740	4850	46.1	2.85	5.4	4.09	15.7	1.48	6.5	1.02	0.186	0.9	0.127	0.85	0.185	0.65	0.066	0.451	0.065	1.04
	Dolomite 8	440	1790	3690	96	1.05	5.9	3.5	8.1	0.6	2.56	0.403	0.092	0.44	0.067	0.58	0.12	0.401	0.061	0.363	0.06	0.16
	Dolomite 10	990	1730	3440	63	2.09	2.8	2.38	5.9	0.53	2.24	0.363	0.069	0.42	0.061	0.54	0.097	0.343	0.052	0.287	0.059	0.248
	Dolomite 11	10300	1440	3930	63	22	19.6	6.5	10.4	0.92	3.13	0.55	0.123	0.574	0.098	0.94	0.156	0.58	0.098	0.59	0.104	0.92
	Dolomite 12	3600	1690	2930	42.5	7.7	7.3	3.41	8.1	0.91	2.58	0.439	0.109	0.52	0.074	0.63	0.115	0.438	0.062	0.359	0.068	0.47
	Dolomite 13	1590	1330	2420	71	6.4	9	3.31	10.6	0.73	2.73	0.44	0.092	0.403	0.063	0.48	0.079	0.345	0.055	0.283	0.043	0.396
	Dolomite 14	450	1720	2540	116	1.28	2.4	3	6.8	0.52	1.64	0.4	0.065	0.28	0.056	0.433	0.112	0.387	0.051	0.32	0.053	0.208
	Dolomite 18	890	1350	2260	63.7	2.96	3.39	4.2	10.3	0.94	3.52	0.62	0.119	0.563	0.087	0.633	0.126	0.444	0.0558	0.369	0.059	0.31
	Dolomite 20	5900	1440	2950	81	36	14	4.22	12.5	0.87	4.4	0.62	0.134	0.47	0.075	0.67	0.135	0.43	0.063	0.73	0.055	0.85
	Dolomite 21	7300	1510	3280	72	17.9	23.7	7.5	14.5	1.32	4.2	0.88	0.198	0.7	0.127	0.84	0.18	0.65	0.094	0.61	0.109	1.29
	Dolomite 22	2420	1760	2400	123	7.2	10.7	2.92	10.4	0.82	2.27	0.59	0.112	0.67	0.089	0.66	0.141	0.52	0.065	0.41	0.071	1.08
	Dolomite 23	11500	2510	4500	85	28.2	27.9	5.7	12.8	1.08	3.9	1.6	0.167	0.79	0.18	1.15	0.175	0.83	0.102	0.68	0.146	1.72
	Dolomite 24	1330	1300	2460	110	6.2	7	4.47	12.8	1.11	3.99	0.7	0.133	0.71	0.097	0.71	0.158	0.562	0.072	0.431	0.07	1.1
	Dolomite 25	2380	1820	3200	73	6.7	7.5	4.77	8.3	1	2.52	0.56	0.112	0.6	0.098	0.7	0.167	0.65	0.059	0.47	0.061	0.543
	Dolomite 26	730	1820	3140	87	2.99	3.31	4.46	11.6	0.84	3.33	0.65	0.126	0.62	0.12	0.86	0.157	0.63	0.076	0.469	0.092	0.408
	Dolomite 28	4800	2170	4120	60	15.7	10.5	5.64	15.4	1.08	4.6	0.71	0.15	0.8	0.131	0.8	0.153	0.61	0.093	0.57	0.088	1.18
	Dolomite 29	1290	2040	3570	78	3.54	3.5	4.3	6.7	0.56	2.44	0.381	0.078	0.491	0.083	0.66	0.132	0.466	0.09	0.388	0.065	0.418
	Dolomite 30	430	2070	3510	102	2.9	1.49	3.35	7	0.62	2.5	0.35	0.076	0.51	0.081	0.68	0.14	0.52	0.06	0.479	0.0496	0.274
	Dolomite 31	510	1740	3410	101	1.7	1.93	4.1	7.8	0.67	2.28	0.375	0.067	0.407	0.075	0.6	0.116	0.342	0.058	0.371	0.053	0.43
	Dolomite 33	3310	1810	4500	59	7.9	19.9	3.31	6.9	0.64	2.79	0.49	0.096	0.54	0.084	0.625	0.156	0.77	0.067	0.443	0.091	0.47
	Dolomite 40	510	1890	2800	133	1.48	3.1	3.64	9.6	0.74	2.03	0.48	0.079	0.42	0.078	0.57	0.133	0.5	0.065	0.39	0.059	0.41
	Average	2859.5	1732	3322.7	82.423	8.6	8.94	4.21	10.06	0.85	3.13	0.594	0.112	0.561	0.092	0.691	0.139	0.525	0.0692	0.444	0.0719	0.65
	St. Dev.	3214.8	297.9	728.53	24.381	9.49	7.53	1.22	2.923	0.26	1.109	0.283	0.038	0.152	0.0293	0.163	0.027	0.135	0.0158	0.124	0.0242	0.424

INDIVIDUAL DOLOMITE GEOCHEMICAL DATA (CONTINUED)

DV 5.3	Dolomite 4	3100	1030	1130	129	5	7.3	5	9	0.74	3.13	0.46	0.123	0.46	0.06	0.48	0.097	0.289	0.056	0.275	0.04	0.332
	Dolomite 5	5000	720	1340	97	13.8	15.2	7	20.7	1.68	6.2	1.07	0.247	0.9	0.133	1.02	0.198	0.483	0.071	0.448	0.061	0.66
	Dolomite 6	1290	583	1040	101	3.48	5.7	6.55	17.5	1.44	6.43	0.79	0.204	0.73	0.108	0.77	0.156	0.474	0.0596	0.351	0.0462	0.271
	Dolomite 7	1360	365	890	46.7	3.45	7.6	6.3	17.3	1.44	6.2	0.83	0.208	0.74	0.105	0.66	0.127	0.296	0.051	0.309	0.038	0.246
	Dolomite 8	1900	469	930	87	4.09	7.1	10.6	27.5	2.35	7.5	1.32	0.305	1.16	0.171	0.95	0.171	0.527	0.0623	0.374	0.0499	0.285
	Dolomite 9	1960	660	860	77	8.2	10.1	6.26	20.6	1.51	4.72	0.91	0.2	0.83	0.112	0.81	0.164	0.44	0.049	0.325	0.049	0.41
	Dolomite 11	5600	482	1090	81	9	14.2	7.76	18.4	1.46	5.91	0.99	0.201	0.89	0.105	0.8	0.142	0.497	0.0735	0.466	0.071	0.717
	Dolomite 15	2370	600	730	180	6	8.7	4.8	10.6	1.05	3.4	0.68	0.101	0.392	0.067	0.369	0.096	0.263	0.049	0.24	0.0354	0.353
	Dolomite 17	4180	500	1200	103	9.2	15.5	7.3	16.9	1.79	5.31	0.9	0.201	0.72	0.105	0.76	0.153	0.436	0.053	0.379	0.06	0.53
	Dolomite 18	1090	1070	1370	148	3.27	5.3	8.4	19.3	1.42	4.74	0.83	0.205	0.75	0.101	0.6	0.158	0.336	0.044	0.31	0.044	0.285
	Dolomite 21	3300	850	650	138	5.8	9.3	7.2	19.4	2.34	6.4	1.14	0.26	1.18	0.156	1.19	0.191	0.53	0.078	0.52	0.075	2.24
	Dolomite 22	11500	840	1470	160	23.6	32.5	9.6	19.4	1.97	7.5	1.31	0.303	1.11	0.154	1.07	0.193	0.62	0.094	0.64	0.096	1.24
	Dolomite 23	2470	920	900	212	5.7	14.1	8.8	17.6	1.54	4.1	0.89	0.164	0.76	0.102	0.74	0.141	0.44	0.05	0.4	0.068	0.58
	Dolomite 25	2170	771	511	139	5.6	8.3	6.61	15.4	1.48	4.31	0.83	0.156	0.83	0.107	0.753	0.163	0.476	0.07	0.405	0.07	0.59
	Dolomite 28	6600	501	1010	73	10.9	21.8	8.6	19.4	2.01	6.2	1.04	0.272	1.04	0.112	0.88	0.162	0.482	0.06	0.457	0.073	0.6
	Dolomite 30	1170	880	640	163	2.92	15.3	6.82	12.8	1.62	4.65	0.81	0.172	0.661	0.093	0.574	0.131	0.363	0.0524	0.336	0.058	0.256
	Dolomite 32	1290	387	582	69.5	2.42	6	11.9	25	3.28	9.8	1.88	0.407	1.52	0.224	1.3	0.246	0.625	0.079	0.524	0.073	0.306
	Dolomite 33	2550	700	660	107	4.29	8.1	7.1	13.3	1.59	4.53	0.98	0.231	0.8	0.115	0.72	0.146	0.369	0.056	0.316	0.055	0.446
	Dolomite 34	1390	1030	640	246	5.3	7.1	5.66	11.9	1.51	3.15	0.63	0.169	0.516	0.09	0.532	0.136	0.39	0.061	0.394	0.062	0.63
	Dolomite 35	9500	650	1030	115	14.1	18.8	11.4	23.5	2.96	8.9	1.39	0.34	1.33	0.165	1.17	0.239	0.61	0.096	0.57	0.106	0.95
	Dolomite 36	720	910	722	123	1.7	3.41	7.29	13.6	1.39	4.35	0.95	0.219	0.8	0.121	0.8	0.176	0.453	0.067	0.41	0.063	0.267
	Dolomite 37	890	605	810	79.6	2.01	3.67	12.8	25.7	2.86	9.2	1.92	0.373	1.52	0.241	1.28	0.217	0.565	0.077	0.58	0.083	0.284
	Dolomite 38	2290	520	560	87	6.1	7.7	5.7	12.3	1.6	3.24	0.76	0.164	0.58	0.095	0.6	0.096	0.283	0.043	0.33	0.054	0.44
	Dolomite 39	700	1090	780	146	1.28	5.6	6.6	13.8	1.36	4.9	0.82	0.137	0.69	0.096	0.59	0.132	0.317	0.063	0.351	0.044	0.298
	Average	3100	714	898	121	6.55	10.8	7.8	17.5	1.77	5.62	1.01	0.22	0.87	0.12	0.81	0.160	0.44	0.06	0.40	0.061	0.55
	St Dev	2773	222	270	48	5.0	6.70	2.1	4.9	0.60	1.90	0.35	0.078	0.303	0.044	0.254	0.04	0.109	0.014	0.103	0.018	0.435
DV 4.4	Dolomite 1	236			190		2.23	4.81	13.2	1.15	4.6	0.65	0.126	0.58	0.104	0.63	0.153	0.456	0.06	0.368	0.056	0.213
	Dolomite 2	440			100		2.7	4.65	13.4	1.07	3.9	0.61	0.124	0.553	0.093	0.61	0.125	0.385	0.047	0.319	0.0469	0.178
	Dolomite 5	2600			119		5.9	8.3	28	2.05	6	1.2	0.266	1.12	0.175	1.06	0.185	0.513	0.078	0.417	0.074	1.89
	Dolomite 7	570			164		2.3	5.3	12.9	1.06	5.3	0.68	0.172	0.65	0.108	0.66	0.137	0.38	0.065	0.41	0.054	0.61
	Dolomite 8	2100			105		6.8	5.5	13.6	1.12	3.54	0.53	0.107	0.54	0.085	0.56	0.122	0.384	0.068	0.303	0.044	0.36
	Dolomite 10	2040			93		5.9	5.4	10.3	1.16	3.9	0.57	0.118	0.62	0.094	0.59	0.119	0.38	0.052	0.298	0.044	0.365
	Dolomite 11	340			110		1.44	4.9	11.1	1.02	3.26	0.5	0.099	0.52	0.093	0.68	0.147	0.57	0.068	0.41	0.047	0.178
	Dolomite 13	440			132		2.33	4.8	10.7	0.93	3.41	0.45	0.136	0.69	0.11	0.61	0.173	0.55	0.086	0.45	0.064	0.21
	Dolomite 14	520			106		3	5.4	13.7	0.99	3.25	0.457	0.117	0.61	0.092	0.71	0.175	0.544	0.061	0.473	0.075	0.409
	Dolomite 15	1750			133		10	6.8	17.6	1.51	5.2	0.75	0.182	0.7	0.11	0.83	0.146	0.506	0.075	0.61	0.065	0.419
	Dolomite 16	1100			124		2.7	5.9	12	0.99	3.68	0.55	0.13	0.59	0.108	0.74	0.17	0.491	0.078	0.48	0.064	0.419
	Dolomite 17	2320			104		6.3	7.3	13.8	1.46	4.52	0.78	0.211	0.86	0.138	0.87	0.151	0.6	0.072	0.515	0.076	0.549
	Dolomite 19	890			98		5.3	5.7	17	1.06	3.9	0.69	0.139	0.59	0.093	0.78	0.166	0.54	0.088	0.64	0.102	0.43

INDIVIDUAL DOLOMITE GEOCHEMICAL DATA (CONTINUED)

	Dolomite 21	660			77		2.61	6.3	15.2	1.23	4.12	0.68	0.142	0.7	0.126	0.76	0.158	0.48	0.062	0.355	0.057	0.32
	Dolomite 23	3400			90		7.4	7.7	15.1	1.66	5.7	1.15	0.237	1.11	0.135	1.01	0.213	0.78	0.086	0.52	0.062	1.36
	Dolomite 27	357			196		2.37	7.7	17.2	1.35	5.5	0.81	0.181	0.85	0.151	1	0.229	0.7	0.099	0.53	0.089	0.64
	Dolomite 32	340			138		2.23	6.6	15.4	1.62	3.96	0.63	0.133	0.71	0.112	0.89	0.184	0.6	0.073	0.54	0.053	0.53
	Dolomite 33	322			88		1.97	5.58	9.8	1.27	5.2	0.94	0.188	1.03	0.163	1.26	0.292	0.85	0.122	0.59	0.099	1.92
	Dolomite 38	2800			113		5.7	5.7	12.5	1.21	4.1	0.7	0.144	0.67	0.125	0.97	0.197	0.67	0.09	0.52	0.081	0.73
	Dolomite 39	1250			86		6.2	6.7	10.9	1.12	4.7	0.75	0.139	0.78	0.125	0.82	0.211	0.584	0.087	0.45	0.071	0.75
	Average	1223.8			118.3		4.27	6.05	14.17	1.25	4.387	0.704	0.155	0.724	0.117	0.802	0.173	0.548	0.0759	0.46	0.0662	0.624
	St. Dev.	993			33		2.38	1.08	4.0	0.28	0.85	0.20	0.04	0.18	0.03	0.19	0.04	0.13	0.02	0.1	0.017	0.513
DV 4.2	Dolomite 2	680			52.1	1.34	5.54	3.34	4.99	0.52	1.81	0.353	0.065	0.45	0.053	0.529	0.093	0.281	0.0314	0.169	0.0267	0.237
	Dolomite 4	910			62.9	2.53	5.9	2.62	6.8	0.66	2.1	0.293	0.072	0.394	0.0499	0.352	0.082	0.205	0.026	0.148	0.03	0.225
	Dolomite 6	1300			66	4.5	7.3	3.05	6.9	0.54	2.21	0.341	0.092	0.307	0.036	0.428	0.083	0.252	0.031	0.147	0.0314	0.225
	Dolomite 7	970			66	1.6	5.58	2.93	6.13	0.57	2.78	0.375	0.07	0.361	0.058	0.372	0.076	0.242	0.0386	0.142	0.033	0.252
	Dolomite 8	838			72	1.91	6	3.5	6.52	0.63	2.38	0.5	0.08	0.47	0.064	0.499	0.108	0.289	0.0391	0.178	0.036	0.251
	Dolomite 9	1050			56.5	3.3	5.27	2.57	5.44	0.5	1.77	0.302	0.068	0.324	0.051	0.408	0.072	0.27	0.026	0.152	0.0266	0.238
	Dolomite 10	669			99	2.11	5.6	3.61	8	0.68	2.63	0.316	0.093	0.42	0.069	0.449	0.079	0.275	0.037	0.147	0.0242	0.18
	Dolomite 11	703			68.1	1.93	4.19	5.4	8.2	0.82	3.7	0.55	0.12	0.517	0.065	0.451	0.089	0.287	0.0309	0.196	0.0293	0.345
	Dolomite 13	688			58.5	1.75	3.56	2.79	5.39	0.49	1.87	0.332	0.073	0.289	0.0451	0.342	0.076	0.205	0.0288	0.181	0.0254	0.13
	Dolomite 15	1070			67.7	2.35	5.24	3.56	5.73	0.62	2.3	0.359	0.087	0.383	0.0486	0.399	0.079	0.228	0.0298	0.159	0.0275	0.172
	Dolomite 16	1940			69	4.2	9	3.24	6.2	0.56	1.98	0.372	0.107	0.414	0.073	0.43	0.089	0.309	0.0327	0.232	0.0355	0.297
	Dolomite 17	1180			81	3.46	6.1	3.81	7.3	0.65	2.4	0.396	0.083	0.346	0.066	0.403	0.083	0.252	0.0314	0.246	0.0301	0.279
	Dolomite 20	2380			51.2	5.3	9.3	2.43	6.03	0.5	2.07	0.347	0.083	0.358	0.056	0.336	0.086	0.264	0.039	0.199	0.0336	0.309
	Dolomite 21	940			55	1.96	4.69	2.97	6.55	0.52	2.18	0.397	0.07	0.325	0.048	0.346	0.072	0.259	0.0335	0.179	0.0338	0.162
	Dolomite 22	840			82	1.8	4.36	2.79	5.49	0.59	1.9	0.317	0.065	0.367	0.0476	0.309	0.06	0.185	0.0248	0.201	0.0297	0.164
	Dolomite 24	632			64.8	1.44	3.2	3.1	5.2	0.49	1.93	0.286	0.072	0.299	0.0491	0.325	0.077	0.261	0.0294	0.214	0.0277	0.117
	Dolomite 25	1430			69	3.48	7.5	3.84	9.3	0.93	4.5	0.71	0.109	0.54	0.075	0.54	0.11	0.308	0.0393	0.253	0.0263	0.53
	Dolomite 26	1040			78	1.96	5.8	2.91	5.17	0.46	1.6	0.323	0.074	0.275	0.0356	0.272	0.053	0.189	0.0242	0.197	0.0226	0.156
	Dolomite 29	1080			102	1.86	5.53	3.29	5.62	0.49	1.81	0.357	0.066	0.328	0.0437	0.318	0.064	0.206	0.0283	0.236	0.0211	0.191
	Dolomite 30	890			51.4	3.6	5.34	2.99	5.42	0.5	1.3	0.25	0.056	0.293	0.049	0.434	0.091	0.265	0.0333	0.337	0.0315	0.165
	Dolomite 31	2160			73	2.72	7.8	3.87	6.3	0.58	2.28	0.346	0.085	0.363	0.057	0.389	0.085	0.285	0.0334	0.318	0.0282	0.226
	Dolomite 37	2050			55	3.1	13	2.9	5.21	0.53	1.79	0.293	0.052	0.43	0.053	0.448	0.081	0.297	0.0339	0.299	0.0274	0.224
	Dolomite 38	1330			56.3	1.98	7.88	4.37	6.66	0.6	2.73	0.424	0.081	0.455	0.059	0.458	0.088	0.284	0.0338	0.335	0.0272	0.183
	Dolomite 39	1050			54.7	2.08	6.14	3.55	5.89	0.6	1.83	0.284	0.067	0.329	0.057	0.418	0.088	0.26	0.0365	0.271	0.0301	0.236
	Average	1159			67.1	2.59	6.24	3.31	6.268	0.58	2.244	0.368	0.079	0.377	0.0545	0.402	0.082	0.257	0.0322	0.214	0.029	0.229
	St. Dev.	497			13.7	1.05	2.11	0.65	1.079	0.11	0.682	0.099	0.017	0.072	0.0104	0.069	0.013	0.036	0.0046	0.061	0.0038	0.086
DV 3.5	Dolomite 1	99	1770	7510	40.3	0.97	0.75	1.66	2.94	0.24	0.78	0.179	0.02	0.188	0.0382	0.424	0.105	0.37	0.0325	0.156	0.025	0.012
	Dolomite 2	76.2	1300	4740	41.1	0.41	0.97	1.93	3.54	0.34	1.11	0.222	0.055	0.26	0.039	0.318	0.091	0.255	0.0273	0.178	0.0225	0.03
	Dolomite 3	92.4	1840	7850	43.4	0.42	0.79	1.59	3.11	0.29	1.01	0.132	0.039	0.246	0.0452	0.365	0.111	0.398	0.04	0.189	0.0266	0.019
	Dolomite 4	78.8	1570	5490	36.1	0.37	0.58	1.47	2.71	0.3	0.78	0.154	0.025	0.17	0.0334	0.309	0.08	0.252	0.0326	0.156	0.0186	0.012

INDIVIDUAL DOLOMITE GEOCHEMICAL DATA (CONTINUED)

	Dolomite 5	900	1130	3960	70	1.72	4.14	2.6	4.8	0.57	1.34	0.22	0.052	0.267	0.0428	0.243	0.059	0.164	0.0268	0.143	0.0163	0.116
	Dolomite 6	720	1490	4770	66	3.9	4.41	2.18	6.2	0.51	1.7	0.273	0.049	0.222	0.0345	0.263	0.054	0.192	0.0234	0.157	0.0173	0.135
	Dolomite 7	320	1760	6900	91	0.86	2.38	2.59	4.34	0.5	1.02	0.231	0.041	0.271	0.0436	0.351	0.08	0.245	0.0349	0.146	0.0228	0.054
	Dolomite 8	630	1150	6400	93	2.83	3.88	2.14	4.6	0.41	1.6	0.225	0.049	0.213	0.0301	0.217	0.042	0.156	0.0187	0.119	0.0188	0.093
	Dolomite 9	1470	1500	5390	62.5	2.67	3.72	3.32	6.07	0.7	1.72	0.249	0.066	0.348	0.0544	0.322	0.075	0.213	0.0302	0.18	0.0204	0.148
	Dolomite 10	684	1220	3820	57.2	2.46	3.88	2.75	5.36	0.67	2.06	0.268	0.051	0.335	0.0439	0.314	0.062	0.184	0.0236	0.125	0.0177	0.106
	Average	507	1473	5683	60.1	1.66	2.55	2.22	4.37	0.45	1.31	0.215	0.045	0.252	0.0405	0.313	0.076	0.243	0.0290	0.155	0.0206	0.073
	St. Dev.	461	265	1427	20.5	1.24	1.62	0.59	1.27	0.16	0.44	0.047	0.014	0.058	0.0070	0.061	0.022	0.082	0.0063	0.023	0.0035	0.053
DV 2.0	Dolomite 1	575			575	0.81	6.42	2.41	4.7	0.56	1.78	0.304	0.063	0.33	0.0492	0.302	0.065	0.182	0.0198	0.122	0.0206	0.102
	Dolomite 2	238			238	0.69	3.94	2.27	4.26	0.5	1.75	0.291	0.051	0.311	0.034	0.261	0.053	0.164	0.0175	0.114	0.0149	0.087
	Dolomite 3	570			570	1.53	8.2	2.22	5.25	0.56	1.88	0.328	0.059	0.356	0.0417	0.335	0.064	0.191	0.0182	0.12	0.0133	0.13
	Dolomite 4	259			259	0.79	6.33	2.19	7.5	0.74	2.34	0.417	0.074	0.38	0.049	0.399	0.073	0.231	0.0234	0.137	0.0137	0.14
	Dolomite 5	109			109	0.23	2.46	2.23	4.6	0.42	1.41	0.234	0.043	0.177	0.0338	0.255	0.045	0.117	0.0184	0.083	0.0116	0.029
	Dolomite 6	194			194	0.41	3.75	3.96	9.4	0.96	3	0.45	0.094	0.5	0.046	0.35	0.08	0.209	0.0279	0.147	0.0213	0.053
	Dolomite 7	466			466	1.43	8.1	3.08	7.3	0.52	2.26	0.372	0.069	0.308	0.0467	0.36	0.069	0.182	0.0182	0.106	0.0155	0.076
	Dolomite 8	400			400	0.62	4.66	2.94	5.9	0.52	1.95	0.384	0.069	0.263	0.046	0.347	0.07	0.185	0.0208	0.137	0.0168	0.062
	Dolomite 9	289			289	0.61	3.68	2.94	5.42	0.59	1.98	0.287	0.061	0.293	0.051	0.326	0.084	0.202	0.0309	0.146	0.0254	0.081
	Dolomite 11	527			527	0.98	6.1	2.69	5.9	0.58	2.23	0.326	0.07	0.297	0.0406	0.282	0.06	0.153	0.0154	0.104	0.0182	0.132
	Dolomite 12	350			350	0.79	4.8	2.65	5.6	0.59	2.05	0.379	0.074	0.362	0.066	0.411	0.079	0.211	0.024	0.134	0.0223	0.203
	Dolomite 13	1200			1200	3.6	10.4	3.07	5.81	0.57	2.14	0.377	0.09	0.374	0.057	0.32	0.075	0.198	0.037	0.122	0.024	0.217
	Dolomite 14	725			725	2.24	6.6	1.93	4.63	0.47	1.72	0.33	0.063	0.282	0.0356	0.262	0.054	0.156	0.0198	0.125	0.0183	0.185
	Dolomite 15	564			564	2.25	6.35	2.62	5.4	0.49	1.91	0.315	0.063	0.323	0.0335	0.219	0.059	0.157	0.0302	0.11	0.0183	0.166
	Dolomite 16	536			536	2.09	5.57	3.72	6.78	0.87	2.57	0.413	0.083	0.471	0.0576	0.431	0.113	0.279	0.0249	0.163	0.031	0.154
	Dolomite 18	225			225	0.3	3.16	2.16	3.68	0.42	1.61	0.272	0.049	0.261	0.0392	0.255	0.071	0.199	0.0235	0.128	0.0255	0.06
	Dolomite 19	455			455	0.82	5.53	2.9	6.23	0.58	2.09	0.334	0.053	0.281	0.039	0.257	0.064	0.164	0.0168	0.101	0.0213	0.088
	Dolomite 20	400			400	0.88	6.1	3.3	6	0.71	2.36	0.318	0.063	0.356	0.046	0.3	0.072	0.216	0.0183	0.127	0.0172	0.111
	Average	449			449	1.17	5.68	2.74	5.8	0.59	2.06	0.341	0.066	0.329	0.045	0.315	0.069	0.189	0.0225	0.124	0.0194	0.115
	St. Dev.	248.47			248	0.87	1.98	0.56	1.3	0.15	0.37	0.056	0.014	0.075	0.009	0.060	0.015	0.036	0.0058	0.019	0.005	0.054
DV 0.0	Dolomite 1	3540			95	18.6	12.9	5.65	17.8	1.9	7	1.21	0.247	1.08	0.166	1.14	0.241	0.553	0.068	0.33	0.06	0.9
	Dolomite 2	2560			92	10.8	12.2	5.7	17.3	1.91	6.7	1.04	0.272	1.27	0.152	1	0.241	0.532	0.073	0.361	0.047	2.4
	Dolomite 3	890			167	5.22	6.7	8.3	36.1	4.41	13.2	2.45	0.399	2.43	0.294	1.57	0.288	0.689	0.076	0.37	0.054	1.8
	Dolomite 7	2950			141	10.3	13.2	5.6	18.8	2.24	6.7	1.09	0.257	1.15	0.174	1.16	0.224	0.523	0.053	0.353	0.052	0.543
	Dolomite 9	1420			87	5.3	6.4	3.67	14.4	1.34	4.05	0.611	0.158	0.71	0.106	0.74	0.152	0.426	0.0521	0.239	0.0349	0.373
	Dolomite 11	1990			107	5.7	7.8	4.54	16.8	1.55	5.61	0.735	0.155	0.83	0.109	0.76	0.19	0.476	0.0523	0.292	0.042	0.372
	Dolomite 12	1650			124	5.5	7.8	3.53	12.3	1.17	3.72	0.55	0.117	0.529	0.085	0.62	0.109	0.287	0.0381	0.184	0.0294	0.264
	Dolomite 13	4100			99	17.2	11.8	5.28	18.8	2.06	9.6	0.93	0.214	1.01	0.154	1.11	0.209	0.555	0.082	0.428	0.075	0.68
	Dolomite 14	1290			94	5.5	8	3.26	15.2	1.59	5.5	0.64	0.145	0.76	0.108	0.73	0.167	0.342	0.0466	0.273	0.037	0.342
	Dolomite 15	720			76	3.42	5.2	4.8	18.3	2.8	7.3	1.06	0.23	1.16	0.119	0.76	0.135	0.291	0.0315	0.162	0.0261	0.157
	Dolomite 16	2520			108	11.5	10.6	4.44	16.7	1.56	5.99	0.81	0.184	0.77	0.112	0.7	0.142	0.407	0.0495	0.299	0.0399	0.432

INDIVIDUAL DOLOMITE GEOCHEMICAL DATA (CONTINUED)

	Dolomite 20	2040			113	9.2	10.2	4.8	15.3	2.11	7.7	1.02	0.217	1.01	0.151	0.99	0.195	0.54	0.063	0.383	0.0543	0.526
	Dolomite 21	1530			78	6.8	10.6	4.54	16.5	1.58	6.2	0.95	0.195	0.87	0.149	0.82	0.171	0.49	0.052	0.393	0.047	0.46
	Dolomite 28	1730			149	8.4	8.2	4.27	15.8	1.82	6.8	1.05	0.215	0.94	0.154	0.93	0.181	0.558	0.064	0.454	0.055	0.81
	Dolomite 30	1710			122	6	7.7	5	15.5	1.42	7	1.16	0.217	0.86	0.134	0.79	0.191	0.517	0.061	0.28	0.0461	0.425
	Dolomite 31	3000			82	6.74	9.8	5.56	23	1.71	7.4	1.18	0.276	1.01	0.142	1	0.194	0.504	0.06	0.365	0.048	0.489
	Dolomite 34	1780			140	8.9	9.8	5.24	21.2	1.97	8.4	1.27	0.25	0.98	0.13	0.83	0.169	0.543	0.064	0.415	0.051	0.569
	Dolomite 35	3320			104	13.8	14.7	5.87	23.1	2.26	8.4	1.27	0.261	1.01	0.16	1.19	0.204	0.64	0.077	0.409	0.056	0.77
	Dolomite 36	2230			65	13	13.3	5.5	20.5	1.85	8.1	1.14	0.256	1.15	0.186	1.13	0.221	0.66	0.07	0.402	0.048	0.74
	Dolomite 37	1550			79	8	8.6	6.6	17.4	2.21	7.9	1.19	0.256	0.94	0.138	0.88	0.195	0.553	0.07	0.35	0.045	0.68
	Dolomite 38	860			60	4.7	5.9	3.52	12.1	1.23	5.3	0.707	0.156	0.66	0.104	0.727	0.156	0.495	0.073	0.343	0.041	0.311
	Dolomite 39	1940			65.2	7.6	10.4	4.26	15	1.29	4.85	0.71	0.16	0.77	0.113	0.8	0.179	0.527	0.065	0.331	0.055	0.46
	Dolomite 40	1610			78	14.2	8.21	5.63	16.8	1.77	5.83	1.03	0.202	0.84	0.133	0.85	0.18	0.522	0.058	0.307	0.0366	0.423
	Average	2040			101	9.0	9.6	5.0	18.0	1.90	6.92	1.03	0.219	0.99	0.142	0.92	0.188	0.506	0.061	0.336	0.047	0.649
	St. Dev.	878			29	4.1	2.6	1.1	4.9	0.67	1.98	0.38	0.060	0.36	0.042	0.22	0.039	0.102	0.013	0.074	0.011	0.502
DV A. 20	Dolomite 3	1060			89		7	9.6	35.9	3.9	14.3	2.59	0.365	1.95	0.299	1.65	0.292	0.71	0.098	0.465	0.077	0.26
	Dolomite 4	1620			146		7.6	9.2	45	4.8	15.3	3.04	0.52	2.4	0.319	1.64	0.333	0.9	0.117	0.58	0.081	0.334
	Dolomite 5	414			94		3.48	6.6	27.1	4.12	11.3	2.73	0.457	1.87	0.261	1.44	0.304	0.88	0.079	0.56	0.072	0.242
	Dolomite 6	880			89		4.31	9.2	31	4.3	16.2	2.82	0.495	2.12	0.32	1.93	0.327	0.84	0.104	0.54	0.088	0.256
	Dolomite 7	1040			81		4.75	8.9	26.6	3.65	11.9	2.26	0.411	1.72	0.255	1.7	0.321	0.84	0.112	0.525	0.074	0.261
	Dolomite 9	427			64		3.13	5.51	33	3.2	11.8	1.95	0.304	1.4	0.207	1.16	0.223	0.61	0.074	0.322	0.06	0.146
	Dolomite 10	1160			90		4.95	6.6	22.3	2.67	8.1	1.54	0.266	1.38	0.191	1.08	0.224	0.58	0.076	0.408	0.057	0.335
	Dolomite 12	2090			95		10	9.7	30.5	3.36	11.6	2.12	0.402	1.67	0.24	1.57	0.271	0.79	0.116	0.544	0.081	0.496
	Dolomite 14	1470			79		10.7	7.5	26.4	2.46	8.7	1.57	0.294	1.43	0.241	1.23	0.27	0.6	0.079	0.439	0.063	0.395
	Dolomite 16	2890			90		10.1	8.9	29	2.86	10.3	1.79	0.413	1.58	0.224	1.49	0.292	0.66	0.1	0.435	0.086	0.487
	Dolomite 17	3100			101		7.9	11.8	40.6	5	15.5	3.15	0.55	2.38	0.331	2.16	0.387	1.41	0.134	0.72	0.111	0.61
	Dolomite 18	5500			112		11.9	8	45	3.26	12.1	2	0.416	1.79	0.284	1.45	0.298	0.85	0.099	0.63	0.079	0.54
	Dolomite 19	1890			67		6.95	7.72	23.9	2.44	8.9	1.79	0.326	1.43	0.227	1.38	0.3	0.75	0.109	0.483	0.081	0.401
	Dolomite 22	3040			117		13.9	10.6	27	3.29	11.1	1.82	0.418	1.56	0.218	1.18	0.246	0.67	0.077	0.42	0.062	0.71
	Dolomite 24	2050			90		13.7	8.3	26.1	3.01	10.2	1.6	0.376	1.47	0.236	1.39	0.254	0.67	0.098	0.5	0.065	0.47
	Dolomite 25	1790			70		8.2	9.7	29.2	3.31	11.7	2.08	0.389	1.77	0.274	1.54	0.296	0.86	0.105	0.58	0.089	0.62
	Dolomite 26	3660			87		11.9	9.4	23.6	2.7	8.4	1.73	0.31	1.46	0.222	1.26	0.243	0.71	0.098	0.557	0.078	0.53
	Dolomite 27	1100			71		5.31	8.1	39	4.69	14.9	3.15	0.484	2.06	0.329	1.87	0.339	0.81	0.113	0.568	0.076	0.409
	Dolomite 28	980			137		5.15	10.3	30.6	5.4	14.8	2.55	0.54	2.47	0.344	2.17	0.382	0.98	0.128	0.67	0.103	0.336
	Dolomite 29	1950			77.4		6.37	11.3	34.8	4.37	15.7	2.82	0.548	2.18	0.334	1.98	0.369	0.97	0.126	0.618	0.092	0.434
	Dolomite 30	9700			140		19.7	10	32	2.98	11.5	2.69	0.44	1.93	0.248	1.6	0.313	0.96	0.105	0.75	0.098	1.04
	Dolomite 31	1080			65		5.9	6.4	20.9	3.11	9.4	1.78	0.323	1.22	0.221	1.18	0.21	0.52	0.071	0.366	0.057	0.259
	Dolomite 32	1310			109		5.9	9.3	30	3.8	11.9	2.29	0.372	1.54	0.264	1.74	0.322	0.73	0.084	0.44	0.068	0.365
	Dolomite 35	1110			72		5.19	7.1	32.5	3.49	10.7	2.18	0.49	2.06	0.244	1.44	0.272	0.81	0.076	0.447	0.067	0.422

INDIVIDUAL DOLOMITE GEOCHEMICAL DATA (CONTINUED)

	Dolomite 37	1680			88		6.7	8.5	26.4	3.9	12.4	2.38	0.45	1.72	0.257	1.58	0.301	0.84	0.081	0.46	0.076	0.357
	Dolomite 38	1380			60		4.8	8.2	27.4	3.43	14.3	2.3	0.396	2.12	0.256	1.55	0.286	0.63	0.091	0.486	0.071	0.313
	Dolomite 40	1350			86		5	11.3	36.3	4.87	17.5	3.17	0.545	2.4	0.346	2.09	0.4	0.87	0.104	0.545	0.092	0.309
	Average	2064			91		7.8	8.8	30.8	3.6	12.2	2.29	0.419	1.82	0.266	1.57	0.30	0.79	0.098	0.521	0.078	0.420
	St. Dev.	1875			23		3.8	1.6	6.3	0.8	2.6	0.52	0.084	0.36	0.046	0.31	0.05	0.18	0.018	0.102	0.014	0.181
DV A. 18	Dolomite 2	4000	670	2780	91	5.4	10.2	14.4	54	6.1	17.4	2.89	0.66	2.22	0.325	1.89	0.314	0.9	0.103	0.604	0.088	0.475
	Dolomite 3	10600	840	4700	168	17.5	22.7	14	51.5	5	15.6	2.53	0.534	2.18	0.301	1.77	0.317	0.95	0.119	0.86	0.098	0.88
	Dolomite 5	2390	546	14900	103	3.49	7.2	13.8	47.8	6.13	20.9	4.02	0.736	3.27	0.43	2.5	0.462	1.16	0.148	0.772	0.116	0.89
	Dolomite 6	4200	540	4500	82	9.5	12.3	12.5	38.8	4.5	13.6	2.44	0.492	1.94	0.263	1.36	0.252	0.83	0.097	0.67	0.101	0.54
	Dolomite 7	8100	740	3330	92	11.2	19	12.5	44	3.51	12.1	1.88	0.418	1.52	0.207	1.31	0.243	0.78	0.099	0.519	0.086	0.631
	Dolomite 9	9700	570	2050	159	25.5	63	15.9	62	8.6	29.7	5.13	1.15	4.9	0.6	3.15	0.59	1.42	0.183	0.92	0.115	5.9
	Dolomite 10	14500	650	3180	105	33	35	14.4	36.5	4.9	12.3	2.06	0.44	1.51	0.211	1.33	0.255	0.87	0.1	0.72	0.106	1.56
	Dolomite 11	2180	870	3270	107	101	78	11.5	35.8	4.48	13.2	2.06	0.42	1.75	0.27	1.56	0.322	1.01	0.151	0.814	0.167	0.617
	Dolomite 12	4300	596	1910	126	13	10	17	46.1	5.53	21.4	3.29	0.633	2.83	0.426	2.42	0.449	1.19	0.173	0.96	0.14	0.91
	Dolomite 14	7100	590	1960	122	16.7	17.2	15.4	43.1	5.5	18.9	2.91	0.592	2.14	0.317	1.75	0.297	0.76	0.121	0.62	0.1	1.08
	Dolomite 15	12300	438	3400	111	24.4	45	14.6	42.1	5.9	16.6	3.35	0.62	2.5	0.355	2.04	0.353	0.94	0.112	0.96	0.127	1.11
	Dolomite 16	11000	750	3780	141	33.3	34.1	13.3	48.4	4.25	14.5	2.62	0.47	1.82	0.267	1.53	0.307	0.99	0.14	0.91	0.115	1.78
	Dolomite 17	2150	680	1810	112	9.5	13.7	13.4	39.1	4.1	14.5	2.55	0.453	1.96	0.273	1.49	0.308	0.96	0.126	0.8	0.124	0.609
	Dolomite 18	5600	610	2720	114	12.1	16.6	12.1	46.2	3.71	14.3	2.6	0.486	1.85	0.281	1.69	0.376	0.87	0.144	0.76	0.116	0.76
	Dolomite 19	560	940	1900	115	1.9	3.74	15.2	48	4.71	16.2	2.69	0.606	2.57	0.334	2.06	0.392	1.06	0.118	0.73	0.104	0.253
	Dolomite 20	8500	510	2150	94	18.5	20	16.1	52	5.71	19.6	2.97	0.68	2.56	0.378	2.32	0.37	1.17	0.158	0.9	0.13	0.94
	Dolomite 21	5800	590	2560	150	11.4	18.8	10.4	29.5	3.27	12.4	1.9	0.442	1.74	0.25	1.25	0.275	0.84	0.118	0.73	0.108	1.19
	Dolomite 22	12300	760	3480	112	21	25.5	16.5	53	5.01	18.6	2.85	0.67	2.66	0.317	2.18	0.376	1.12	0.126	0.88	0.146	1.2
	Dolomite 23	8100	780	2910	112	17.1	18.5	12.3	29.5	3.28	12.6	2.22	0.464	1.84	0.278	1.58	0.325	0.88	0.09	0.7	0.117	1.16
	Dolomite 24	8900	670	4140	105	19.3	18.3	16.9	48.5	5.21	17.5	3.01	0.631	2.44	0.361	2.02	0.378	1.06	0.135	1.02	0.124	1.05
	Dolomite 25	7000	547	2210	128	13.2	18	12.8	37.9	5.4	16.3	2.82	0.663	2.57	0.375	1.89	0.381	1.04	0.123	0.93	0.117	2.17
	Dolomite 26	7400	490	2730	95	14	16.3	17.3	45.8	5.08	18.7	2.98	0.71	2.75	0.359	2.11	0.384	1.1	0.154	0.8	0.137	1.04
	Dolomite 27	7700	660	8300	100	12.8	18.4	19.6	45.9	4.72	15.9	2.48	0.534	2.44	0.315	2.02	0.393	1.09	0.151	0.92	0.091	0.74
	Dolomite 28	2650	920	2430	73	5	8.9	7.4	38	4.2	10	1.6	0.364	1.49	0.192	1.69	0.269	0.8	0.101	0.62	0.075	0.405
	Dolomite 31	2120	720	1880	139	3.13	5.8	14.6	41	6.1	17.9	2.71	0.543	2.51	0.336	1.8	0.408	1.13	0.125	0.91	0.111	0.455
	Dolomite 32	9900	880	3430	91	12	19.5	11.5	38.2	4.05	14.1	2.55	0.494	2.1	0.246	1.57	0.305	0.82	0.114	0.79	0.09	0.77
	Dolomite 33	4100	671	2960	82	7.2	10.1	14.2	37.7	4.36	15.1	2.52	0.585	2.25	0.335	1.79	0.325	0.92	0.111	0.716	0.106	0.63
	Dolomite 34	4700	860	1850	93	7.1	14.3	8.6	36	3.43	11	1.82	0.339	1.33	0.212	1.38	0.219	0.76	0.095	0.72	0.078	0.54
	Dolomite 35	3500	690	2250	122	5.6	10.6	13.6	40.3	4.8	18.2	2.55	0.59	2.38	0.292	1.9	0.332	0.85	0.109	0.71	0.093	0.61
	Dolomite 36	3200	446	2270	91	7.1	11.3	13.3	47	4.95	18.8	3.54	0.7	2.79	0.334	2.49	0.396	1.08	0.149	0.85	0.121	0.424
	Dolomite 37	1660	658	1840	97	3.2	5.1	13.1	34.4	4.55	15.1	2.32	0.502	2.08	0.29	1.76	0.358	0.89	0.118	0.7	0.104	0.377
	Dolomite 38	7900	940	3800	131	34	21.7	19.1	70	7.9	29.4	5.7	1.11	4.9	0.58	3.74	0.75	1.68	0.245	1.22	0.183	6.4
	Dolomite 39	4260	550	1940	91	5.1	10.4	21.5	51	5.25	18.7	2.78	0.7	2.63	0.308	2.09	0.369	1	0.125	0.77	0.116	0.46
	Dolomite 40	3000	557	2830	71	5.6	7.4	13.4	42.1	4.43	14.2	2.26	0.475	2.02	0.249	1.52	0.256	0.73	0.091	0.554	0.0634	0.3

INDIVIDUAL DOLOMITE GEOCHEMICAL DATA (CONTINUED)

	Average	6217	674	3299	110	15.9	19.6	14.2	44.2	4.96	16.6	2.78	0.585	2.37	0.320	1.91	0.356	0.99	0.129	0.80	0.112	1.14
	St. Dev.	3560	141	2394	23	17.4	15.7	2.9	8.5	1.15	4.32	0.84	0.174	0.78	0.090	0.52	0.101	0.20	0.031	0.14	0.024	1.34
DV P. 5	Dolomite 1	990			77.00	2.57	6.3	9.1	26.7	3.2	14.4	2.43	0.417	1.88	0.297	1.92	0.341	0.94	0.128	0.72	0.099	0.69
	Dolomite 2	4510			82.00	9.6	13.9	14.6	28.7	3.99	14.5	2.5	0.608	2.34	0.329	2.47	0.482	1.32	0.167	0.94	0.12	1.09
	Dolomite 3	187			61.30	0.44	2.04	15.8	41.4	5.64	23.4	4.02	0.754	3.41	0.499	2.99	0.512	1.35	0.167	0.81	0.116	0.296
	Dolomite 4	920			86.00	1.69	4.39	14.5	53	7.1	31.2	6	0.98	4.61	0.65	3.4	0.55	1.4	0.173	1.03	0.134	0.68
	Dolomite 5	1080			73.70	2.31	6.43	13.9	31.6	4.49	19.4	3.33	0.605	2.72	0.422	2.14	0.438	1.09	0.126	0.77	0.104	0.538
	Dolomite 6	3600			80.00	6.2	13.4	13.5	35.7	4.41	19.7	3.44	0.631	2.76	0.44	2.94	0.512	1.54	0.159	0.94	0.113	0.838
	Dolomite 7	382			79.00	2.47	4.13	10.3	28.3	3.45	14.7	3.1	0.55	2.71	0.436	2.31	0.44	1.16	0.133	0.69	0.12	0.58
	Dolomite 8	760			59.80	1.48	5	9.9	25.7	3.55	13	2.79	0.52	2.04	0.338	2.39	0.38	1.28	0.109	0.76	0.098	0.336
	Dolomite 9	454			74.00	0.97	3.32	11	34	4.59	20.1	3.65	0.603	3.07	0.448	2.5	0.492	1.4	0.163	0.86	0.111	0.328
	Dolomite 10	456			57.20	1.21	5.07	11.9	33.7	3.43	15.4	3.21	0.496	2.37	0.394	2.51	0.453	1.26	0.142	0.82	0.121	0.284
	Dolomite 11	166			85.80	2.29	2.33	23.8	56.4	8.4	41.6	6.89	1.06	5.31	0.68	3.6	0.556	1.39	0.151	0.87	0.123	0.53
	Dolomite 12	900			73.80	3.1	4.03	12.7	32.1	4.06	16.3	3.54	0.57	2.59	0.42	2.47	0.482	1.22	0.137	0.85	0.127	0.615
	Dolomite 13	550			66.50	2.95	3.33	15.5	34.2	4.61	18.3	3.79	0.606	3.06	0.478	2.74	0.507	1.34	0.171	0.85	0.129	0.356
	Dolomite 14	245			79.60	2.5	2.43	16.9	46.9	6.75	31.6	5.82	0.94	4.28	0.563	2.83	0.474	1.12	0.132	0.82	0.1	0.49
	Dolomite 15	42			70.80	1.13	1.09	34.6	74.6	9.81	40.4	8.49	1.3	6.17	0.96	4.78	0.82	2.07	0.213	1.21	0.177	0.444
	Dolomite 17	113			65.90	0.39	2.5	22.4	47.3	7.21	33.3	5.77	0.99	4.56	0.661	3.51	0.603	1.62	0.177	0.99	0.12	0.51
	Dolomite 18	840			83.10	3.5	5.6	22.8	69	9	37	6.9	1.2	5.31	0.79	3.65	0.561	1.42	0.154	0.97	0.131	0.57
	Dolomite 19	410			77.30	1.47	3.79	13.6	32.1	5.4	19.9	4.32	0.744	3.27	0.498	2.64	0.432	1.11	0.128	0.7	0.106	0.309
	Dolomite 20	790			78.00	2.4	5.8	21.9	57	7	29.7	5.6	0.93	5.2	0.62	3.59	0.52	1.27	0.124	0.82	0.124	0.64
	Average	916			74.3	2.6	5.0	16.2	41.5	5.58	23.9	4.50	0.76	3.56	0.52	2.91	0.503	1.33	0.150	0.86	0.120	0.533
	St. Dev.	1161			8.6	2.1	3.4	6.3	14.5	2.03	9.4	1.73	0.26	1.29	0.17	0.69	0.100	0.24	0.025	0.13	0.018	0.206

VITA

John Michael Callen spent his childhood living in several cities throughout the south before eventually spending his high school years in northern Louisiana. His parents were educators in science and math, resulting in his keen interest in everything outdoors and nature-related. Despite his indecision beginning college, his undergraduate advisor, Dr. David Bieler, persuaded him to take an Introductory Geology class at Centenary College of Louisiana, sparking an passion that has not abated to this day.

After working in the petroleum industry, further cementing his interest in geology and future goals, for several years and graduating, John Michael entered graduate school at Louisiana State University. A shared interest in carbonates and sedimentary depositional systems led him to a pairing with his graduate advisor, Dr. Achim Herrmann.